

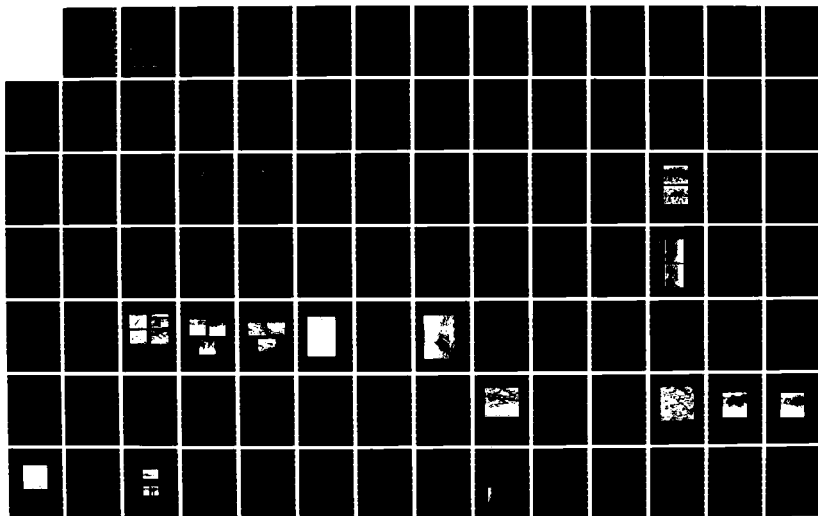
AD-A168 173

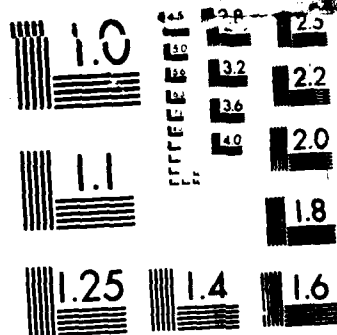
THE USGS (US GEOLOGICAL SURVEY) X- C- AND L-BAND SAR
DATA COLLECTION PROG. (U) ENVIRONMENTAL RESEARCH INST
OF MICHIGAN ANN ARBOR RADAR DIV E S KASISCHKE AUG 85
ERIM-173000-4-T F/G 17/9

1/2

UNCLASSIFIED

NL





MICROCOPY RESOLUTION TEST CHART

2

AD-A168 173

173000-4-T

Topic Report

THE USGS X-, C-, AND L-BAND SAR
DATA COLLECTION PROGRAM

E.S. KASISCHKE

Radar Division

AUGUST 1985

DTIC
SELECTED
MAY 19 1986
SAD

[Handwritten signature]

DTIC FILE COPY

Intera Environmental Consultants, Inc.
11999 Katy Freeway Suite 610
Houston, Texas 77079
Technical Monitor: Joseph Pearson

U.S. Geological Survey
12201 Sunrise Valley Drive
Reston, Virginia 22092
Technical Monitor: John Jones

Contract No. 14-08-0001-21748

ENVIRONMENTAL
RESEARCH INSTITUTE OF MICHIGAN
BOX 8618 • ANN ARBOR • MICHIGAN 48107

86 5 19 012

TECHNICAL REPORT STANDARD TITLE PAGE

1. Report No. 173000-4-T		2. Government Accession No.		3. Recipient's Catalog No.	
4. Title and Subtitle The USGS X-, C- and L-Band SAR Data Collection Program				5. Report Date August 1985	
				6. Performing Organization Code	
7. Author(s) Eric S. Kasischke				8. Performing Organization Report No. 173000-4-T	
9. Performing Organization Name and Address Environmental Research Institute of Michigan P. O. Box 8618 Ann Arbor, MI 48107-8618				10. Work Unit No.	
				11. Contract or Grant No. 14-08-0001-21748	
12. Sponsoring Agency Name and Address Intera Environmental Consultants, Inc. 11999 Katy Freeway, Suite 610 Houston, TX 77079 See Page ii				13. Type of Report and Period Covered Topic Report November 1983 to August 1985	
				14. Sponsoring Agency Code	
15. Supplementary Notes The technical monitors for this work are Joseph Pearson (Intera) and John Jones (USGS)					
16. Abstract This report presents the results of a data collection program performed for the U.S. Geological Survey. Twenty-two passes of high resolution (3m), multifrequency (X-, C- and L-band) and multipolarization (VV and VH) imagery were collected over five test sites within the North Carolina Digital Project Area. The SAR used for this program was the ERIM/CCRS CV-580 SAR System. This report presents diagrams of the ground swath of each SAR pass, along with representative SAR imagery which illustrates the high quality of the data set. The engineering assessment performed on the SAR imagery is discussed. The optical and digital SAR data products generated for this program are summarized, including the first-order geometric and radiometric corrections applied to the digital data.					
17. Key Words Synthetic Aperture Radar Multifrequency Multipolarization North Carolina Digital Project Area Vegetation.			18. Distribution Statement The distribution of this report is unlimited		
19. Security Classif. of this report Unclassified		20. Security Classif. of this page Unclassified		21. No. of Pages 116 + xiv	22. Price

Unclassified

SECURITY CLASSIFICATION OF THIS PAGE (When Data Entered)

12. Continued

U.S. Geological Survey
12201 Sunrise Valley Drive
Reston, VA 22042

Unclassified

SECURITY CLASSIFICATION OF THIS PAGE (When Data Entered)

ACKNOWLEDGMENTS

The success of the X-, C- and L-band SAR data collection and processing activities conducted for the USGS in April 1984 is due in large part to the assistance of numerous organizations and individuals who we would like to acknowledge at this time.

Special thanks go to the crew of the ERIM/CCRS CV-580 SAR (Messrs. W. Bayer, S. Bertrand, A. Gignac, R. Gould and S. Bertrand), whose extra efforts insured the success of the SAR data collection mission.

C. Richardson, J. Edeburn and S. Davidson are thanked for assisting in identifying and locating the various test sites.

C. Ager and M. Powers of the USGS assisted in the deployment of the reference reflectors, and their help was greatly appreciated. D. Krohn and A. Kover, also of the USGS, provided technical inputs during the flight planning phase of the experiment.

Finally, individuals at ERIM who assisted in the data collection, processing and report preparation activities include B. Beatty, D. Clarke, C. Caruthers, J. Clinthorne, J. Lyden, R. Rau, F. Smith and L. Sutherland.

TABLE OF CONTENTS

PREFACEiii

ACKNOWLEDGEMENTSv

LIST OF FIGURESix

LIST OF TABLESxiii

1. INTRODUCTION 1

2. CV-580 SAR SYSTEM DESCRIPTION 7

3. DATA DESCRIPTION17

 3.1 SAR Data17

 3.1.1 USGS-1 (8 April 1984 - 13:06 to 16:24 EST)20

 3.1.2 USGS-2 (9 April 1984 - 11:27 to 13:45 EST)31

 3.1.3 USGS-3 (10 April 1984 - 15:59 to 17:58 EST)38

 3.2 SAR Calibration Data45

 3.4 Digitized SAR Data53

 3.4.1 Geometric Correstion of SAR Data57

 3.4.2 Radiometric Correction64

 3.4.3 Digitally-Processed SAR Data71

 3.5 Engineering Assessment71

4. SUMMARY79

REFERENCES81

APPENDIX A:83

APPENDIX B:89

APPENDIX C:109

APPENDIX D:115

LIST OF FIGURES

1. Location of North Carolina Digital Project Area (NCDPA) Test Sites	2
2. Locations of Test Sites A, B and C of the NCDPA	3
3. Locations of Test Sites D and E of the NCDPA	4
4. Schematic Diagram of CV-580 X/C/L SAR System	9
5. Schematic Diagram of CV-580 SAR System Transmitter/Receiver	10
6. Schematic Diagram of CV-580 SAR System X/L Calibration Signal Generator	12
7. CV-580 SAR System Signal Recording and Processing Options	15
8. CV-580 SAR Ground Coverage During USGS-1, Pass 1	22
9. CV-580 SAR Ground Coverage During USGS-1, Pass 2	23
10. CV-580 SAR Ground Coverage During USGS-1, Pass 3	24
11. CV-580 SAR Ground Coverage During USGS-1, Pass 4	25
12. CV-580 SAR Ground Coverage During USGS-1, Pass 5	26
13. CV-580 SAR Ground Coverage During USGS-1, Pass 6	27
14. CV-580 SAR Ground Coverage During USGS-1, Passes 7 and 9	28
15. CV-580 SAR Ground Coverage During USGS-1, Pass 8	29
16. Optically-Processed X- and L-Band SAR Imagery of Pilot Mountain (USGS-1, Pass 7, 8 April 1984)	30
17. CV-580 SAR Ground Coverage During USGS-2, Pass 1	33
18. CV-580 SAR Ground Coverage During USGS-2, Pass 2	34
19. CV-580 SAR Ground Coverage During USGS-2, Pass 3	35
20. CV-580 SAR Ground Coverage During USGS-2, Passes 4 and 5	36
21. CV-580 SAR Ground Coverage During USGS-2, Passes 6 and 7	37
22. CV-580 SAR Ground Coverage During USGS-3, Pass 1	40

LIST OF FIGURES
 (Continued)

23. CV-580 SAR Ground Coverage During USGS-3, Passes 2 and 3	41
24. CV-580 SAR Ground Coverage During USGS-3, Pass 4	42
25. CV-580 SAR Ground Coverage During USGS-3, Pass 5	43
26. Optically-Processed X- and C-Band SAR Imagery of Pilot Mountain (USGS-3, Pass 4; 10 April 1984)	44
27. Approximate Locations of Reference Reflectors Within the Asheboro Calibration Array	47
28. Approximate Locations of Reference Reflectors Within the Duke Forest Calibration Array	48
29. Typical Calibrated Reflectors Deployed at the Asheboro and Duke Forest Calibration Arrays	49
30. Optically-Processed X-, C- and L-Band SAR Imagery of the Duke Forest Calibration Array	50
31. Optically-Processed X-, C- and L-Band SAR Imagery of the Asheboro Airport Calibration Array	51
32. Image of L-Band Calibration Signals	52
33. A Dihedral Corner Reflector Being Deployed in the Field	54
34. Locations of Dihedral Corner Reflectors	55
35. Slant Range Versus Ground Range Perspective in an Imaging Radar System	61
36. Calculation of the Aircraft Altitude (h) From Two Known Ground Locations (A and B)	65
37. Illustration of the Effects of Range Fall-off, X- and L-Band Antenna Pattern, and Laser Illumination Pattern	67
38. Non-Corrected Hybrid-Digitized L-Band SAR Data From USGS-2, Pass 5	69
39. Radiometric Correction Applied to USGS-2, Pass 5	70

LIST OF FIGURES
(Continued)

40. Radiometrically- and Geometrically-Corrected L-Band SAR Data From USGS-2, Pass 572

41. Digitally-Processed X-Band SAR Data Collected Over the Duke Forest Calibration Array73

42. Digitally-Processed C-Band SAR Data Collected Over the Duke Forest Calibration Array74

43. Digitally-Processed L-Band SAR Data Collected Over the Duke Forest Calibration Array75

44. Examples of Image Characteristics Found on USGS-NCDPA X-Band SAR Data77

LIST OF TABLES

1. CV-580 SAR System Parameters	8
2. CV-580 SAR System X-, C- and L-Band SAR Data Recording Capability	14
3. Summary of USGS NCDPA Multichannel SAR Flights	18
4. Summary of SAR and Aircraft Parameters During USGS-1 (8 April 1984)	21
5. Summary of SAR and Aircraft Parameters During USGS-2 (9 April 1984)	32
6. Summary of SAR and Aircraft Parameters During USGS-3 (10 April 1984)	39
7. Summary of Calibrated Corner Reflectors Used During USGS-NCDPA SAR Overflights	46
8. Locations of Dihedral Reflectors	55
9. Summary of Digitized NCDPA Data Set	58

USGS X-, C- AND L-BAND SAR DATA COLLECTION PROGRAM

1
INTRODUCTION

This report presents a summary of the multi-channel (i.e., multi-frequency and multipolarization) synthetic aperture radar (SAR) data set collected for the United States Geological Survey (USGS) during the Side-Looking Airborne Radar (SLAR) Data Acquisition Program. This report specifically discusses data collected over the North Carolina Digital Project Area (NCDPA). This SAR data collection was conducted between 8 and 10 April 1984 over four forested test sites in central North Carolina (see Figures 1 through 3).

The objective of this data collection program was to provide USGS scientists with a data set which could be used to determine whether or not geologically-stressed, vegetated areas could be discriminated using multi-channel SAR data. In order to achieve this goal, the SAR data must have a high degree of radiometric and geometric fidelity. To assist in obtaining this fidelity, a set of calibrated corner reflectors and a set of geometric reference reflectors were deployed near the four test sites.

During the data collection period, three SAR missions were flown, with 22 passes of imagery being collected. Two missions (16 passes) were flown with the SAR collecting X- and L-band data, and one mission (6 passes) was flown with the SAR collecting X- and C-band data.

There are five chapters in this report, including this introduction. Chapter 2 describes the ERIM/CCRS CV-580 SAR System used to collect the data for this project. Chapter 3 documents the data collection and processing performed, including: (1) coverage maps and SAR system parameters; (2) a discussion of the calibrated corner reflector array; (3) a discussion of the geometric reflectors; (4) a discussion of the digitally-recorded data; and (5) an engineering

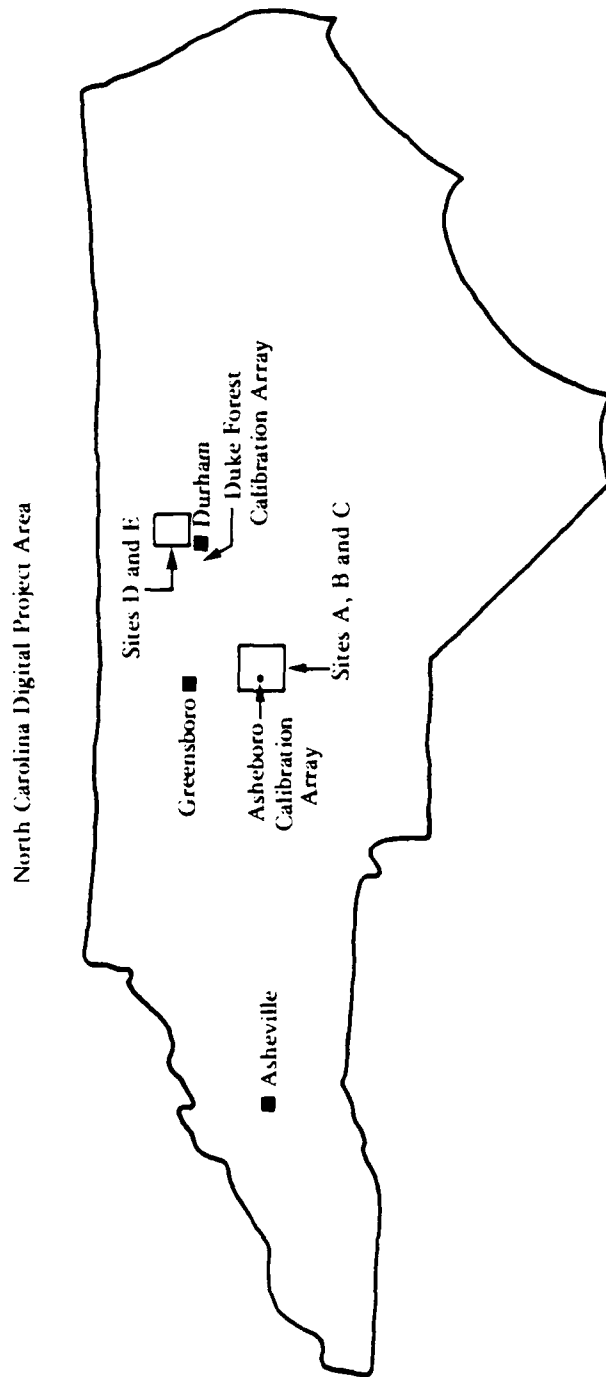


Figure 1. Location of North Carolina Digital Project Area (NCDPA) Test Sites

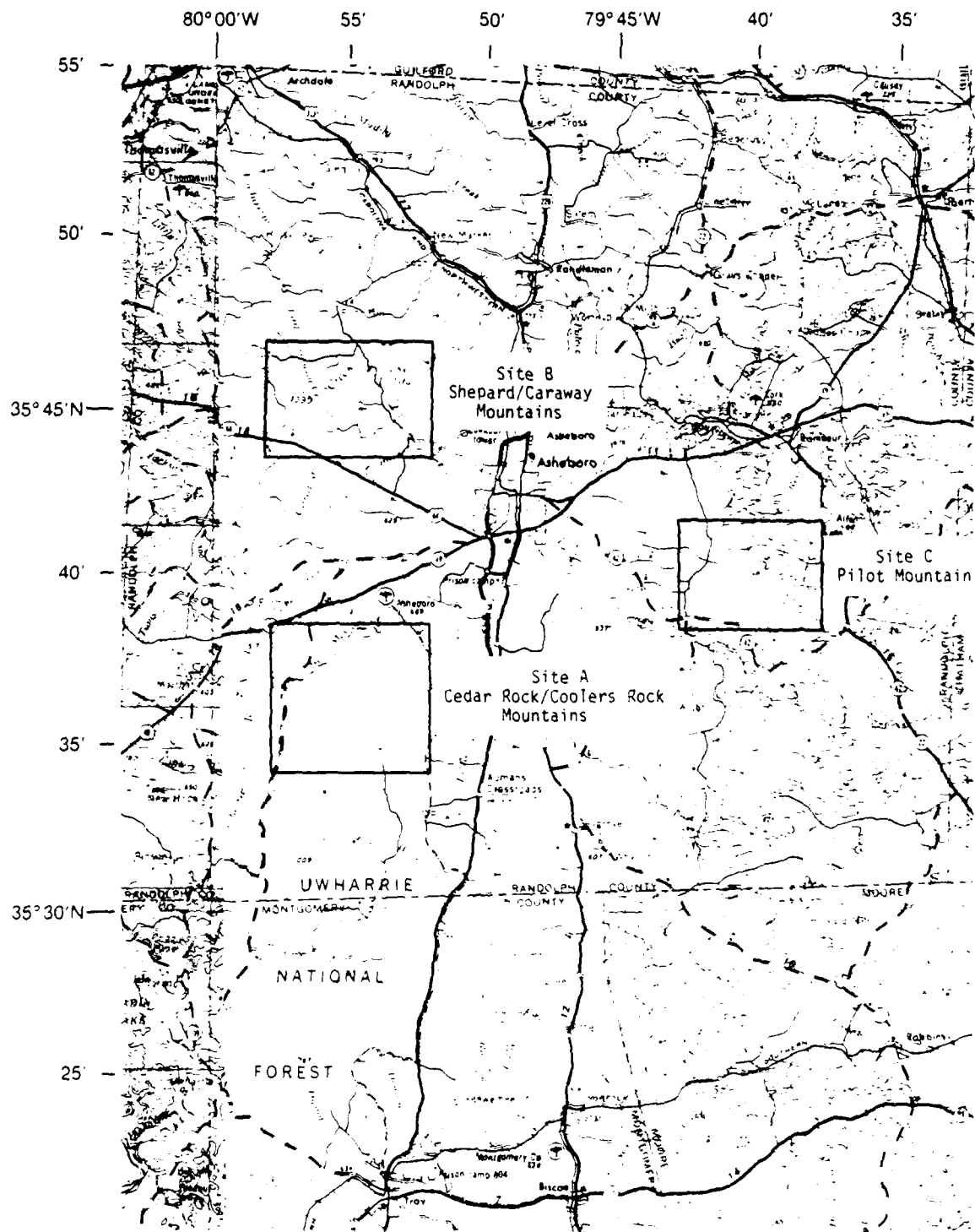


Figure 2. Locations of Test Sites A, B and C of the NCDPA (after USGS Raleigh 1:250000 Quad Sheet)

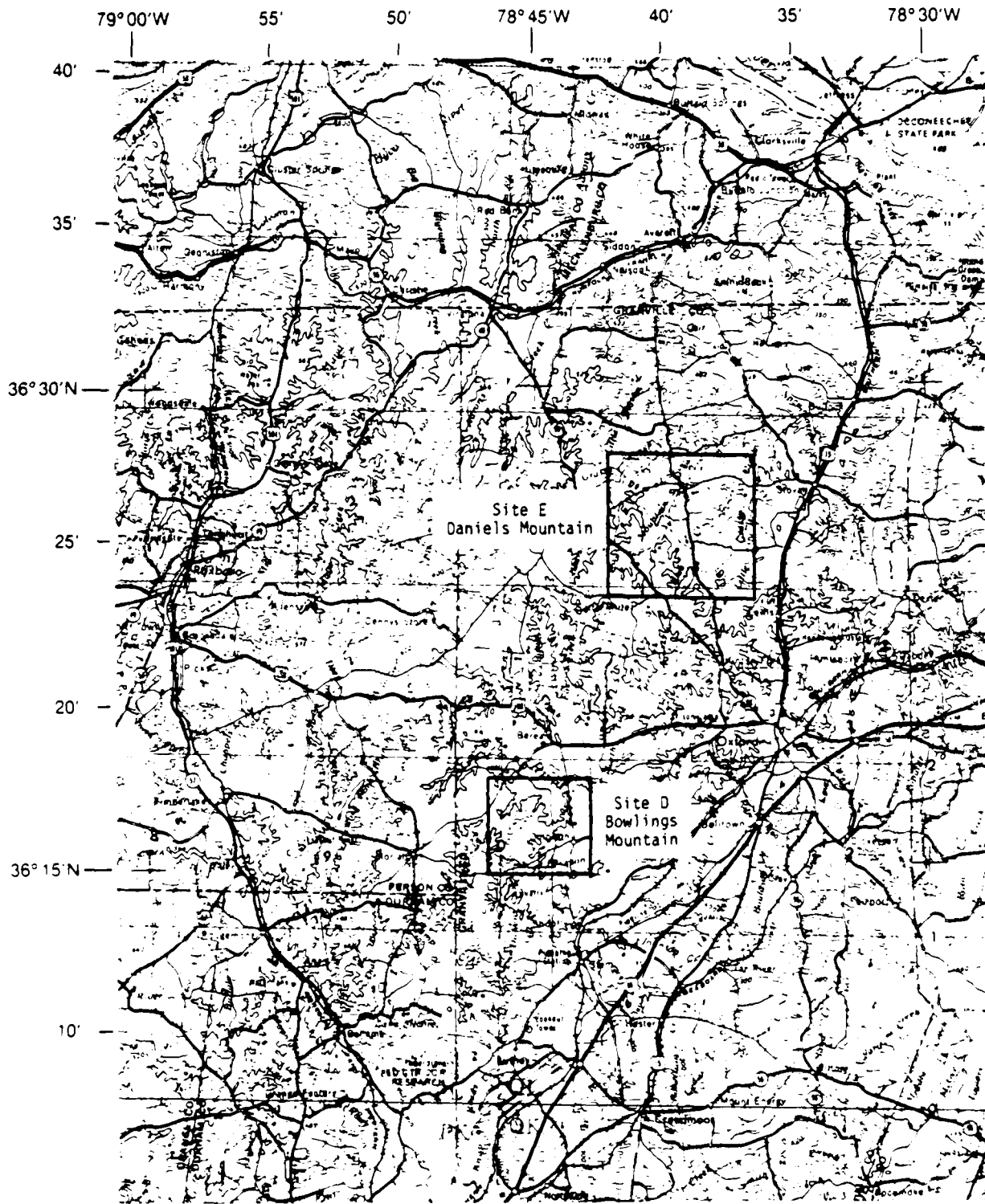


Figure 3. Locations of Test Sites D and E of the NCDPA (after USGS 1:250000 Greensboro Quad Sheet)

assessment of the SAR data. Finally, Chapter 4 summarizes the principal results of this program.

There are four appendices to this report. Appendix A discusses the basic manner in which the X- and L-band SAR imagery collected during this experiment may be calibrated. Appendix B describes the dihedral reflectors deployed during the SAR data collection. Appendix C describes the Hybrid Image Processing Facility used to digitize the SAR data for this program. Appendix D discusses the formats of the digitally-recorded SAR data set.

2
CV-580 SAR SYSTEM DESCRIPTION

From 1978 through 1984, ERIM operated a multifrequency and multi-polarization SAR in conjunction with the Canada Center for Remote Sensing (CCRS). This SAR was maintained through a leasing agreement between ERIM and CCRS and is called the CV-580 SAR System. This facility was used extensively over the past six years in a variety of oceanographic and terrestrial research programs. The leasing agreement between ERIM expired the end of CY84. At this time, the CV-580 SAR System is not available for U.S. Government sponsored research programs. Efforts are underway to transfer this system into a U.S.-owned aircraft (Shuchman, et al., 1984).

The CV-580 SAR System was essentially an X-band radar to which an L-band and a C-band capability was added. Because of this configuration, the X-band channels were always available, and, in addition, one could operate either the L-band or the C-band channels simultaneously with the X-band channel. For each frequency band, two orthogonal polarizations were available. The radar could transmit either horizontal or vertical polarization and receive both the parallel and perpendicular-polarized returns. The radar antenna could be pointed so as to image on either side of the aircraft. Table 1 summarizes the relevant radar parameters for this system.

Figure 4 presents a functional diagram of the CV-580 SAR System. The major components of the SAR are its antennas, the transmitters and receivers, the calibration signal generator, the optical film recorders, the digital tape recorder and the X-band real-time processor.

Figure 5 presents a more detailed diagram of the reference oscillators, transmitters and receivers of the SAR system. This diagram shows how the L-band and C-band wavelengths are returned to X-band.

TABLE 1
 CV-580 SAR SYSTEM PARAMETERS

<u>Parameter</u>	<u>X-Band</u>	<u>C-Band</u>	<u>L-Band</u>
Center Frequency	9.35 GHz	5.3 GHz	1.185 GHz
Wavelength	3.2 cm	5.7 cm	23.5 cm
Nominal Altitude	7 km	7 km	7 km
Nominal Platform Velocity	250 knots	250 knots	250 knots
Swath Width/Channel (slant range)	5.2 km	5.2 km	5.2 km
Incidence Angle	0° - 90°	0° - 90°	0° - 90°
FM Rate	33.3 MHz/μsec	33.3 MHz/μsec	33.3 MHz/μsec
Pulse Length	2.7 μsec	2.7 μsec	1.8 μsec
Bandwidth	89 MHz	89 MHz	60 MHz
Azimuth Beamwidth	1.15°	2.5°	8°
Nominal Slant Range Resolution	3 m	3 m	3 m
Nominal Azimuth Resolution	3 m	3 m	3 m
Azimuth Scale Factor (Approx.)	15,000	15,000	41,500
Range Scale Factor (Approx.)	196,000	196,000	196,000
Data Recording	Real Time Image	Real Time Image	
	Opt. Sig. Film	Opt. Sig. Film	Optical Signal Film
	Dig. Tape (HDDT)	Digital Tape	Digital Tape

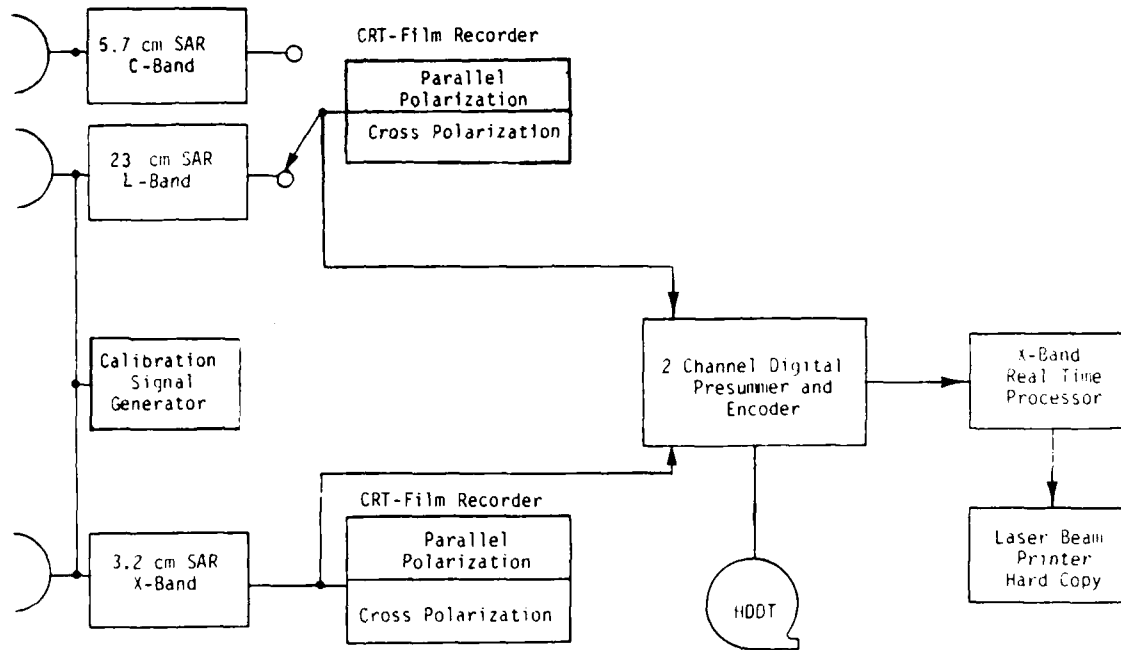


Figure 4. Schematic Diagram of CV-580 X/C/L SAR System

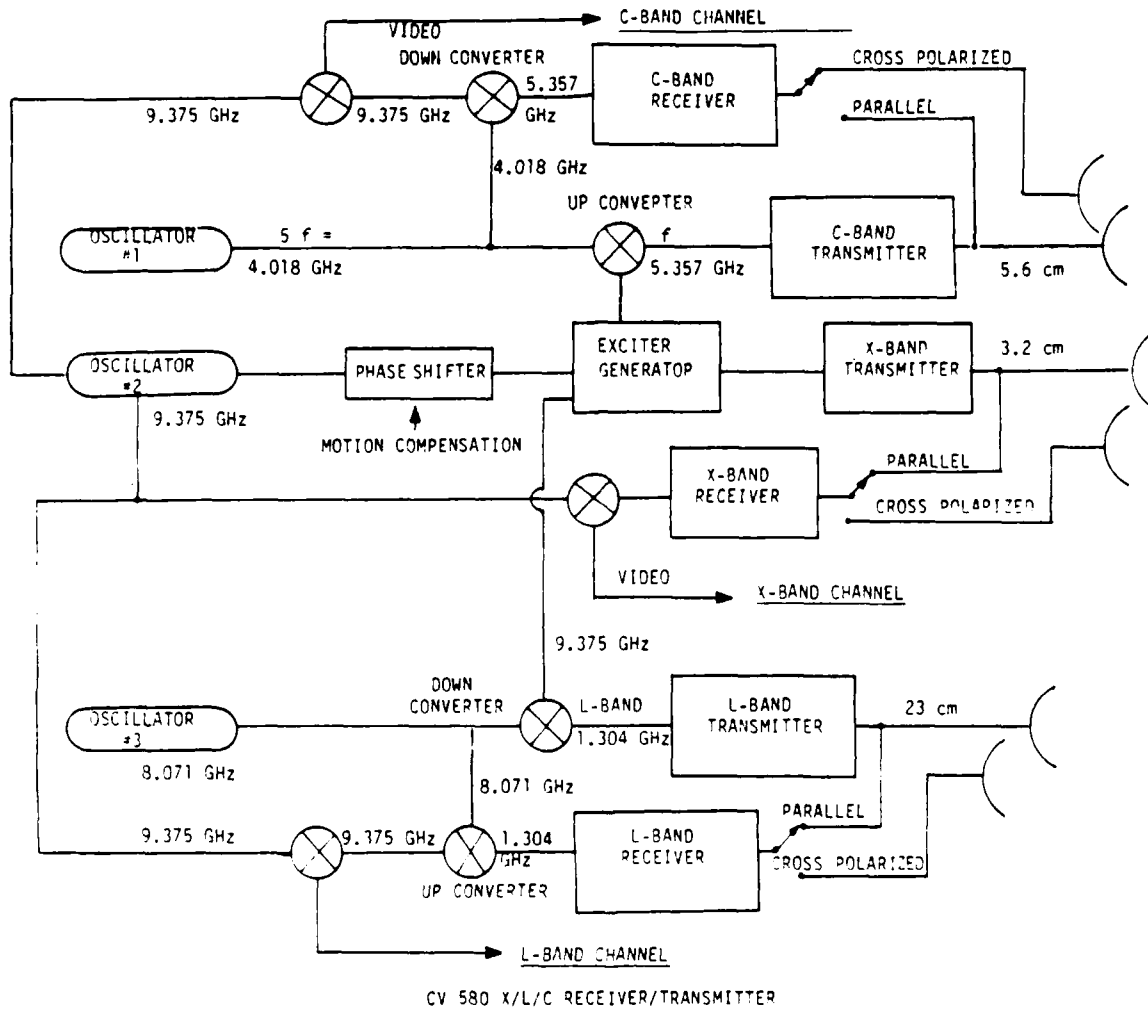


Figure 5. Schematic Diagram of CV-580 SAR System Transmitter/Receiver

Figure 6 presents a diagram of the calibration signal generator (CSG) system, which is used as a monitoring and reference source for the periodic verification of the SAR's system transfer function. The calibration signal generator produces synthetic target signals which are added into the radar receiver (Walker and Larson, 1981; Larson, et al., 1981; 1982; 1985). The form of the synthetic target corresponds to a given range, and the intensity is controlled by an accurate calibrated R.F. attenuator. At specific times during the imaging flight, the calibration signals are inserted into the receiver at the antenna terminals, so that the radar receiver detects them as a radar return. Using a sequence of such signals with different intensities, along with the processed signals from the corner reflectors, a calibration curve can be produced of output signal power versus radar cross section (σ_0). When combined with measurements of precision corner reflectors, CSG measurements can be used to achieve absolute calibration of the SAR (see Walker and Larson, 1981; or Larson, et al., 1985). The synthetic targets from the CSG can be recorded both optically and digitally, but only at X- and L-band.

The three SARs which comprised the CV-580 SAR System are similar in that they all use the synthetic aperture technique to produce imagery with fine cross-range resolution. These SARs used pulse compression to achieve fine resolution in the range dimension. Each recording channel was adjusted to produce imagery of a selected swath parallel to the flight direction. The width of the imaged swath was determined by the range increment of signals displayed on the recording system. The displacement of the recorded swath from the flight line was adjustable by the radar operator. The CV-580 SAR System is extensively described by Rawson, et al. (1975).

The SAR phase histories were recorded onboard the aircraft both optically on 70 mm film and digitally on high density digital tape (HDDT). The optical recording system recorded four data channels,

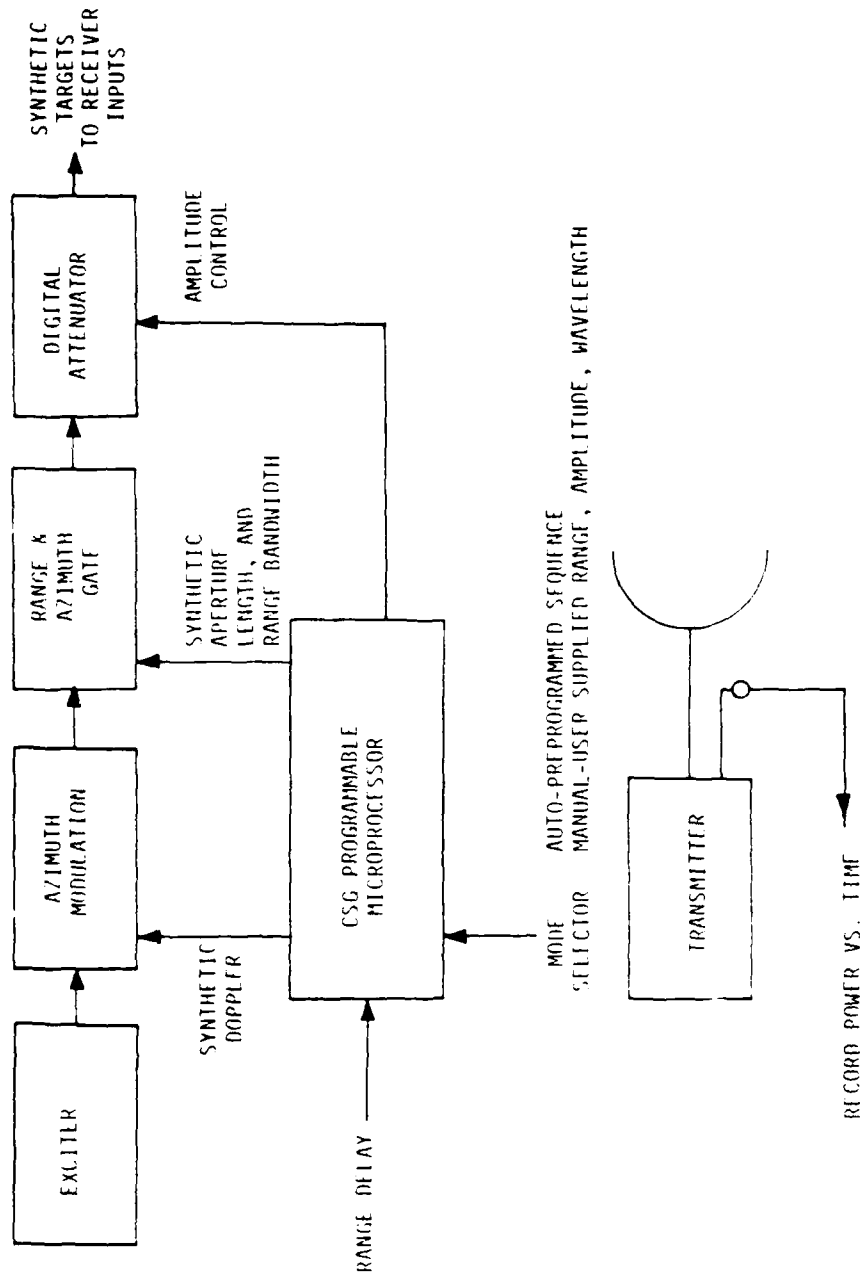


Figure 6. Schematic Diagram of CV-580 SAR System X/L Calibration Signal Generator

while the digital system was restricted to recording only two of the four data channels during data collection. In addition to the optical and digital recorders, a real-time digital SAR processor onboard the CV-580 generated X-band imagery. The real-time imagery was not intended to be of high quality, but provided "quick-look" data necessary for system performance evaluation and planning purposes during data collection missions. It was also used to select digital data of interest for subsequent processing and analysis. Table 2 presents the various data recording options available on the system. Figure 7 schematically illustrates the various SAR data recording and processing options.

TABLE 2
 CV 580 SAR SYSTEM X-, C- AND L-BAND SAR DATA RECORDING CAPABILITY

SAR Mode	Optical Recording (C Recorders)		Digital Recording (A+B)		Real-Time Processor (Channels)		Comments
	Channels	Swath	Channels	Swath	Resolution	Swath	
X band wide swath	1 (2 films)	20 km	A and B	12 km 20 km	3 m 6 m	Near range 12 km	Data buffer required
4 channel X, C or X, L	4	5.2 km	A any channel B X, C, L, like, cross	6 km	3 m	X- or C-band Channel A only	Scene illumination depends on altitude and incidence angle range
3 channel X, C or X, L	3	10 km 5.2 km	A and B, wide swath channel or A, B independent assignment	12 km 6 km	3 m 6 m	X- or C-band Channel A only	Wide swath channel illumination strongly affected by antenna pattern and imaging geometry
2 channel X, C or X, L	2	10 km	A and B (either channel)	12 km	3 m	Channel A if not L-band	As above

Note: 1. The extended swath recording modes enhance the system signal to noise for weak returns on the optical recordings only.

2. An X band signal film will contain approximately 215 nautical miles of data, a high density digital tape will contain approximately 130 nautical miles of data.

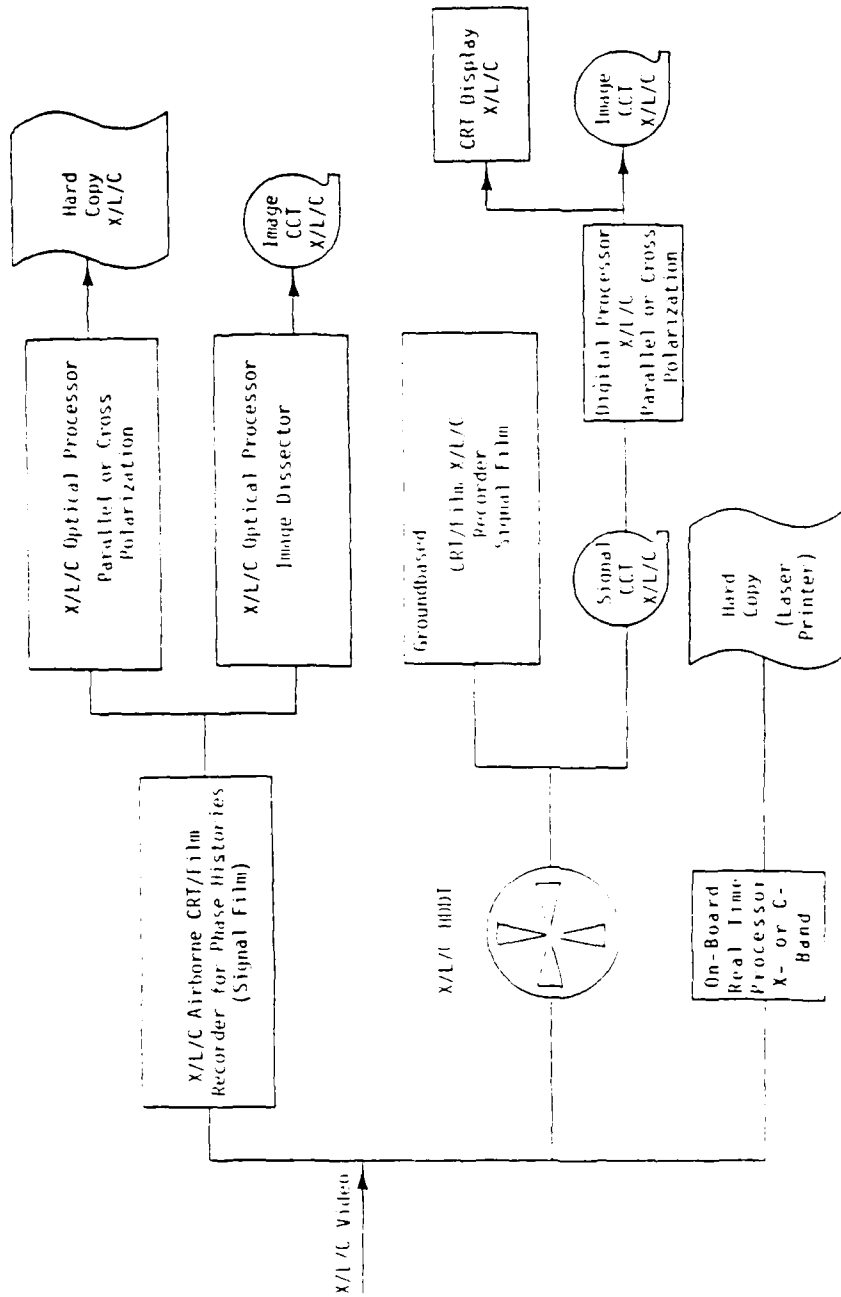


Figure 7. CV-580 SAR System Signal Recording and Processing Options

3
DATA DESCRIPTION

This chapter contains a summary of all multi-channel SAR data collection missions conducted during the USGS North Carolina program, as well as a description of all SAR data processing performed at ERIM. This chapter also contains a description of the calibration and geometric reflector arrays which were deployed, as well as a description of the digital SAR image products which were generated.

3.1 SAR DATA

There were five test sites within the North Carolina Digital Project Area (NCDPA). These sites are:

- A. Cedar Rock/Coolers Rock Mountains
- B. Shepard/Caraway Mountains
- C. Pilot Mountains
- D. Bowlings Mountain
- E. Daniels Mountain

The locations of these sites are presented in Figures 1 through 3. Three SAR data collection missions were flown over these sites on 8 through 10 April 1984 with the CV-580 SAR System. A total of 22 passes of SAR imagery were collected. These missions are summarized in Table 3.

During the NCPDA data collection, the CV-580 SAR System was configured in its two-frequency, narrow swath mode. In this mode, four channels of SAR data were recorded optically on SAR signal film and two channels recorded digitally on high density digital tape. Each optically-recorded channel has a slant-range swath width of 5.4 km and each digital channel has a slant-range swath width of 6.1 km.

In the two frequency, narrow swath mode, either horizontally (H) or vertically (V) polarized microwave energy is transmitted in two

TABLE 3
SUMMARY OF USGS NCDPA MULTICHANNEL SAR FLIGHTS

Date	Mission	Pass	Area*	Time (EST)	Frequency and Polarization**																	
					X-VV	X-HH	X-VH	X-HV	L-VV	L-HH	L-VH	L-HV	C-VV	C-VH								
8 April 1984	USGS-1	1	T	13:06-13:10	±		±															
		2	T	13:34-13:40	±		±															
		3	C	13:56-13:59	±		±															
		4	C	14:20-14:25	±		±															
		5	A	14:41-14:46	±		±															
		6	A	15:05-15:09	±		±															
		7	A/C	15:27-15:31	±		±															
		8	T	15:50-15:56	±		±															
		9	A	16:21-16:24	±		±															
9 April 1984	USGS-2	1	T	11:27-11:31	±		±															
		2	T	11:51-11:56	±		±															
		3	C	12:13-12:18	±		±															
		4	A	12:33-12:40	±		±															
		5	C	12:59-13:04	±		±															
		6	E	13:28-13:32	±		±															
		7	D	13:43-13:45	±		±															
10 April 1984	USGS-3	1	T	15:59-16:04	±		±															
		2	B	16:16-16:21	±		±															
		3	A	16:33-16:40	±		±															
		4	A/C	16:58-17:02	±		±															
		5	E	17:34-17:38	±		±															
		6	D	17:56-17:58	±		±															

*Areas

- A - Cedar Rock/Coolers Rock Mountains
- B - Shepard/Caraway Mountains
- C - Pilot Mountains
- A/C - Cedar Rock/Coolers Rock/Pilot Mountains
- D - Bowlings Mountain
- E - Daniels Mountain
- T - Test Flight

**

± - Data Recorded Optically
± - Data Recorded Optically and Digitally

frequencies (X- and L-band or X- and C-band). Both like (HH or VV) and cross (HV or VH) backscattered energy from each frequency is recorded optically, resulting in four channels of data. Two of the four channels are recorded digitally.

X- and L-band SAR data were collected on 8 and 9 April 1984 and X- and C-band data were collected on 10 April 1984. The frequency and polarization combinations which were optically- and digitally-recorded are also summarized in Table 3.

In the remainder of this section, we will discuss the SAR data collected during each of the three missions. For each SAR mission, a table summarizing the aircraft ground tracks and SAR parameters are presented. Diagrams which present the ground location of each pass are also included, as are representative examples of SAR imagery.

3.1.1 USGS-1 (8 April 1984 - 13:06 to 16:24 EST)

The purpose of this mission was to collect multipolarization X- and L-band SAR data over the NCDPA. Three passes of SAR imagery were collected over a test area to verify the operational status of the CV-580 SAR System. Six passes of SAR imagery were collected over Test Sites A, and B and C, including one pass over the calibrated corner reflector array.

The aircraft and SAR system parameters for the USGS-1 mission are summarized in Table 4. In Table 4, all latitudes and longitudes represent the positions to the near edge of the swath. The locations of the ground coverage during each SAR pass of the USGS-1 mission are presented in Figures 8 through 15. Figure 16 presents optically-processed X- and L-band SAR imagery of Pilot Mountain collected during Pass 7. The SAR data collected during this mission was all of excellent quality.

TABLE 4. SUMMARY OF SAR AND AIRCRAFT PARAMETERS DURING USGS-1 (8 APRIL 1984)

CV-580 AIRCRAFT PARAMETERS

PASS	HEADING (TRUE)	VELOCITY (KNOTS)	ALTITUDE (FEET)	START TIME (EDT)	STOP TIME (EDT)	START LATITUDE	START LONGITUDE	STOP LATITUDE	STOP LONGITUDE
1	78	301	20000	18:06:25	18:10:26	35:58.4	79:14.9	36:03.7	78:47.6
2	258	218	20000	18:34:21	18:39:53	36:04.5	78:47.9	35:59.6	79:14.2
3	180	262	20000	18:55:51	18:59:21	35:48.9	79:48.9	35:27.1	79:49.6
4	0	252	20000	19:19:57	19:24:44	35:26.9	79:53.6	35:48.7	79:52.7
5	203	253	20000	19:41:20	19:46:04	35:47.5	79:41.6	35:28.0	79:51.7
6	23	279	20000	20:05:00	20:09:16	35:26.3	79:47.9	35:46.5	79:37.6
7	75	318	20000	20:27:02	20:30:38	35:36.5	80:01.8	35:43.9	79:35.6
8	258	223	20000	20:50:08	20:55:30	36:04.5	78:48.5	35:59.6	79:14.2
9	203	252	20000	21:21:38	21:24:02	35:46.4	79:38.2	35:35.4	79:43.8

SAR PARAMETERS

PASS	WAVELENGTHS	LOOK	ANTENNA DEPRESSION ANGLE	POLARIZATION		DIGITAL CHANNEL	RANGE DELAY (USEC)	GAIN SETTINGS (dB ATTENUATION)				TRANS POWER (WATTS)	
				TRANS	REC			X-B OPT.	L-B OPT.	X-B DIG.	L-B DIG.	X-B	L-B
1	X,L	R	28	V	VH	XV, XVH	50	30	33	14	42	1744	4608
2	X,L	L	28	V	VH	XV, LVV	55	30	33	14	42	1743	5193
3	X,L	R	28	V	VH	XV, LVV	55	30	33	16	44	1719	5290
4	X,L	L	28	V	VH	XV, LVV	55	30	33	16	44	1762	4457
5	X,L	L	28	V	VH	XV, LVV	55	30	33	16	44	1755	5121
6	X,L	R	28	V	VH	XV, LVV	55	30	33	16	44	1758	4957
7	X,L	R	27	V	VH	XV, LVV	55	30	33	16	44	1690	4820
8	X,L	L	27	H	HV	XHH, LHH	55	30	33	16	44	1732	4589
9	X,L	L	30	V	VH	X'V, LVV	55	30	33	16	44	1724	4662

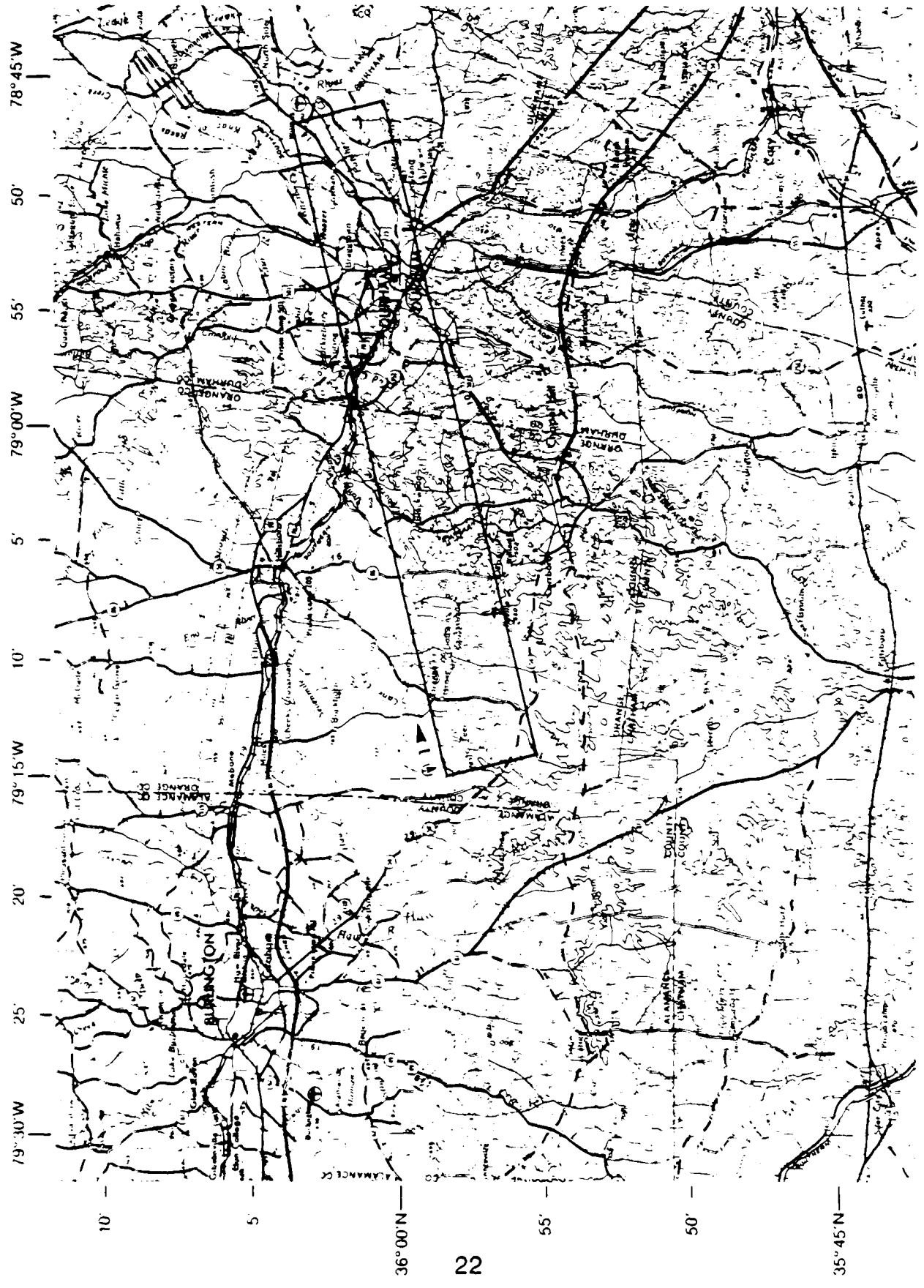


Figure 8. CV-580 SAR Ground Coverage During USGS-1, Pass 1
 (after USGS Greensboro and Raleigh 1:250000 Quad Sheet)

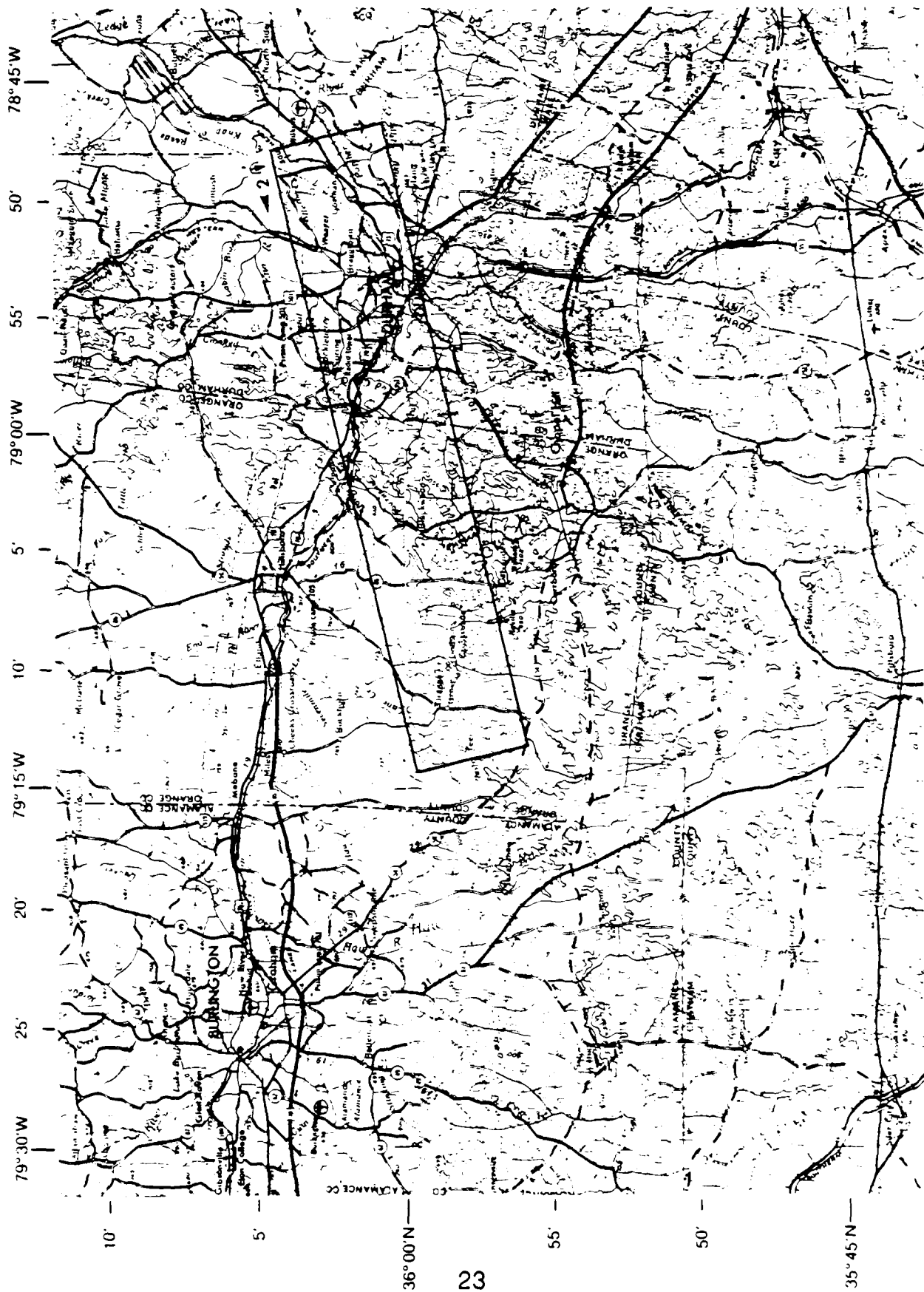


Figure 9. CV-580 SAR Ground Coverage During USGS-1, Pass 2
 (after USGS Greensboro and Raleigh 1:250000 Quad Sheet)

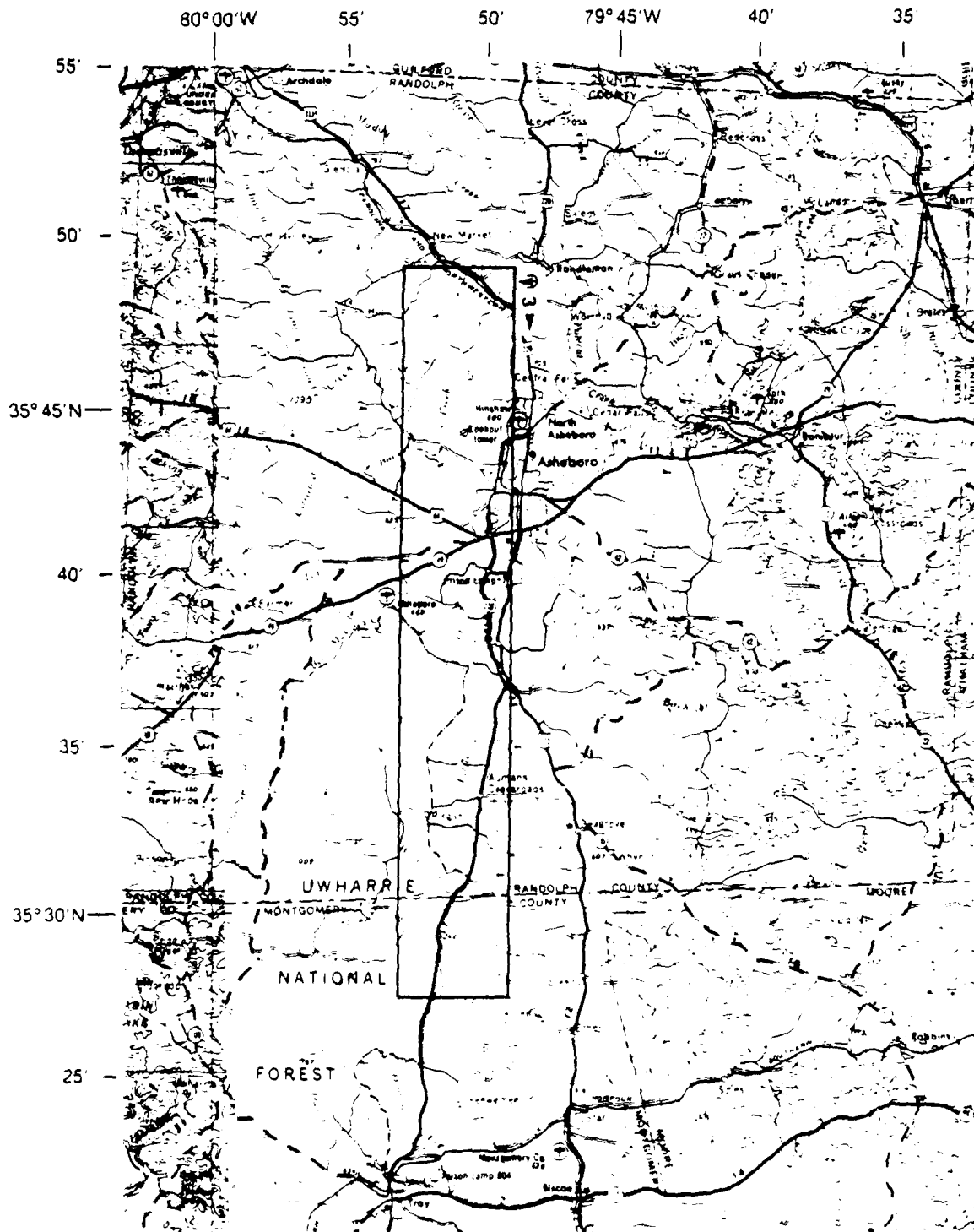


Figure 10. CV-580 SAR Ground Coverage During USGS-1, Pass 3
(after USGS Raleigh 1:250000 Quad Sheet)

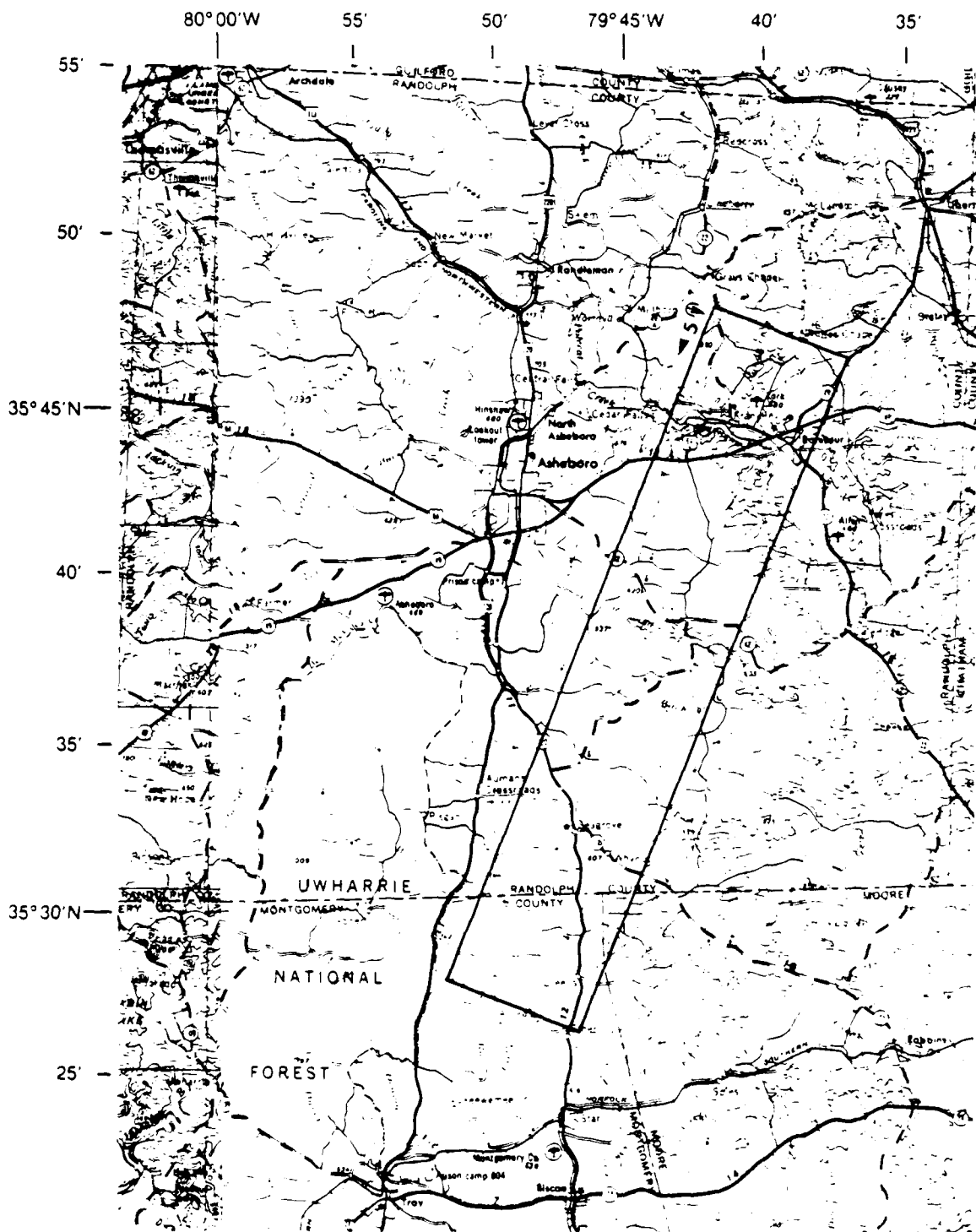


Figure 12. CV-580 SAR Ground Coverage During USGS-1, Pass 5
(after USGS Raleigh 1:250000 Quad Sheet)

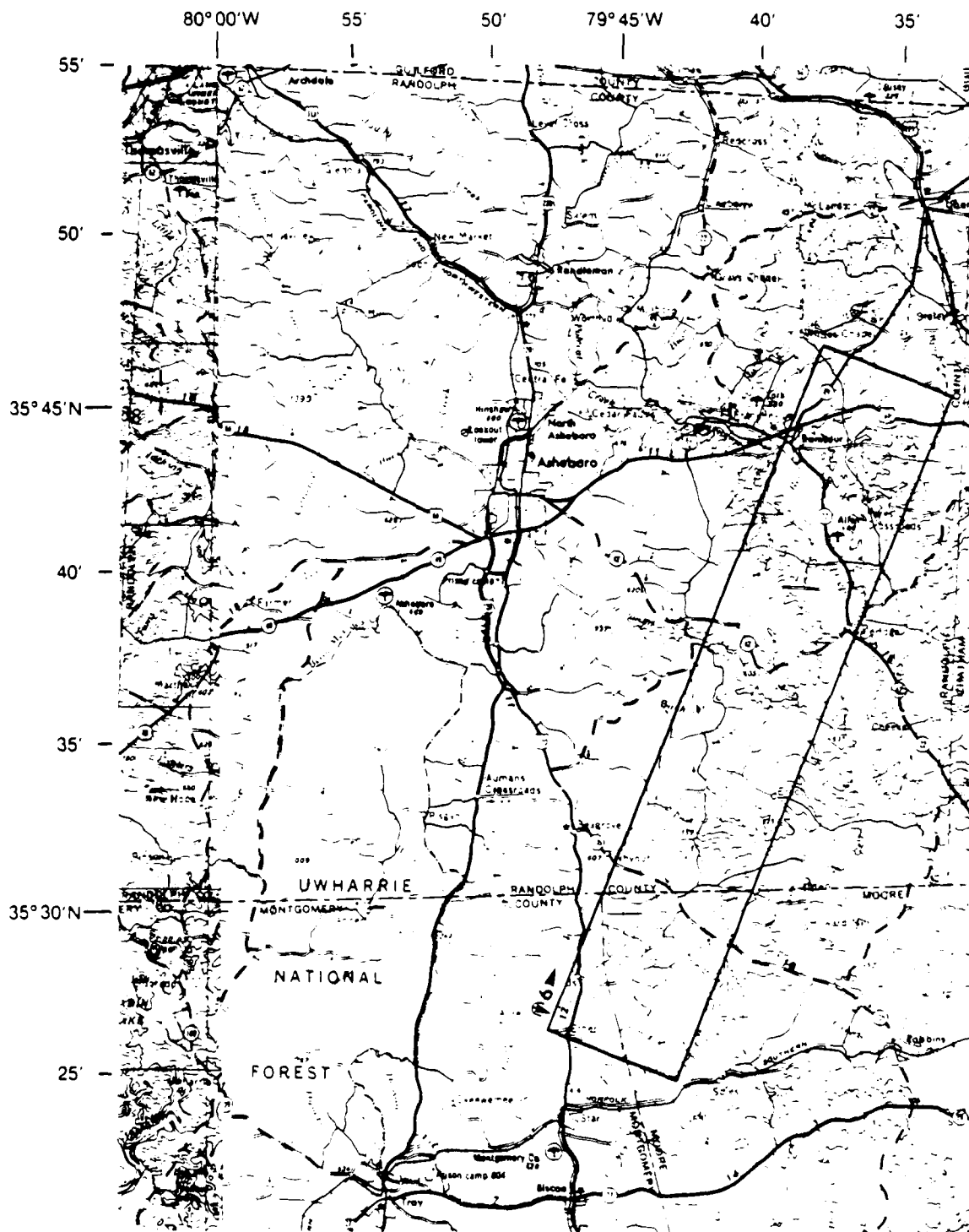


Figure 13. CV-580 SAR Ground Coverage During USGS-1, Pass 6
(after USGS Raleigh 1:250000 Quad Sheet)

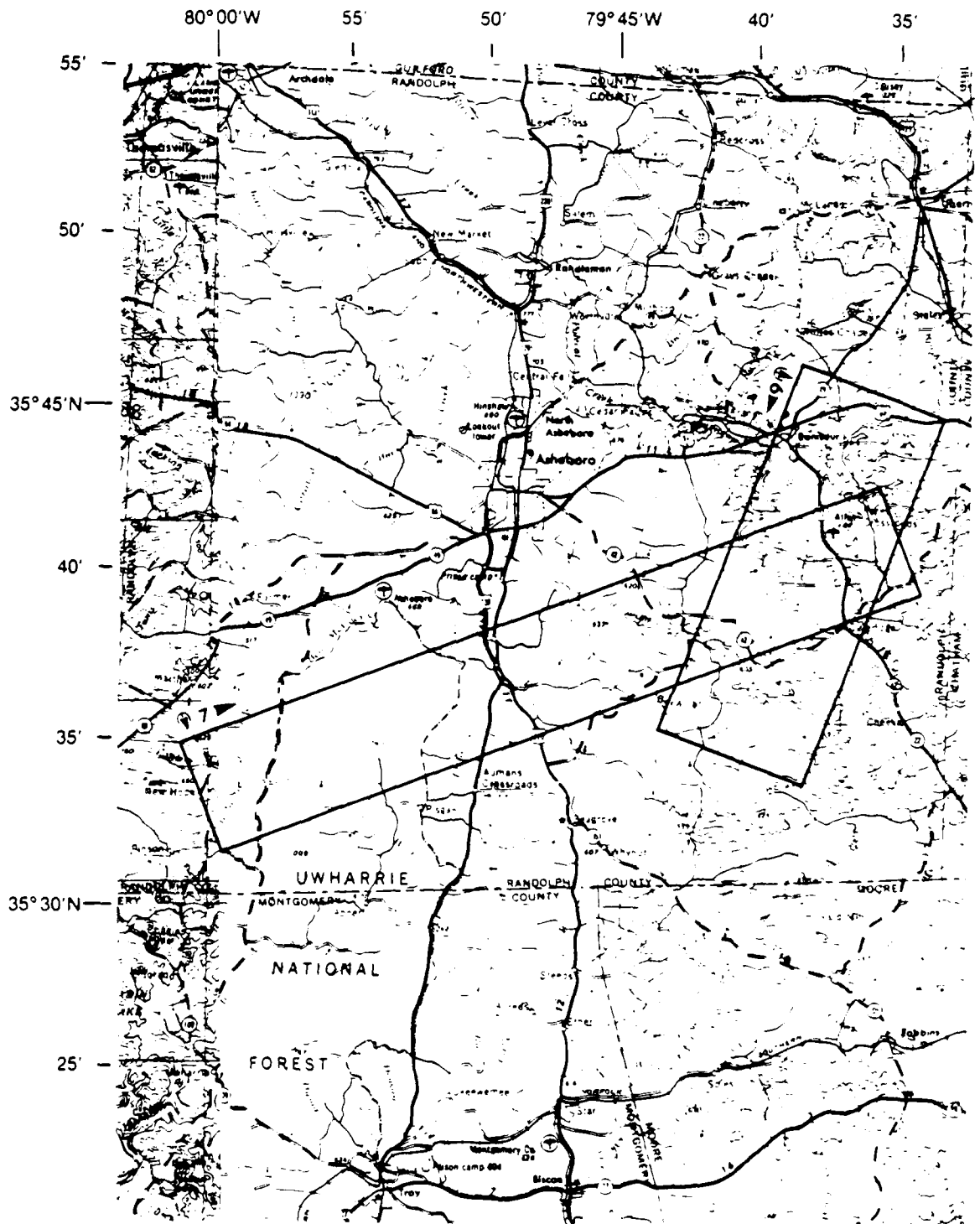


Figure 14. CV-580 SAR Ground Coverage During USGS-1, Passes 7 and 9 (after USGS Raleigh 1:250000 Quad Sheet)

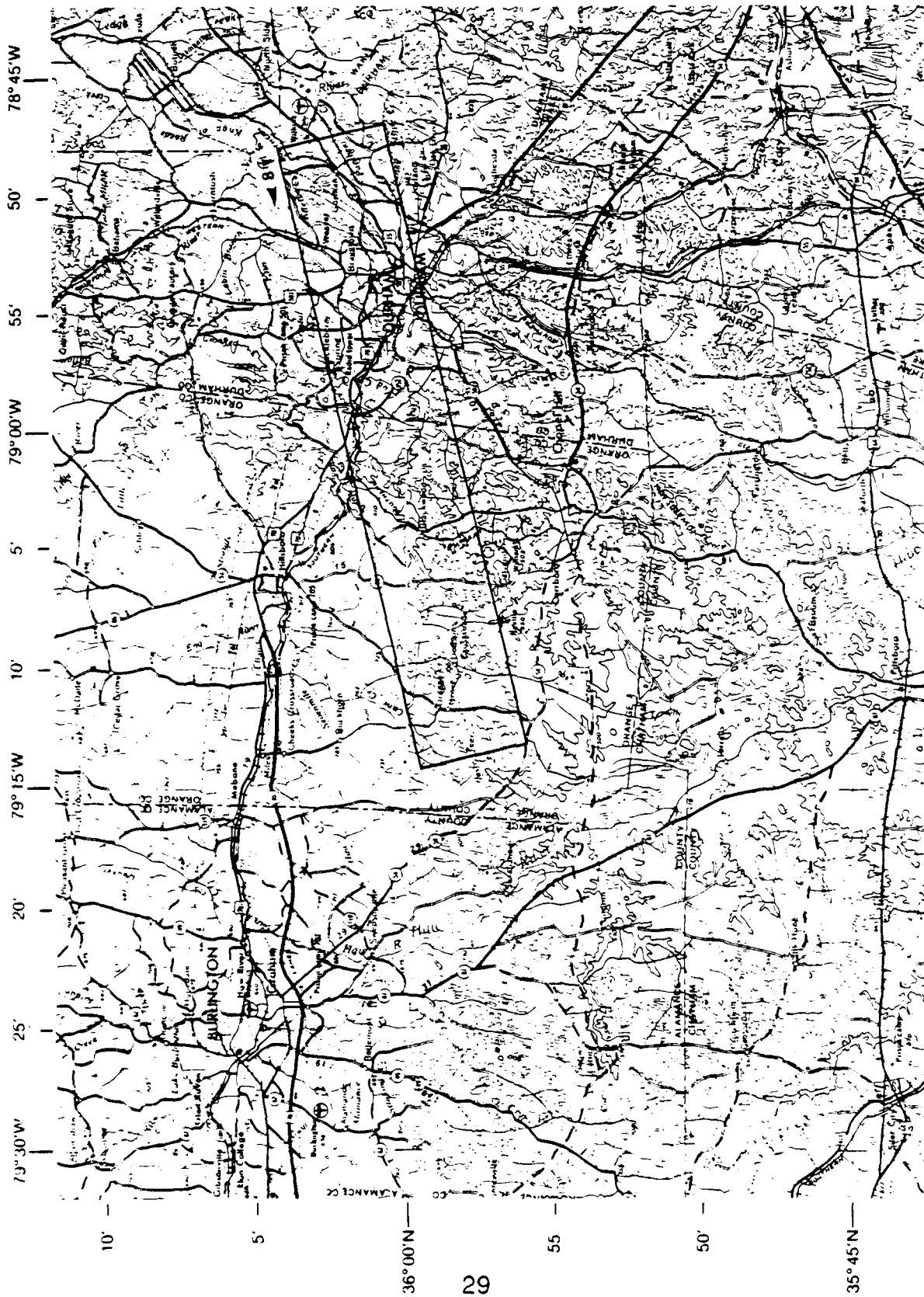
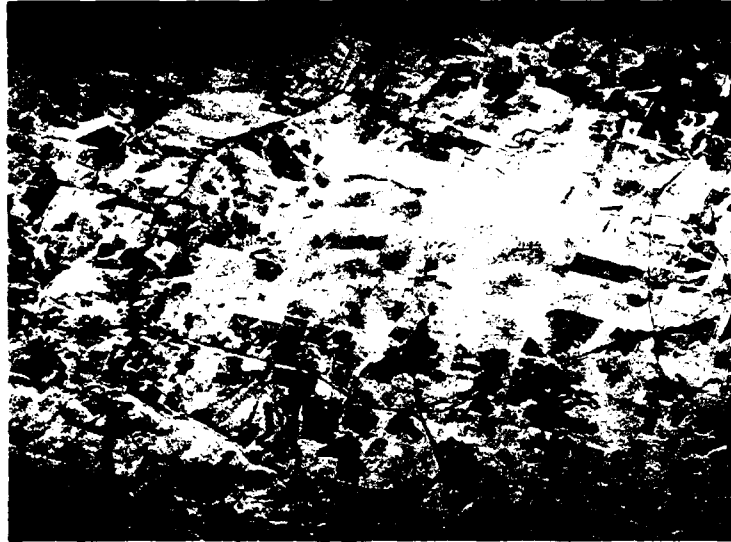
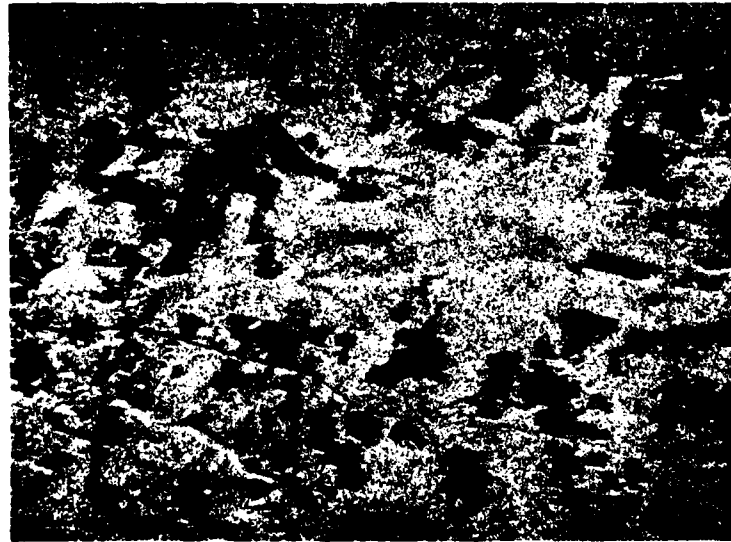


Figure 15. CV-580 SAR Ground Coverage During USGS-1, Pass 8
 (after USGS Greensboro and Raleigh 1:250000 Quad Sheet)



X-Band



L-Band

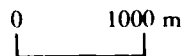


Figure 16. Optically-Processed X- and L-Band SAR Imagery of Pilot Mountain (USGS-1, Pass 7, 8 April 1984)

3.1.2 USGS-2 (9 April 1984 - 11:27 to 13:45 EST)

The purpose of this mission was to collect multipolarization X- and L-band SAR data over the NCDPA. Two passes of SAR imagery were collected over a test area to verify the operational status of the CV-580 SAR system. Five passes of SAR imagery were collected over Test Sites A, B, C, D, and E including one pass over the calibrated corner reflector array.

The aircraft and SAR system parameters for the USGS-2 mission are summarized in Table 5. The locations of the ground coverage during each SAR pass of the USGS-2 mission are presented in Figures 17 through 21. The SAR data collected during this mission was all of high quality.

TABLE 5. SUMMARY OF SAR AND AIRCRAFT PARAMETERS DURING USGS-2 (9 APRIL 1984)

CV-580 AIRCRAFT PARAMETERS

PASS	HEADING (TRUE)	VELOCITY (KNOTS)	ALTITUDE (FEET)	START TIME (EDT)	STOP TIME (EDT)	START LATITUDE	START LONGITUDE	STOP LATITUDE	STOP LONGITUDE
1	78	283	20000	16:26:34	16:30:52	35:59.6	79:14.3	36:04.6	78:48.3
2	258	270	20000	16:50:37	16:56:07	36:04.2	78:47.6	35:59.5	79:13.3
3	180	264	20000	17:13:12	17:17:48	35:47.8	79:49.0	35:26.4	79:49.3
4	22	265	20000	17:33:02	17:39:52	35:24.2	79:49.4	35:54.1	79:33.7
5	180	268	20000	17:59:14	18:03:45	35:48.3	79:51.0	35:27.0	79:50.7
6	5	273	20000	18:27:59	18:32:24	36:15.7	78:43.1	36:36.9	78:42.2
7	180	263	20000	18:43:11	18:45:29	36:20.1	78:42.7	36:08.6	78:42.9

SAR PARAMETERS

PASS	WAVELENGTHS	LOOK	ANTENNA DEPRESSION ANGLE	POLARIZATION		DIGITAL CHANNEL	RANGE DELAY (USEC)	GAIN SETTINGS (dB ATTENUATION)				TRANS POWER (WATTS)	
				TRANS	REC			X-B OPT.	L-B OPT.	X-B DIG.	L-B DIG.	X-B	L-B
1	X.L	R	28	H	HV	XHH, XHV	55	27	36	17	45	1726	4810
2	X.L	L	28	H	HV	LHH, LHV	55	27	36	17	45	---	---
3	X.L	R	28	V	VH	XVV, LVV	55	27	36	17	45	1729	5984
4	X.L	R	28	V	VH	XVV, LVV	55	27	36	17	45	1741	5982
5	X.L	R	28	V	VH	XVV, LVV	55	27	36	17	45	1633	5704
6	X.L	R	28	V	VH	XVV, LVV	55	27	36	17	45	1703	6017
7	X.L	R	28	V	VH	XVV, LVV	55	27	36	17	45	1747	5990

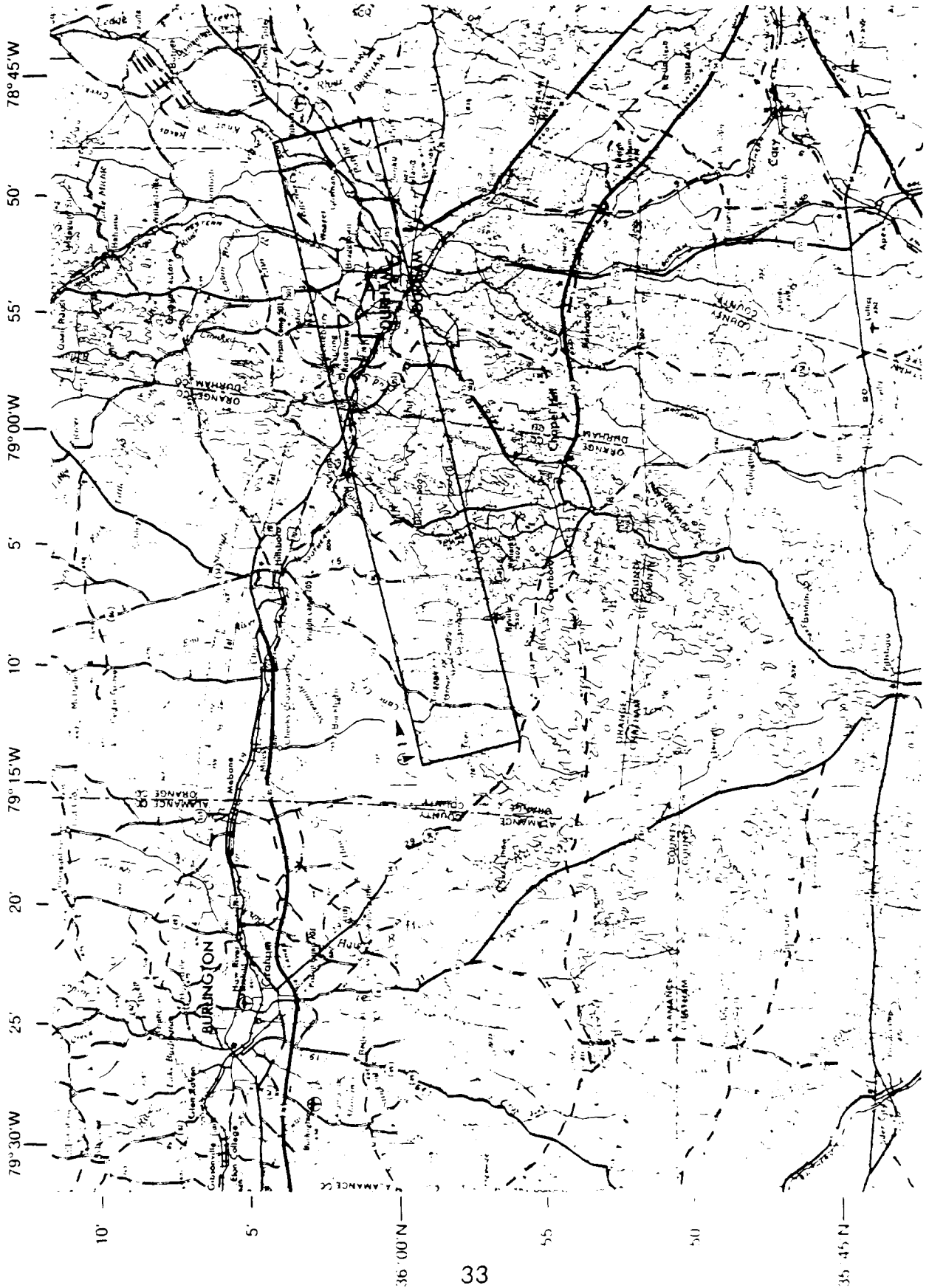


Figure 17. CV-580 SAR Ground Coverage During USGS-2, Pass 1
 (after USGS Greensboro and Raleigh 1:250000 Quad Sheet)

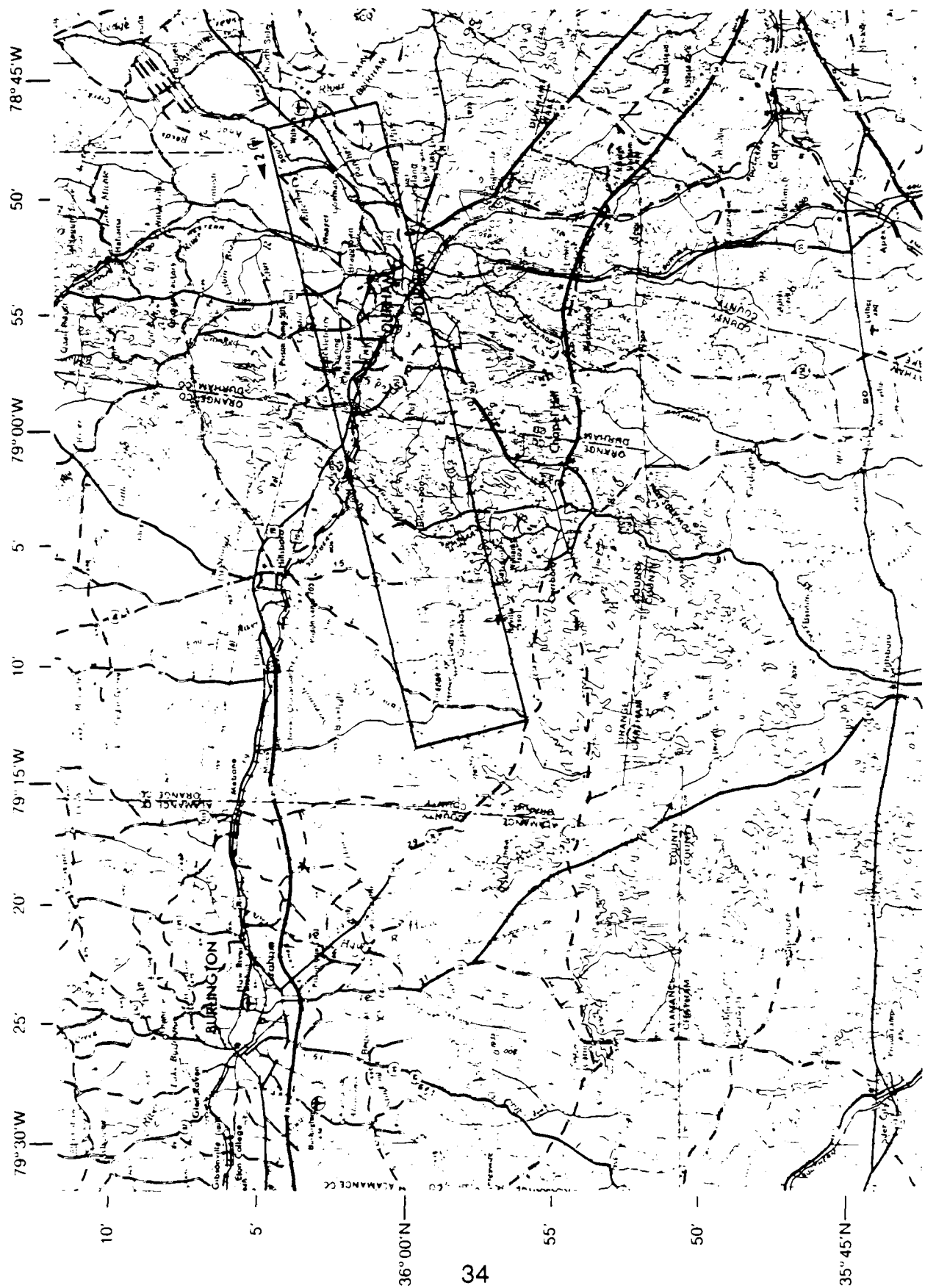


Figure 18. CV-580 SAR Ground Coverage During USGS-2, Pass 2
(after USGS Greensboro and Raleigh 1:250000 Quad Sheet)

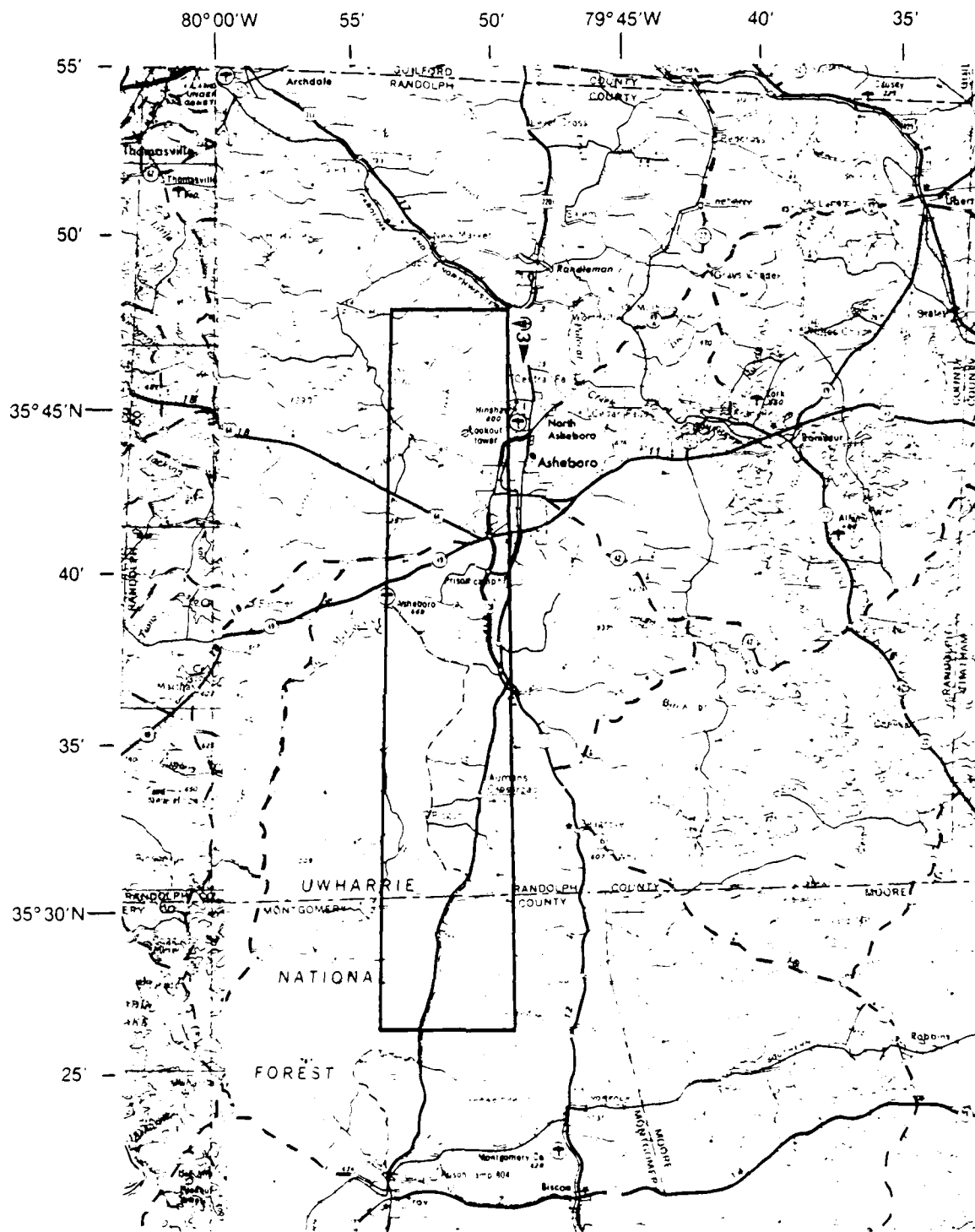


Figure 19. CV-580 SAR Ground Coverage During USGS-2, Pass 3
(after USGS Raleigh 1:250000 Quad Sheet)

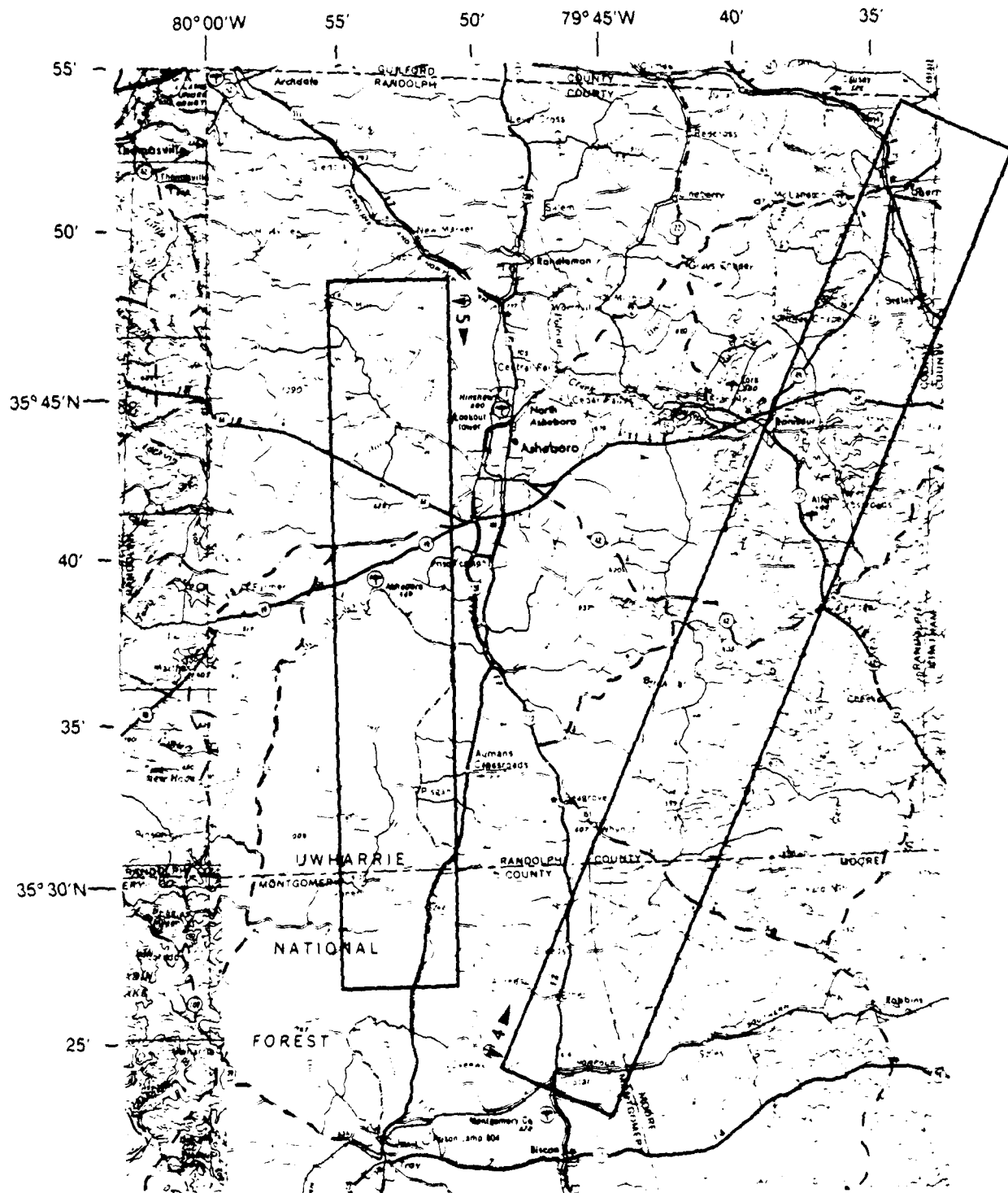


Figure 20. CV-580 SAR Ground Coverage During USGS-2, Passes 4 and 5
(after USGS Raleigh 1:250000 Quad Sheet)

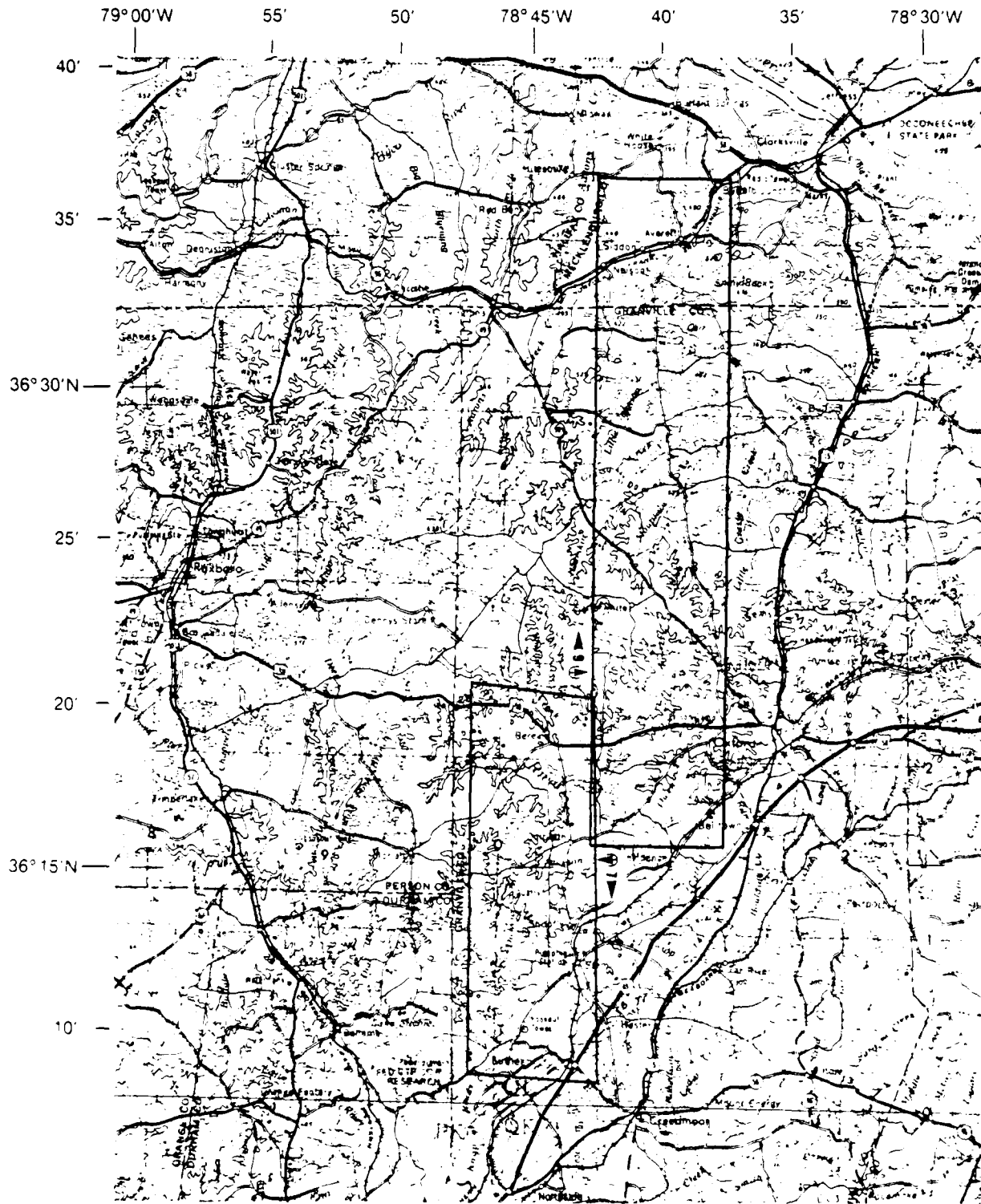


Figure 21. CV-580 SAR Ground Coverage During USGS-2, Passes 6 and 7 (after USGS Greensboro 1:250000 Quad Sheet)

3.1.3 USGS-3 (10 April 1984 - 15:59 to 17:58 EST)

The purpose of this mission was to collect multipolarization X- and C-band SAR imagery over the NCDPA. One pass of SAR imagery was collected over a test area to verify the operational status of the CV-580 SAR System. Five passes of SAR imagery were collected over Test Sites A, B, C, D, and E including one pass over the calibrated corner reflector array.

The aircraft and SAR system parameters for the USGS-3 mission are summarized in Table 6. The locations of the ground coverage of each pass of the USGS-3 mission are presented in Figures 22 through 25. Figure 26 presents optically-processed SAR imagery of Pilot Mountain collected during Pass 4. The SAR data collected during this mission was all of excellent quality.

TABLE 6. SUMMARY OF SAR AND AIRCRAFT PARAMETERS DURING USGS-3 (10 APRIL 1984)

CV-580 AIRCRAFT PARAMETERS

PASS	HEADING VELOCITY (TRUE)	(KNOTS)	ALTITUDE (FEET)	START TIME (EDT)	STOP TIME (EDT)	START LATITUDE	START LONGITUDE	STOP LATITUDE	STOP LONGITUDE
1	258	251	20000	20:59:28	21:04:16	36:03.6	78:49.1	35:58.9	79:15.0
2	180	275	20000	21:16:14	21:20:37	35:47.1	79:51.0	35:26.1	79:51.5
3	22	288	20000	21:33:24	21:39:38	35:23.1	79:48.3	35:51.8	79:34.0
4	75	275	20000	21:57:46	22:02:06	35:37.7	80:03.1	35:43.1	79:38.2
5	5	275	20000	22:34:06	22:38:24	36:14.4	78:43.3	36:34.7	78:42.9
6	180	274	20000	22:56:03	22:58:15	36:19.2	78:42.9	36:08.2	78:42.9

SAR PARAMETERS

PASS	WAVELENGTHS	LOOK	ANTENNA DEPRESSION ANGLE	POLARIZATION		DIGITAL CHANNEL	RANGE DELAY (USEC)		GAIN SETTINGS (dB ATTENUATION)				TRANS POWER (WATTS)	
				TRANS	REC		X-B	L-B	OPT.	DIG.	X-B	L-B	X-B	L-B
1	X,C	L	31	V	VH	XVV,CVV	55	18	20	14	32	1718	3467	
2	X,C	R	29	V	VH	XVV,CVV	55	18	21	14	32	1718	2857	
3	X,C	R	31	V	VH	XVV,CVV	55	22	21	14	31	1701	2599	
4	X,C	R	31	V	VH	XVV,CVV	55	25	21	14	31	1742	2818	
5	X,C	R	31	V	VH	XVV,CVV	55	25	21	14	31	1733	2760	
6	X,C	R	31	V	VH	XVV,CVV	55	25	21	14	31	1733	2747	

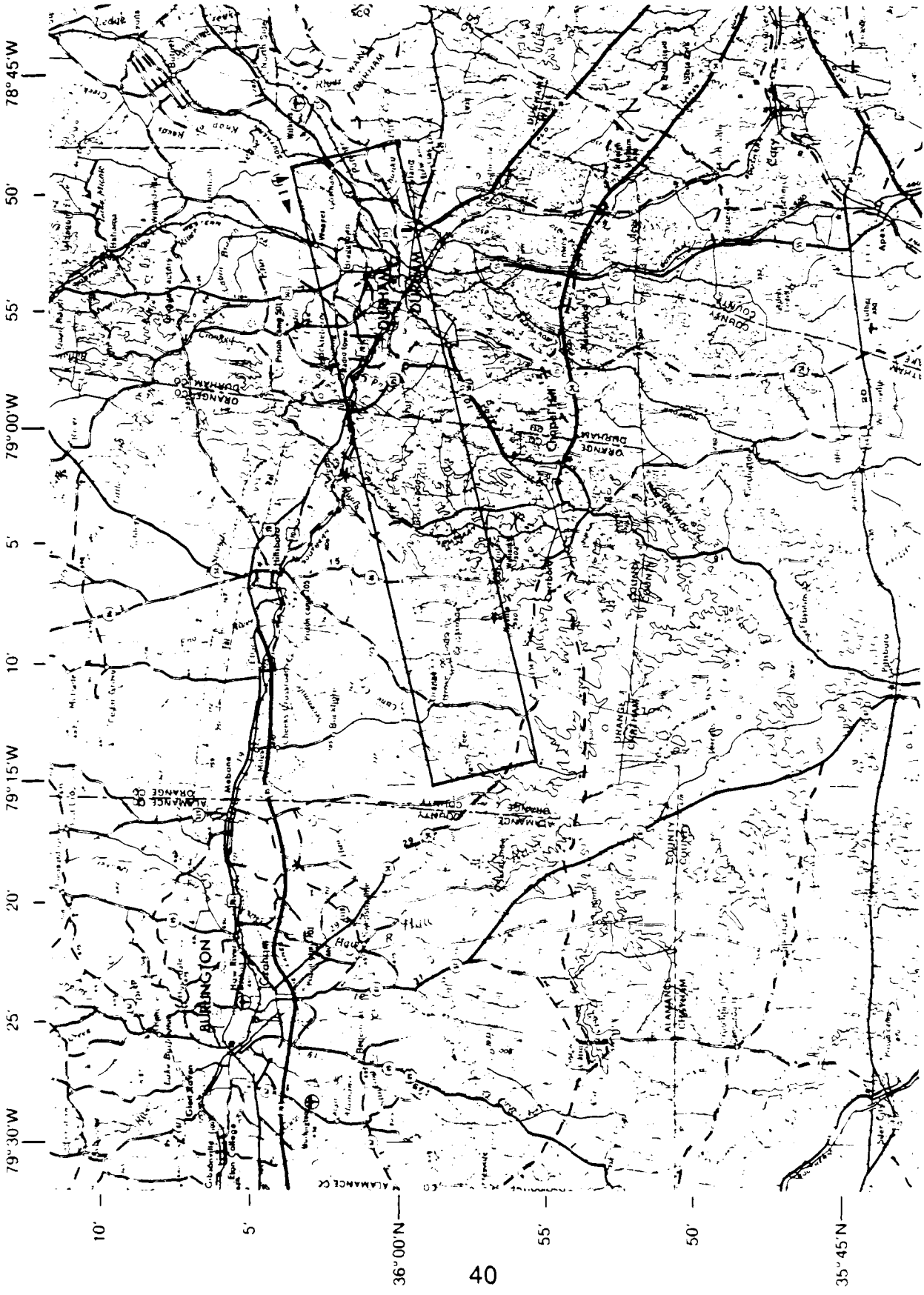


Figure 22. CV-580 SAR Ground Coverage During USGS-3, Pass 1
(after USGS Greensboro and Raleigh 1:250000 Quad Sheet)

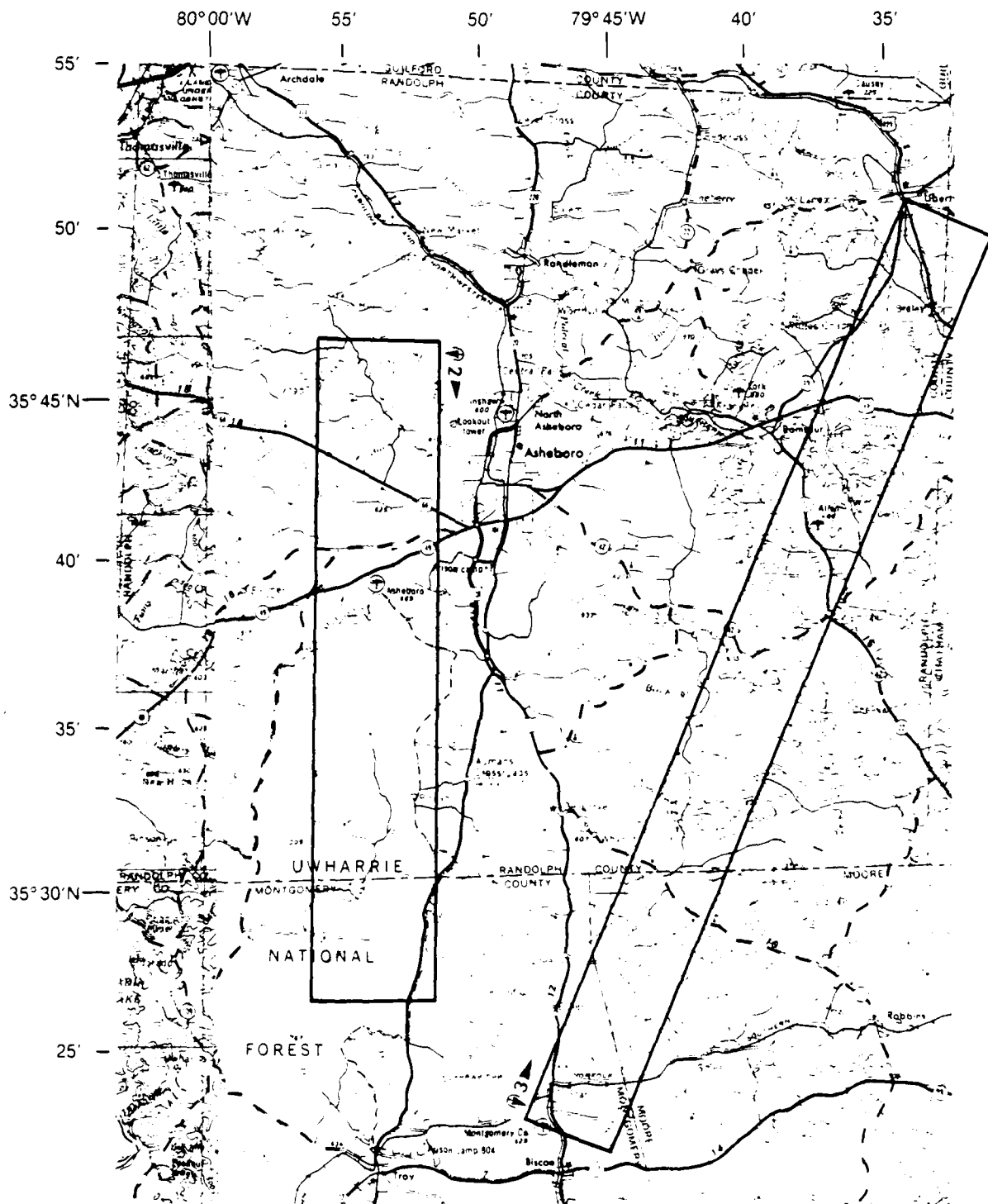


Figure 23. CV-580 SAR Ground Coverage During USGS-3, Passes 2 and 3 (after USGS Raleigh 1:250000 Quad Sheet)

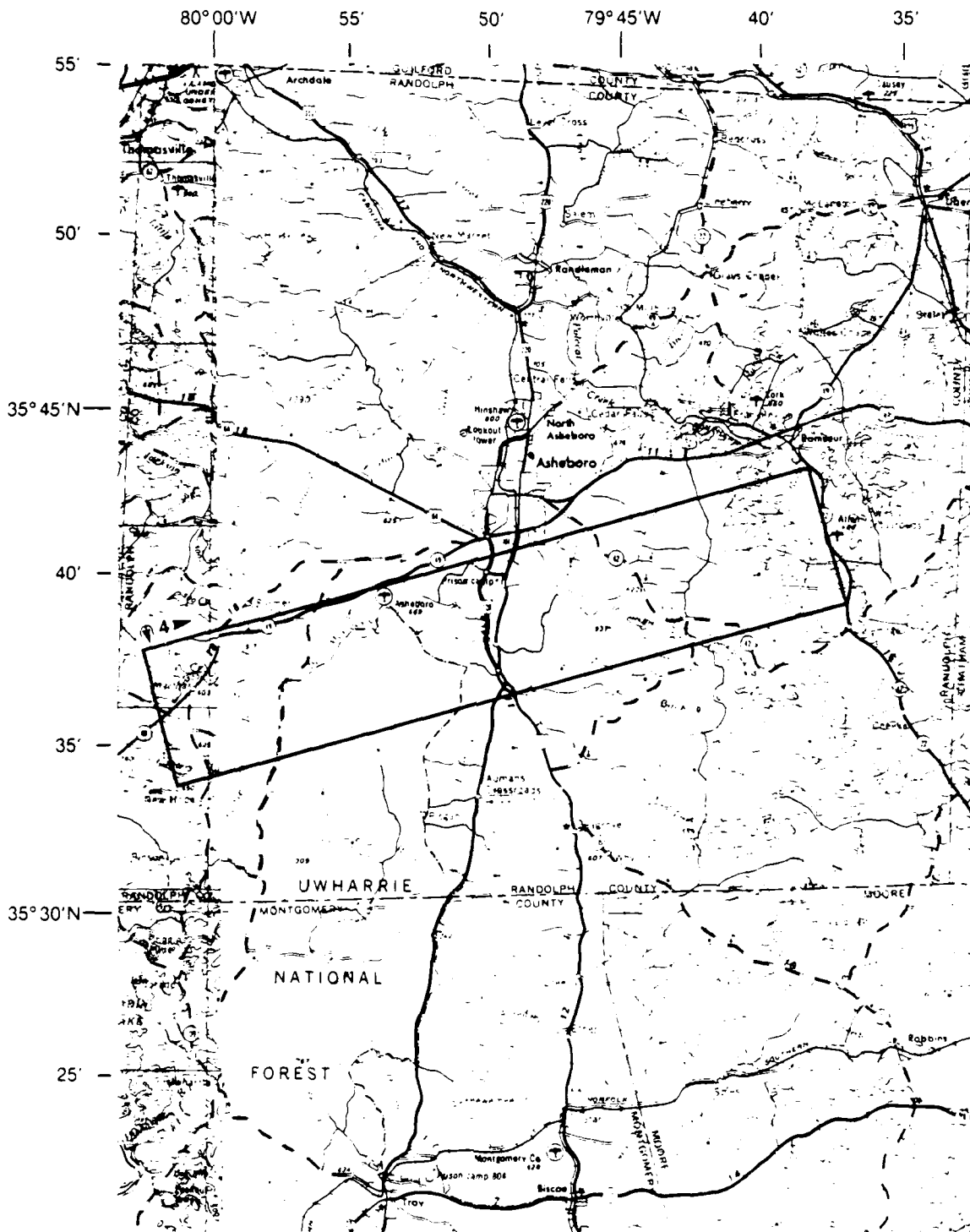


Figure 24. CV-580 SAR Ground Coverage During USGS-3, Pass 4
 (after USGS Raleigh 1:250000 Quad Sheet)

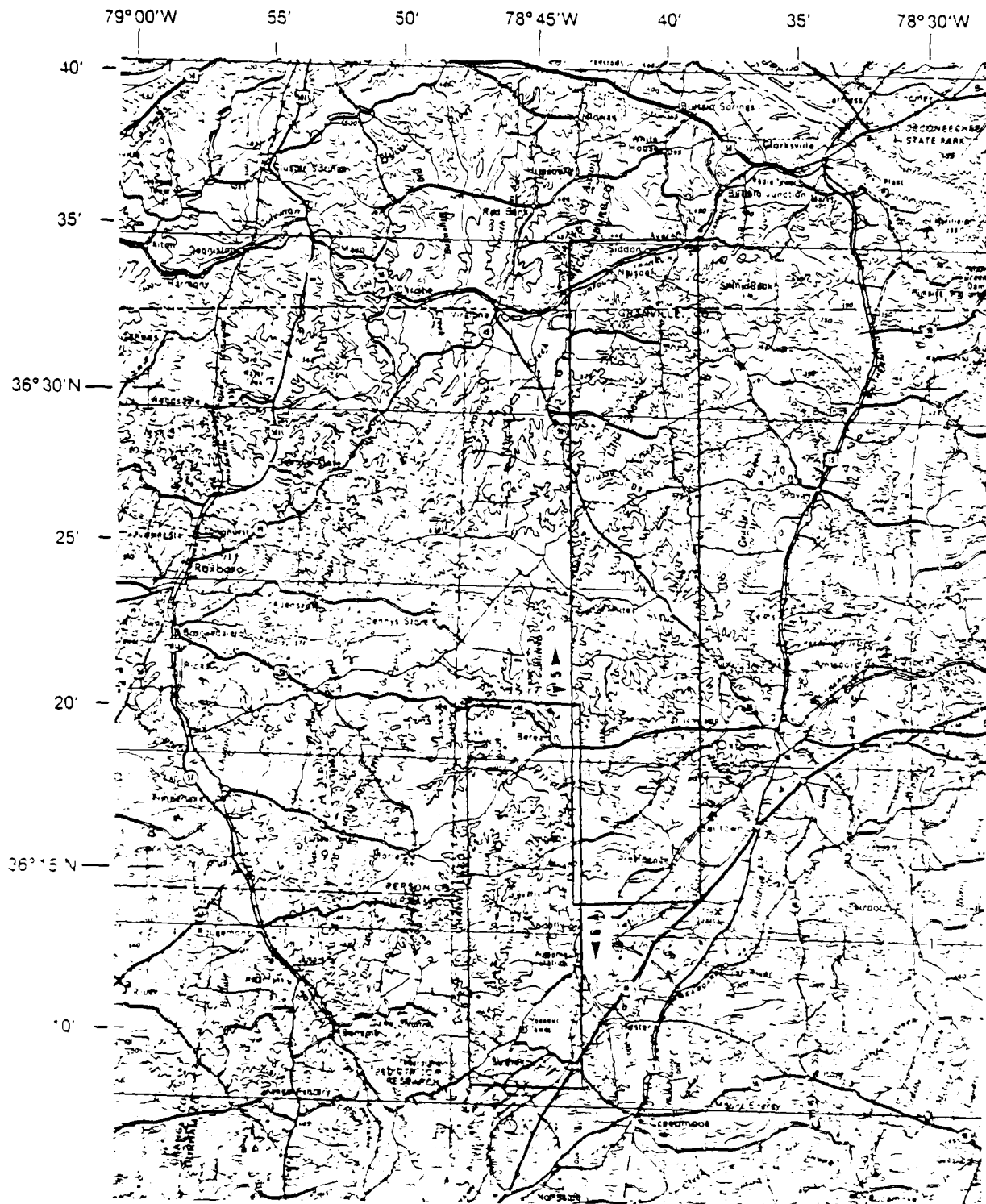


Figure 25. CV-580 SAR Ground Coverage During USGS-3, Pass 5
(after USGS Greensboro 1:250000 Quad Sheet)

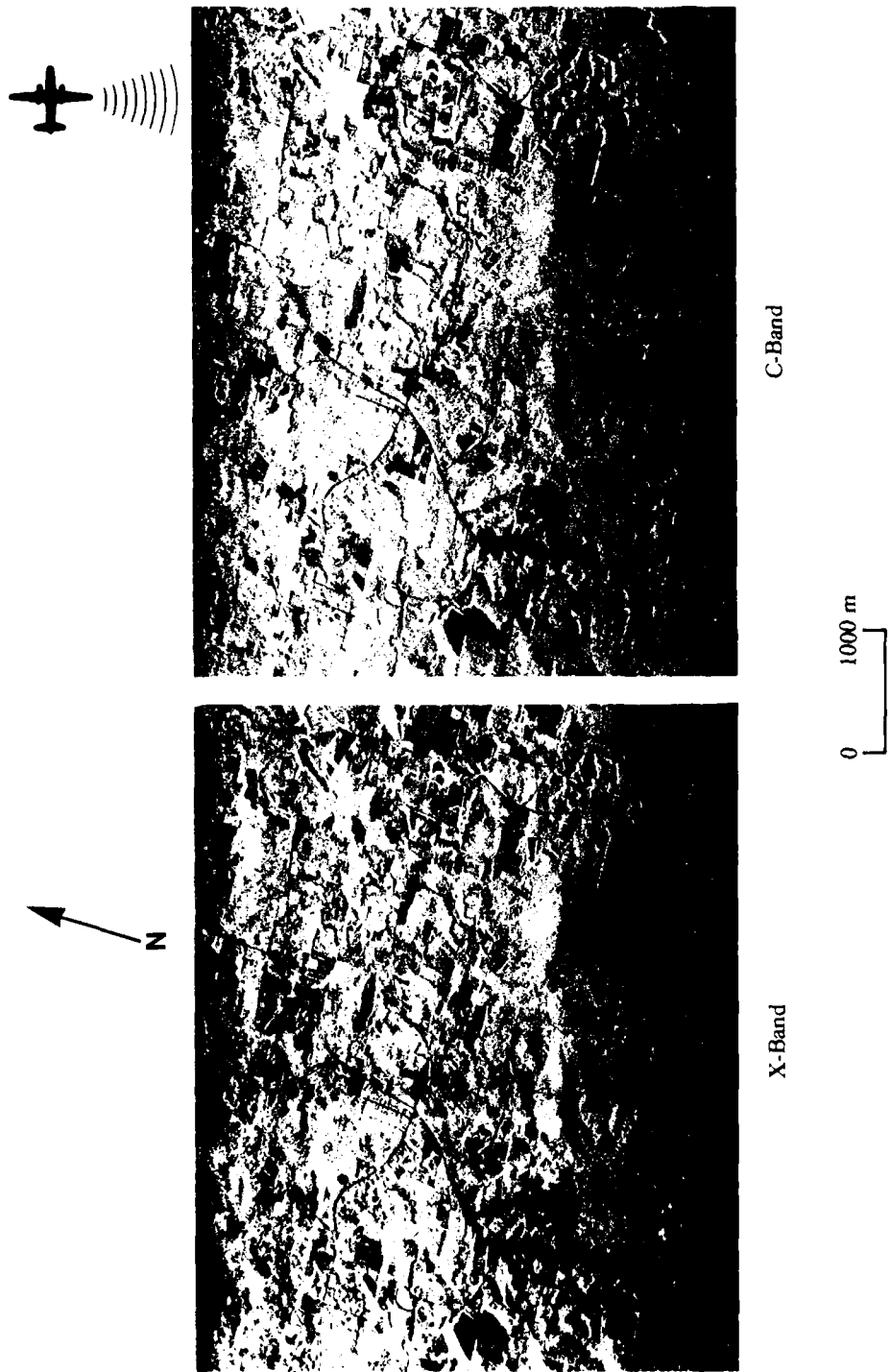


Figure 26. Optically-Processed X- and C-Band SAR Imagery of Pilot Mountain (USGS-3, Pass 4; 10 April 1984)

3.2 SAR CALIBRATION DATA

The data acquired during the USGS-NCDPA flights to assist in the calibration of the SAR imagery are discussed in this section. These data include images of a calibrated corner reflector array and images internally-generated calibration signals. Appendix A to this report discusses calibration of SAR imagery in detail.

The calibrated corner reflectors were located in two separate arrays. These arrays were located at the Asheboro Municipal Airport and at a site in the Duke Forest east of Durham, North Carolina. The locations of these two sites are presented in Figure 1. The Asheboro Array was imaged during three passes, and the Duke Forest Array during six passes.

A total of 31 precision corner reflectors and one active radar calibrator (see Brunfelt and Ulaby, 1984) were deployed in the two arrays. The types and sizes of these reflectors are summarized in Table 7, and their placement within the two arrays illustrated in Figures 27 and 28. Figure 29 is a photograph of typical reflectors used to calibrate SAR imagery, and Figures 30 and 31 contain X-, C- and L-band SAR images of these two arrays.

At specified times during the SAR flights, internal calibration signals were recorded, which are used to calibrate the SAR imagery (see discussion in Chapter 2). Figure 32 presents examples of these internal calibration signals collected at L-band.

3.3 GEOMETRIC REFERENCE REFLECTORS

One of the goals of the USGS-NCDPA data collection program was to provide a multifrequency, multipolarization, digitized SAR data set to evaluate the utility of multi-channel SAR data for the detection of stressed vegetation communities. Implicit in this goal is the capability to merge the multi-channel SAR data.

TABLE 7
 SUMMARY OF CALIBRATED CORNER REFLECTORS USED
 DURING USGS-NCDPA SAR OVERFLIGHTS

Designation	Size (edge of reflector in centimeters)	Type *	Number	Radar Cross Section		
				X-Band (m ²)	C-Band (m ²)	L-Band (m ²)
A	---	ARC	1	---	---	631
B	119	TRI	5	8200	2620	159
C	68	TRI	1	874	280	17
D	61	TRI	4	556	181	11
E	51	TRI	2	300	89	6
F	45	TRI	2	168	54	3
G	22	SQA	1	89	28	2
H	38	TRI	10	85	27	1.5
I	17	SQA	2	30	10	---
J	22	TRI	4	10	3	---

*ARC - Active Radar Calibrator (dual-polarized)
 SQA - Square Trihedral
 TRI - Triangular Trihedral

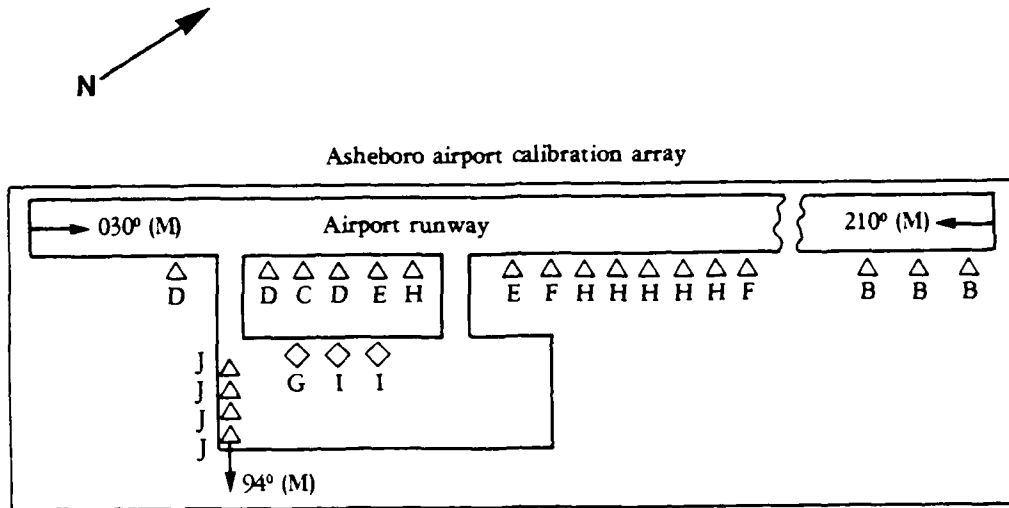


Figure 27. Approximate Locations of Reference Reflectors Within the Asheboro Calibration Array (see Table 7 for reflector parameters)

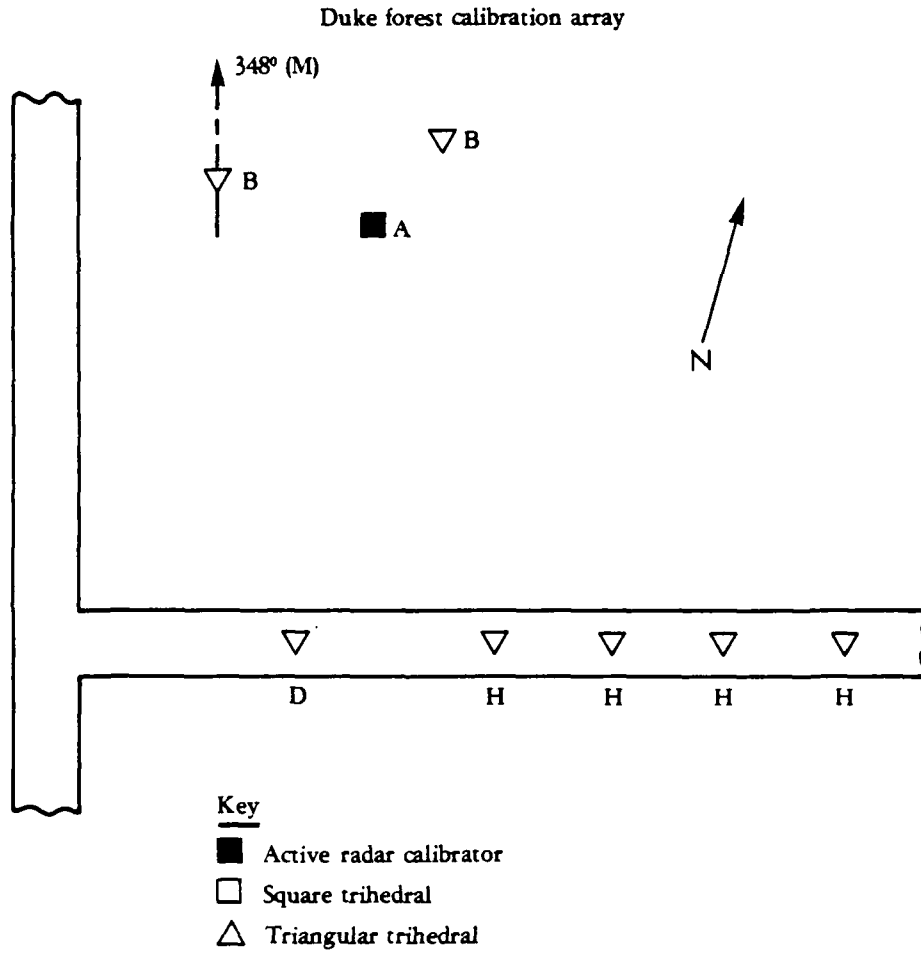
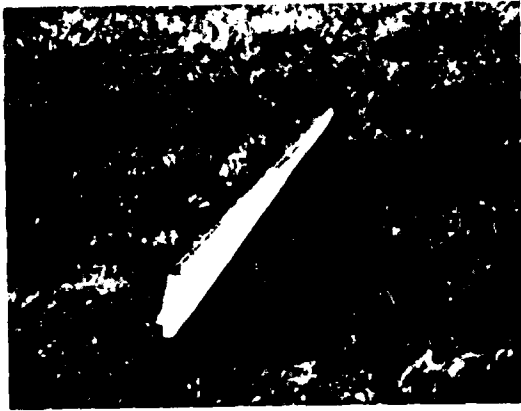
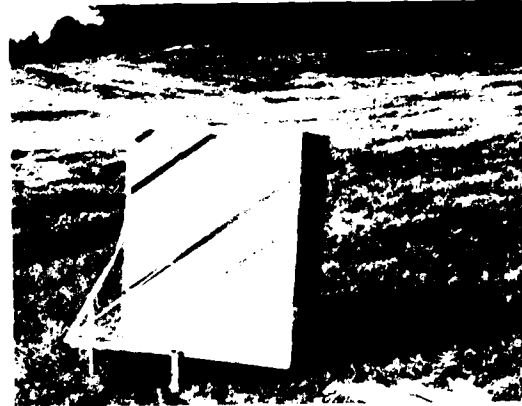


Figure 28. Approximate Locations of Reference Reflectors Within the Duke Forest Calibration Array (see Table 7 for reflector parameters)



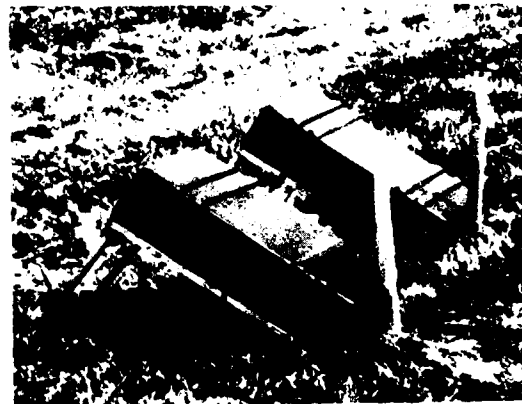
ALUMINUM TRIHEDRAL



STYROFOAM TRIHEDRAL



LUNEBERG LENSE



ACTIVE RADAR CALIBRATOR

FIGURE 29. TYPICAL CALIBRATED REFLECTORS DEPLOYED AT THE ASHEBORO AND DUKE FOREST CALIBRATION ARRAYS

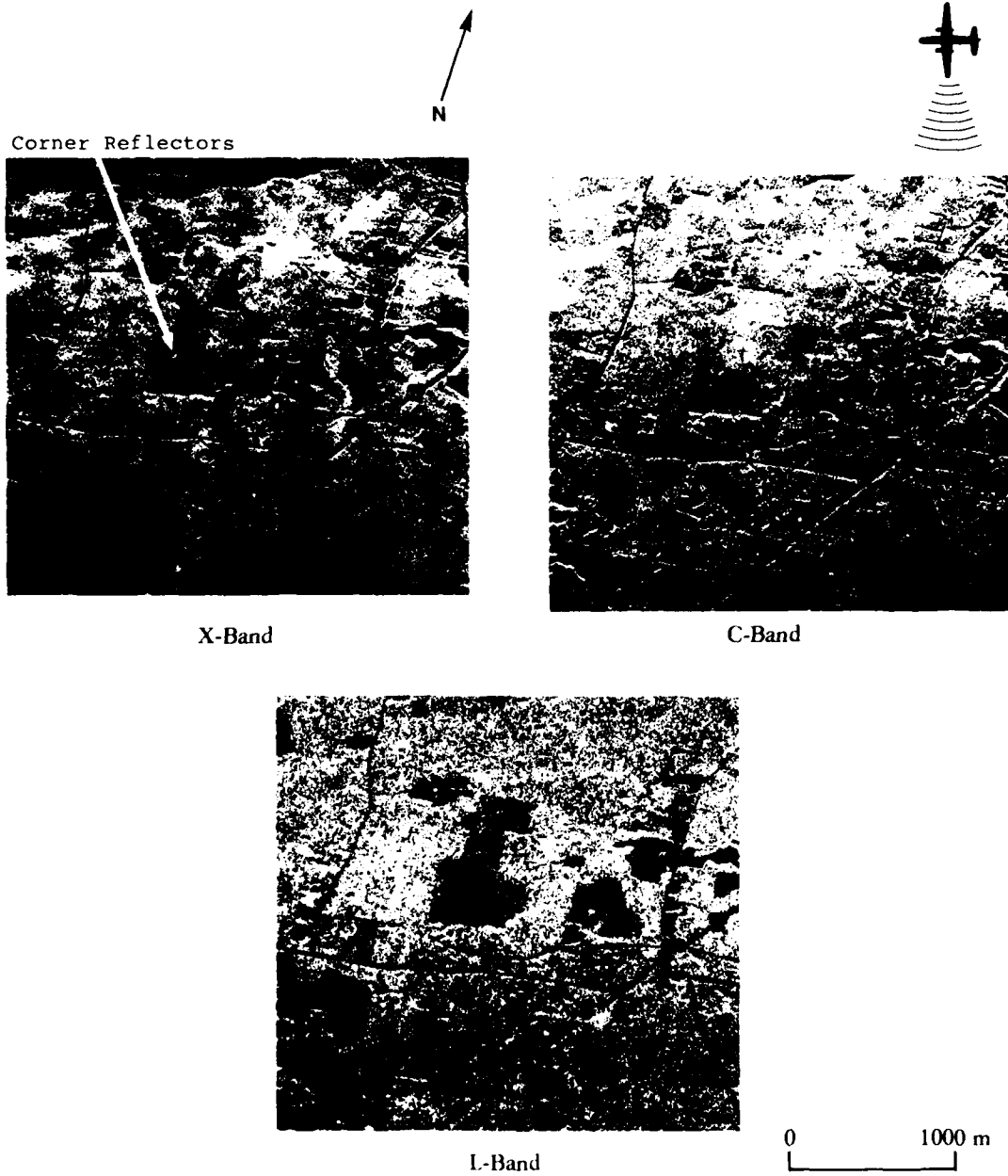


FIGURE 30. OPTICALLY-PROCESSED X-, C- AND L-BAND SAR IMAGERY OF THE DUKE FOREST CALIBRATION ARRAY

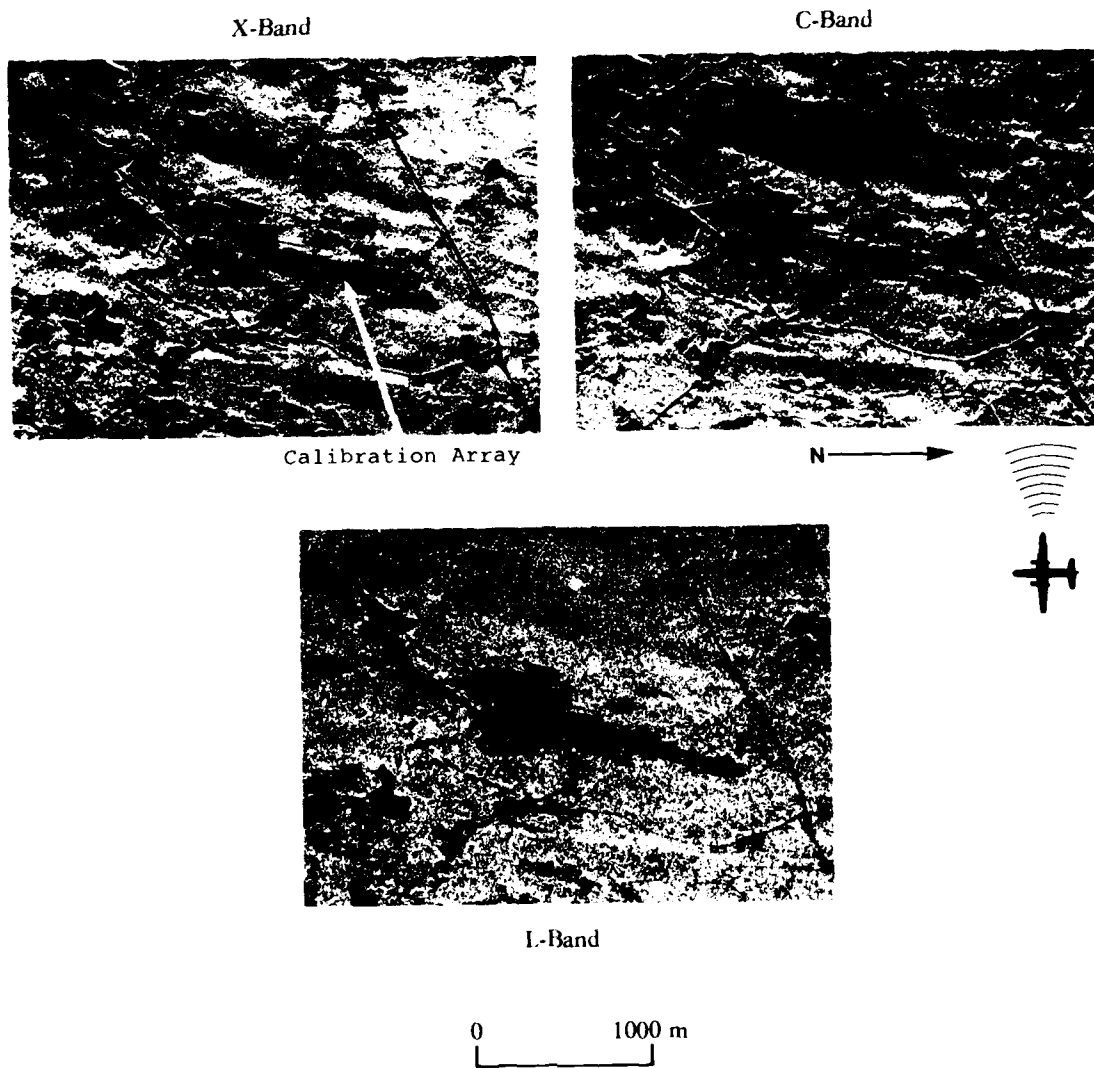


FIGURE 31. OPTICALLY-PROCESSED X-, C- AND L-BAND SAR IMAGERY OF THE ASHEBORO AIRPORT CALIBRATION ARRAY

To assist in this latter objective, a set of specialized radar reflectors were designed and deployed around test areas A and B. These reflectors, called dihedrals because of their design, reflect the incident microwave radiation being transmitted by the SAR in such a way that a return is detected by both the like- and cross-polarized channels of the SAR system. The design and construction of these dihedral reflectors is discussed in more detail in Appendix B, which contains an article which has been submitted for journal publication.

A total of thirteen (13) dihedral reflectors were deployed at nine different sites. Figure 33 presents a photograph of a dihedral reflector, and Figure 34 presents the positions of the nine sites where the dihedrals were deployed. Table 8 lists the latitude and longitude of the positions of the dihedral reflectors.

A review of the SAR imagery indicates that the dihedrals were not detected every time they were within the SAR swath. For the X-band data, the reflectors were detected 72 percent of the time on the like-polarized channel and 81 percent of the time on the cross-polarized channel. For the C-band data, the reflectors were detected 33 percent of the time on the like-polarized channel and 56 percent of the time on the cross-polarized channel. Finally, for the L-band data, the dihedral reflectors were detected 22 percent of the time on the like-polarized channel and 57 percent of the time on the cross-polarized channel.

3.4 DIGITIZED SAR DATA

The primary objective of this data collection program was to generate a multifrequency and multipolarization SAR data set in a digital format. To produce this data set, ERIM's Hybrid Image Processing Facility was used (see Ausherman, et al., 1975, which is included as Appendix C to this report).



Figure 33. A Dihedral Corner Reflector Being Deployed in the Field

TABLE 8
 LOCATIONS OF DIHEDRAL REFLECTORS

<u>Designation</u>	<u>Number of Reflectors</u>	<u>Area</u>	<u>Map</u>	<u>Latitude</u>	<u>Longitude</u>
A	1	Caraway/Shepard Mountains	Glenola Quad (7.5')	35° 46' 28.3"	79° 55' 27.5"
B	1	Caraway/Shepard Mountains	Glenola Quad (7.5')	35° 45' 49.2"	79° 52' 47.9"
C	1	Caraway/Shepard Mountains	Farmer Quad (7.5')	35° 44' 17.0"	79° 57' 58.0"
D	2	Coolers Knob/Cedar Rock Mountains	Farmer Quad (7.5')	35° 38' 49.7"	79° 54' 03.6"
E	2	Coolers Knob/Cedar Rock Mountains	Asheboro Quad (7.5')	35° 36' 35.4"	79° 52' 41.8"
F	1	Needums Mountain	Seagrove Quad (7.5')	35° 31' 55.0"	79° 46' 04.5"
G	1	Needums Mountain	Erect Quad (7.5')	35° 34' 17.1"	79° 44' 54.7"
H	2	Pilot Mountain	Ramseur Quad (7.5')	35° 38' 55.2"	79° 41' 08.9"

Scientists from the USGS selected imagery from twelve separate scenes to be digitized. The images were digitized using an aperture with an equivalent ground size of 3 m by 3 m. The data were then slant-to-ground range corrected and resampled to a pixel size of 3 m by 3 m (see Section 3.4.1 below). A first-order radiometric correction was also applied to the data (see Section 3.4.2). The original uncorrected data are archived at ERIM. The data were then transcribed onto a set of 6 CCTs, with each CCT containing the six channels (X-, C- and L-band; VV and VH polarizations) of data from a specific scene.

Table 9 summarizes the digitized SAR data set. Presented in Table 9 are the CCT number, the file number, IPL tape number where the original data is stored, the area of the scene, the mission and pass of the scene, the frequencies and polarizations of the SAR data for that scene, the number of lines per scene, and the number of pixels per line for each scene. Appendix D presents the format of the CCTs.

As mentioned above, two corrections were applied to the SAR data collected during the USGS-NCDCP. First, a slant-to-ground range correction algorithm was applied to the data. This was followed by an empirical radiometric correction program to remove the effects of the SAR antenna pattern, range fall-off and the illumination pattern of the laser used during digitization of the SAR data. Each of these corrections are discussed in a following section. For an in-depth discussion of calibration of this data, the reader is referred to Appendix A.

3.4.1 GEOMETRIC CORRECTION OF SAR DATA

Because of their sidelooking geometry, SARs produce imagery in the slant range plane. The across-track position of an object in a SAR image is determined by its slant range, the straight line distance of the object from the SAR platform. Ground range, the

TABLE 9
 SUMMARY OF DIGITIZED NCDPA DATA SET

Tape ID	File	IPL ID	Test Area	Mission	Pass	Frequency	Polarization	Lines	Pixels
USGS-CCT1	1	879	C	USGS-3	4	X	VV	2201	2110
	2	879	C	USGS-3	4	X	VH	2201	2110
	3	923	C	USGS-3	4	C	VV	2081	2044
	4	923	C	USGS-3	4	C	VH	2081	2044
	5	878	C	USGS-1	7	X	VV	2201	1980
	6	878	C	USGS-1	7	X	VH	2201	1980
	7	919	C	USGS-1	7	L	VV	2401	1876
	8	919	C	USGS-1	7	L	VH	2401	1874
USGS-CCT2	1	914	A	USGS-3	4	X	VV	2272	2020
	2	913	A	USGS-3	4	X	VH	2272	2020
	3	926	A	USGS-3	4	C	VV	2267	1990
	4	926	A	USGS-3	4	C	VH	2267	1990
	5	918	A	USGS-1	7	X	VV	2075	1980
	6	918	A	USGS-1	7	X	VH	2075	1980
	7	920	A	USGS-1	7	L	VV	2073	1880
	8	920	A	USGS-1	7	L	VH	2073	1880
USGS-CCT3	1	914	A	USGS-3	2	X	VV	3933	2010
	2	914	A	USGS-3	2	X	VH	3933	2010
	3	925	A	USGS-3	2	C	VV	3941	1940
	4	925	A	USGS-3	2	C	VH	3941	1940
	5	916	A	USGS-2	5	X	VV	3661	1990
	6	916	A	USGS-2	5	X	VH	3661	1990
	7	921	A	USGS-2	5	L	VV	3798	1860
	8	921	A	USGS-2	5	L	VH	3798	1860
USGS-CCT4	1	914	B	USGS-3	2	X	VV	1857	2010
	2	914	B	USGS-3	2	X	VH	1857	2010
	3	925	B	USGS-3	2	C	VV	1856	1930
	4	925	B	USGS-3	2	C	VH	1856	1930
	5	916	B	USGS-2	5	X	VV	1809	2000
	6	916	B	USGS-2	5	X	VH	1809	2000
	7	921	B	USGS-2	5	L	VV	1808	1840
	8	921	B	USGS-2	5	L	VH	1808	1840

TABLE 9
 SUMMARY OF DIGITIZED NCDPA DATA SET
 (CONTINUED)

<u>Type ID</u>	<u>File</u>	<u>IPL ID</u>	<u>Test Area</u>	<u>Mission</u>	<u>Pass</u>	<u>Frequency</u>	<u>Polarization</u>	<u>Lines</u>	<u>Pixels</u>
USGS-CC15	1	915	D	USGS-3	5	X	VV	1819	2050
	2	915	D	USGS-3	5	X	VH	1819	2050
	3	927	D	USGS-3	5	C	VV	1815	1970
	4	927	D	USGS-3	5	C	VH	1815	1970
	5	917	D	USGS-2	6	X	VV	1666	1980
	6	917	D	USGS-2	6	X	VH	1666	1980
	7	921	D	USGS-2	6	L	VV	1666	1870
	8	921	D	USGS-2	6	L	VH	1666	1870
USGS-CC16	1	915	E	USGS-3	6	X	VV	1678	2010
	2	915	E	USGS-3	6	X	VH	1678	2010
	3	927	E	USGS-3	6	C	VV	1674	1950
	4	927	E	USGS-3	6	C	VH	1674	1950
	5	917	E	USGS-2	7	X	VV	1661	1990
	6	917	E	USGS-2	7	X	VH	1661	1990
	7	922	E	USGS-2	7	L	VV	1666	1860
	8	922	E	USGS-2	7	L	VH	1666	1860

distance of the object from the ground track of the vehicle, is the representation desired by most image interpreters and analysts.

Figure 35 illustrates the relationship between slant range and ground range. In actuality, the earth's surface is curved, but from aircraft altitudes, the curvature is small enough to be ignored. However, from spacecraft altitudes, the earth's curvature must be accounted for.

In this section, we will discuss the relationship between slant and ground range on a flat, horizontal earth. The relationship between slant and ground range is non-linear, but simple. The trigonometric relationship for flat earth is

$$R_g = R_s \sin \theta , \quad (1)$$

where θ is the incidence angle, R_s refers to slant range, and R_g refers to ground range. The slant range is always smaller than ground range and is highly dependent upon the angle at which the terrain is viewed. However, the relationship between the change in slant range to the change in ground range is

$$\Delta R_g = \Delta R_s / \sin \theta . \quad (2)$$

The relationship between R_g and R_s determines the scale of the image. Because this relationship differs at near range compared to far range, the range scale of the slant range image is not constant. This type of distortion is at its maximum when looking at the nadir of the vehicle, where the incidence angle is 0° . Near the nadir, a comparatively small change in slant range will produce a large change in ground range. As the incidence angle is increased, a smaller and smaller change will occur in ground range for every change in slant range. At the limit when the incidence angle is 90° (the radar beam is grazing the ground and parallel to the ground), there is no distortion, because the change in slant range is identical to the change in ground range. Because of this continuous

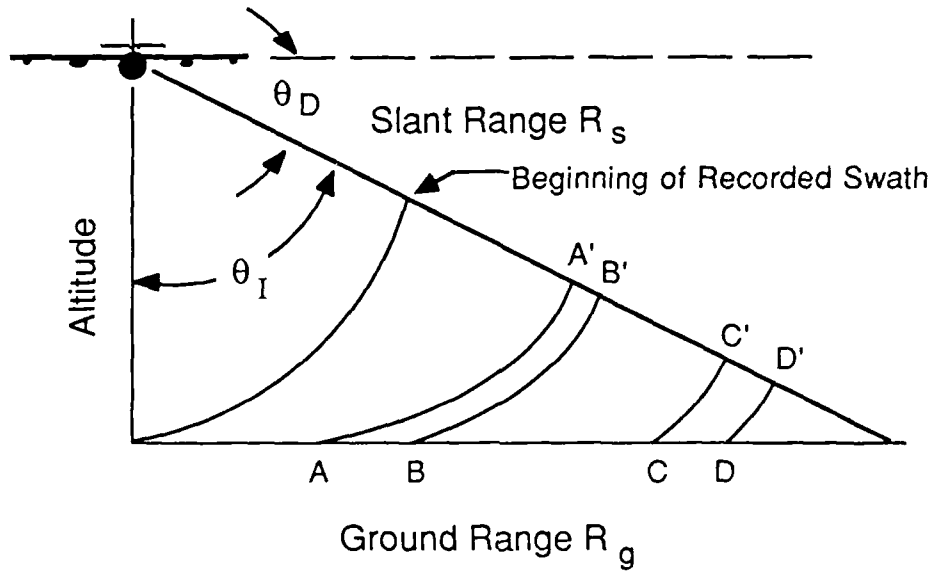


Figure 35. Slant Range Versus Ground Range Perspective in an Imaging Radar System

change in range scale across the image, only one range exists where the slant range scale equals the along-track scale. At nearer range, the map scale will be smaller, and at a farther range the map scale will be larger in the slant range presentation of the image.

The slant-to-ground range distortion can be removed by digitally resampling the data in the range direction. To do this, the slant-ground range relationships can be rewritten as

$$R_g = \sqrt{R_s^2 - h^2}, \quad (3)$$

for the flat earth or low-altitude case, where h is the platform altitude.

Because the range and azimuth scales are not the same after the slant-to-ground range conversion has been applied, the range dimension is usually resampled to match the azimuth line spacing. Two types of resampling techniques are commonly used, depending upon the type of scene, the required accuracy, and the acceptable cost for the correction. The simplest and least expensive resampling technique is the nearest-neighbor method. In this method, a grid is set up having equal intervals of ground range, ΔR_g , beginning at the nearest range sample, R_{g0} . That is, the ground range at grid point n is

$$R_{gn} = R_{g0} + n\Delta R_g. \quad (4)$$

The ground range spacing ΔR_g is usually chosen to equal the distance between samples in the along-track direction, so that the image will have unity aspect ratio when displayed on a device which has pixel elements of equal size in both dimensions.

The resampling is then carried out by considering each value of R_{gn} in turn, and computing the corresponding ground range from Eq. (4). The input range sample nearest to this computed ground range is then copied into the output data set. The maximum error in

the location of any pixel using this method is one half of the ground range distance between pixels. Usually, this is an acceptable error, particularly if the scene reflectivity distribution is relatively smooth.

Another method of resampling interpolates between samples to find the data value at the required location. The same steps as described above are carried out except that instead of choosing the input range sample nearest to the computed slant range for the output pixel under consideration, an interpolation formula is used which involves the data values at several locations surrounding this pixel. Several different interpolation formulas have been used, most of them variations or approximations of a sinc (i.e., $[\sin x]/x$) function (Shuchman, et al., 1977). This procedure results in a theoretically more exact reconstruction of the image but is more difficult to implement and requires more computer time for its operation.

The recorded altitude (h) of the CV-580 aircraft was determined by an altimeter which calculates altitude by measuring the difference in barometric pressure between the aircraft and a point on the ground, usually the air field where the airplane takes off and lands. Naturally occurring variations in atmospheric pressure can result in variations in the actual altitude of the aircraft. Studies have shown that these altitude variations are often as high as 50 m (Lyden, 1983; Kasischke, et al., 1983), which can lead to errors in ground range when calculated using Eq. (3).

During the North Carolina data collection flights, several cold fronts were moving through the area, resulting in an unstable atmosphere. It is therefore very likely that the barometric pressure was variable, resulting in some variation in the recorded aircraft altitude. The slant-to-ground range corrections made on the data used the recorded altitude, and thus some ground-range distortions may be the result of altitude variation.

If a higher degree of accuracy in the slant-to-ground range correction is desired, the following method can be used to determine the aircraft altitude (h).

If there are two points on a SAR image (see Figure 36) whose location can be identified on a map, then we can easily calculate the slant range distance to each point (R_1 and R_2) and the ground range distance (in the range direction) between the two points (G). The depression angle (θ_D) to the second point can be calculated from the law of cosines as

$$\theta_D = \cos^{-1} \left[\left(R_1^2 + G^2 - R_2^2 \right) (2R_1G)^{-1} \right], \quad (5)$$

and the altitude can be calculated

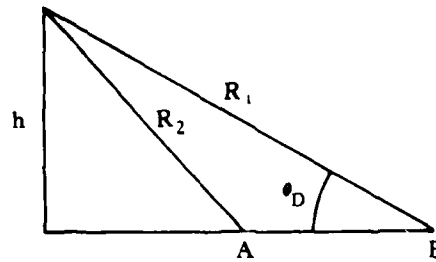
$$h = R_1 \sin \theta_D . \quad (6)$$

Other geometric distortions will be introduced into the image because Eq. (3) assumes a flat earth. Since there are elevation differences within the scene, these will also lead to ground-range variations. These elevation-induced variations can be removed if the SAR data are combined with elevation data (see Jackson, 1983).

3.4.2 RADIOMETRIC CORRECTION

A first-order radiometric correction was applied to the SAR data in order to produce an even illumination pattern across the imaged swath. In this section, we will first discuss the sources of radiometric variation in a SAR scene and then discuss how these variations were normalized.

The intensity (P_I) recorded on the SAR scene is a function of the radar backscatter (σ) for the area being illuminated and a variety of radar parameters. Assuming that the SAR is operating within its linear region, this relationship can be expressed as:



$$h = R_1 \sin \theta_D$$

where

$$\cos \theta_D = \frac{R_1^2 + \overline{AB}^2 - R_2^2}{2 R_1 \overline{AB}}$$

Figure 36. Calculation of the Aircraft Altitude (h) From Two Known Ground Locations (A and B)

$$P_I = \frac{P_T G^2(\theta) \lambda^2 H_s \sigma}{(4\pi)^3 R^4} + P_n \quad (7)$$

where P_T is the transmitted power,

$G(\theta)$ is the antenna gain as a function of the incidence angle, θ ,

λ is the radar wavelength,

H_s is the radar system transfer function or radar system gain,

R is the slant-range distance to the target, and

P_n is the system noise.

Of interest in this discussion are the effects of range (R) and the antenna gain [$G(\theta)$]. If all other SAR parameters are constant, a specific target or feature will have a lower P_I the further out in slant range the target is located because

$$\frac{P_{I2}}{P_{I1}} \sim \frac{R_1^4}{R_2^4} < 1. \quad (8)$$

If we assume that P_{I1} has a value of 1, then the values of P_{I2}/P_{I1} for increasing ranges are illustrated in Figure 37.

The antennas for the X-, C- and L-band SAR each have a unique pattern, with a peak gain or intensity occurring at the center of the antenna beam. The intensity or gain falls off as a function of the angular distance away from the center of the beam, i.e., a target's intensity will be lower at the outside of the beam's center than it will be at the center of the beam.

For the most part, during the North Carolina data collection the antennas' beams were centered at an incidence angle of 62° . Figure 37 also illustrates the expected ratio of P_{I2}/P_{I1} as a

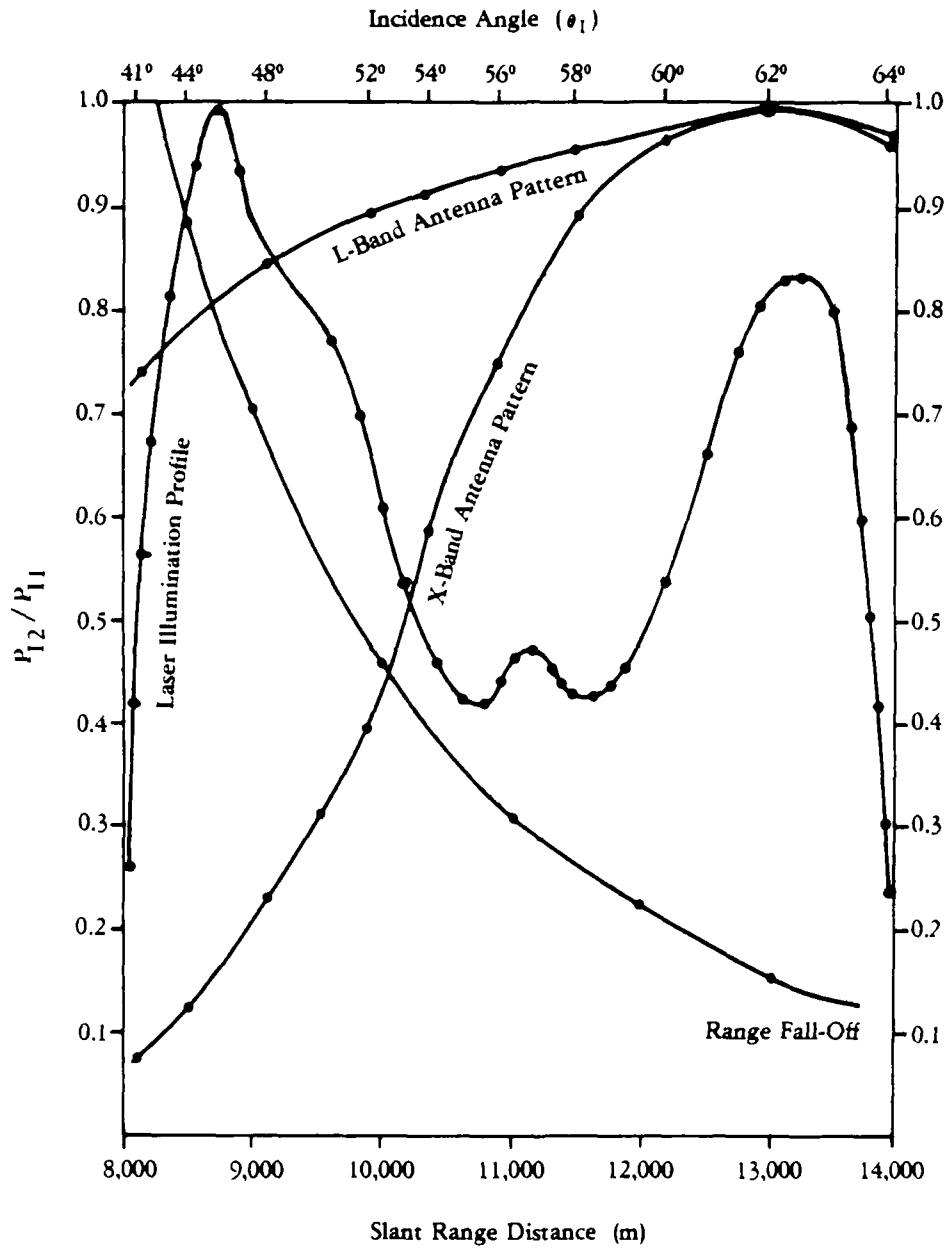


Figure 37. Illustration of the Effects of Range Fall-off, X- and L-Band Antenna Pattern, and Laser Illumination Pattern

function of θ_I , where P_{I1} is the intensity of a target at the center of the antenna beam. We can see that the L-band antenna pattern is fairly flat, whereas the X-band antenna fall-off is rather dramatic. No antenna pattern is yet available for the C-band antenna.

One more factor which will affect the radiometric fidelity of the digital SAR data is the illumination pattern of the laser beam which was used to optically-process SAR data in the HIPF. This pattern is also shown in Figure 37.

To be able to quantitatively compare the intensity values within a given scene or between the same scenes of different frequencies or between the same area on different passes requires calibration of the data. This procedure is discussed in Appendix A. We have applied a first order radiometric correction to the data which has essentially eliminated any range fall-off which may exist in the data. This does not imply the data have been calibrated.

The range variation within a scene was identified by averaging approximately 200 pixels in azimuth and then plotting a running average (of approximately 30 pixels) of pixel intensity versus range. This plot was further smoothed to remove any obvious deviations, and a multiplicative correction value, C_i , calculated as

$$C_i = \frac{S_i}{S_{\max}}, \quad (9)$$

where i is the pixel location in range, S_i is the plot intensity and S_{\max} is the maximum intensity of the curve. A corrected value for each pixel, P'_{Ii} , is then calculated as

$$P'_{Ii} = C_i P_{Ii}. \quad (10)$$

Figure 38 illustrates an L-band image with fall-off in the range dimension. Figure 39 shows the empirical radiometric correction

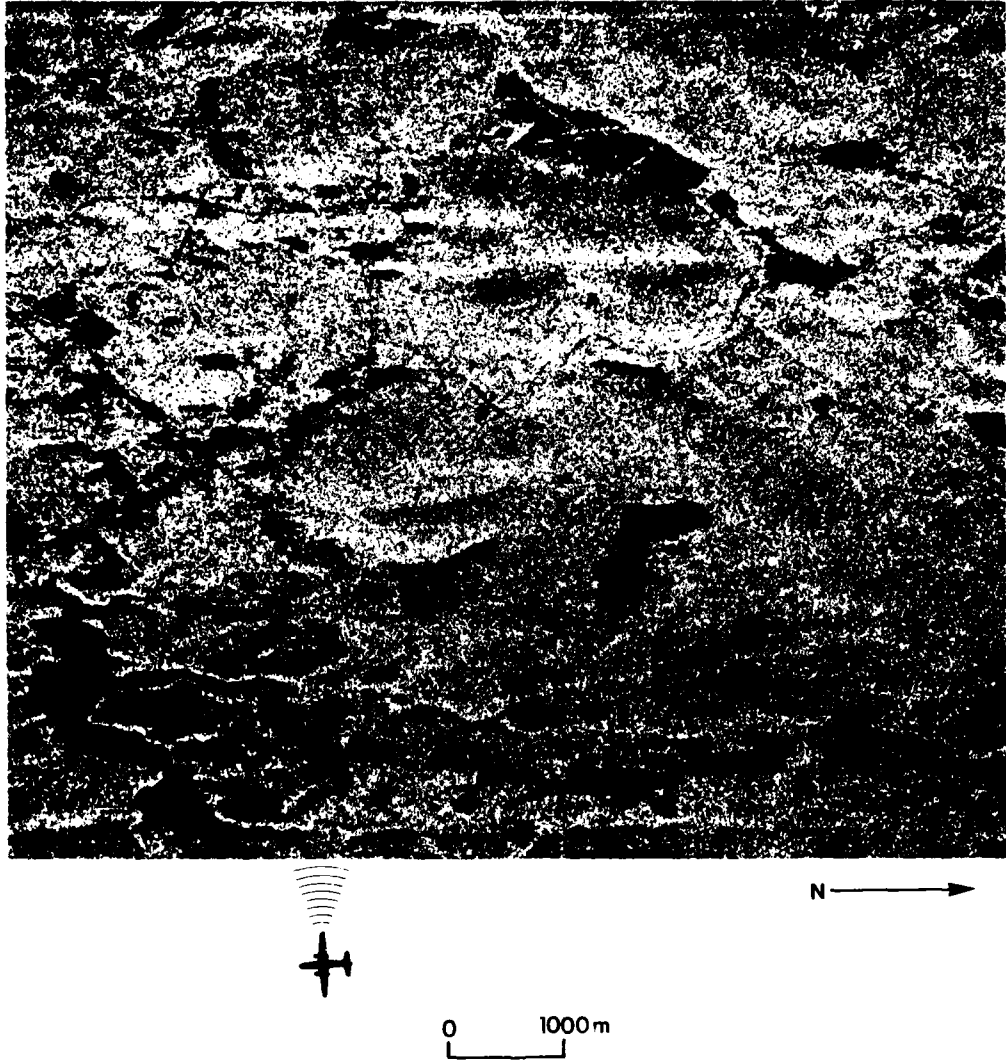


Figure 38. Non-Corrected Hybrid-Digitized L-Band Data From USGS-2, Pass 5

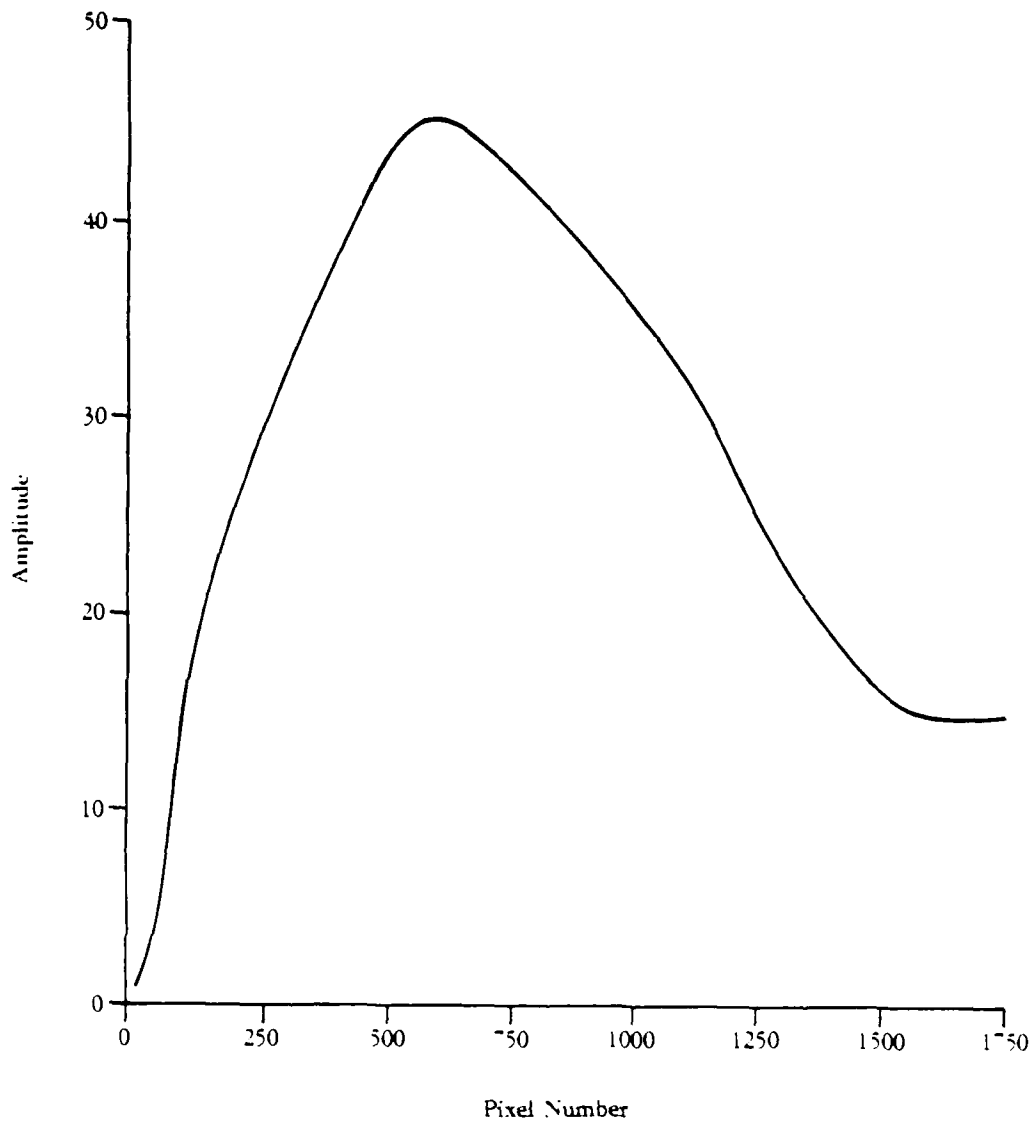


Figure 39. Radiometric Correction Applied to USGS-2, Pass 5 L-Band SAR Data

curve generated for these data. Finally, Figure 40 shows the radio-metrically and geometrically corrected data.

3.4.3 DIGITALLY-PROCESSED SAR DATA

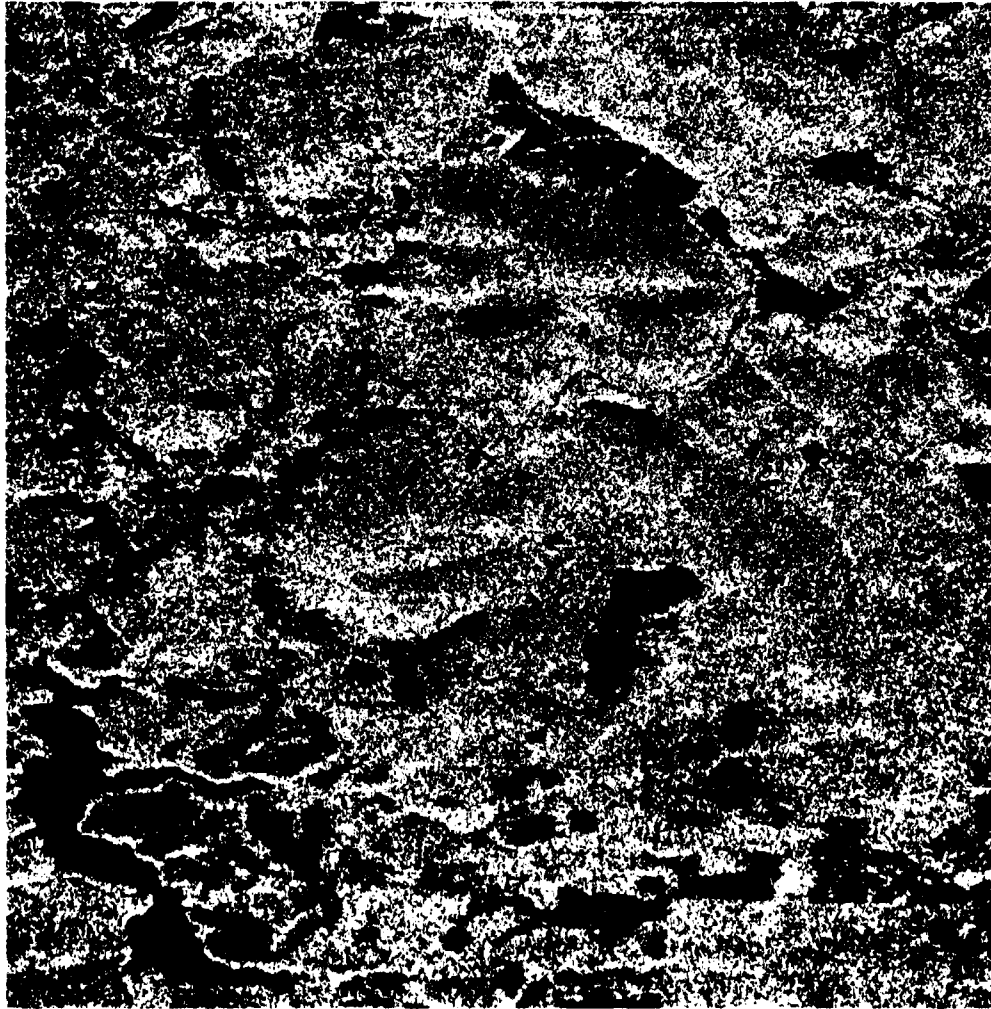
Another method to obtain digital SAR image is to digitally process the SAR signal histories recorded on the high density digital tape (HDDT). During the USGS-NCDPA program, two channels of SAR data were recorded on HDDT during each pass (see Table 3). These data are presently archived at ERIM. Figures 41 to 43 present examples of imagery generated from digitally-recorded data. These images are all from the Duke Forest area surrounding the calibration array (see Figure 30).

3.5 ENGINEERING ASSESSMENT

Immediately after optically processing the SAR imagery from a data collection program, ERIM engineers and scientists perform an engineering assessment on the data. These engineers and scientists have extensive experience in SAR image interpretation and recognize image characteristics which are indicative of SAR system malfunctions. During this engineering assessment, a rigorous set of guidelines is followed. The degree to which each image characteristic is present is noted. The following rating criteria is used:

- + slight reduction in image quality,
- * moderate reduction in image quality, or
- severe reduction in image quality.

In addition to noting the types and severity of the characteristics present in the imagery, the overall quality of each pass of imagery is rated using the following categories:



0 1000m

FIGURE 40. RADIOMETRICALLY AND GEOMETRICALLY CORRECTED
L-BAND SAR DATA FROM USGS-2, PASS 5



Figure 41. Digitally-Processed X-Band SAR Data Collected Over the Duke Forest Calibration Array (USGS 3, Pass 1, 10 April 1984)

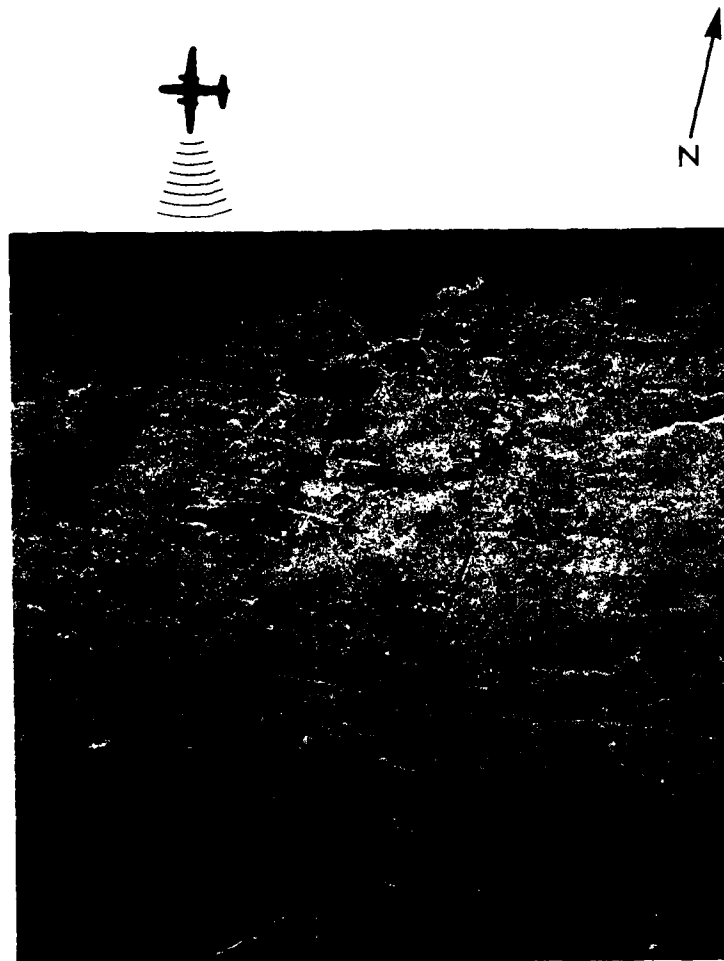


Figure 42. Digitally-Processed C-Band SAR Data Collected Over the Duke Forest Calibration Array (USGS 3, Pass 1, 10 April 1984)

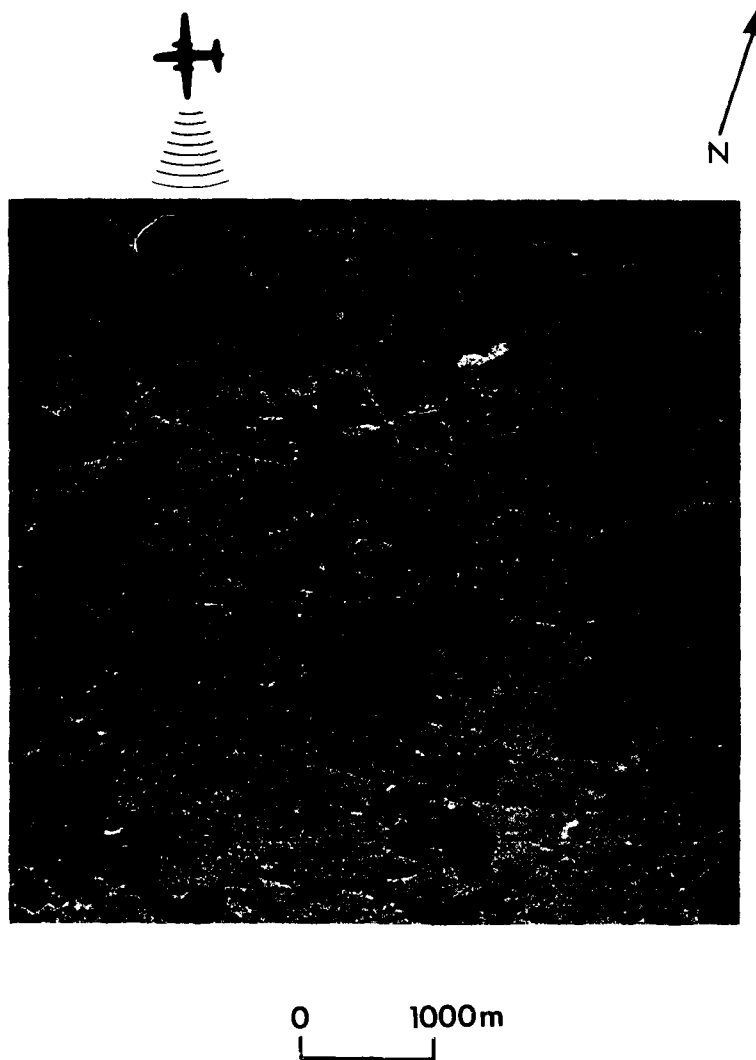


Figure 43. Digitally-Processed L-Band SAR Data Collected Over the Duke Forest Calibration Array (USGS 2, Pass 2, 9 April 1984)

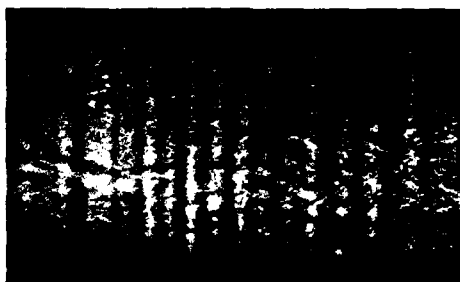
- 7 Excellent imagery
- 6
- 5 Good imagery
- 4
- 3 Fair imagery
- 2
- 1 Poor imagery
- 0 Data not recorded or of insufficient quality to be useful.

A rating of excellent implies that the data are of the highest quality and require no additional precision processing. A rating of good implies that there are slight or moderate image perturbations present, which usually can be removed through precision processing of the imagery. A rating of fair implies there is much useable data present, and that the moderate to severe image perturbations may be removed through precision processing. A rating of poor implies that the severe image perturbations generally cannot be removed through precision processing.

Only two image characteristics were noted during the engineering assessment of the USGS-NCDPA SAR data set, and these were noted only on the X-band data. These two characteristics were modulation intensity variations and film transport runaways.

Excessive aircraft motion caused by areas of high turbulence during data collection sometimes create a range-oriented banded pattern within the imagery. These bands are referred to as modulation intensity variations. This type of image characteristic is most often found in X-band data. Figure 44 presents an example of a set of modulation intensity variations from USGS-2, Pass 7.

A periodic malfunction of the camera which recorded X-band data resulted in gaps in the recorded SAR signal histories. These gaps result in blank areas on the output imagery. Figure 44 presents an example of X-band imagery where this film-drive runaway occurred



(a) Modulation Intensity Variation
(USGS-2, Pass 7)



(b) Film Transport Runaway
(USGS-2, Pass 7)

Figure 44. Examples of Image Characteristics Found on USGS-NCDPA X-Band SAR Data

during USGS-1, Pass 7. No data are lost due to these runaways, but the optically processed imagery from passes where this problem occurred will have to be mosaiced in order to produce a continuous image.

The image characteristics noted on the X-band SAR imagery were all slight in nature, and did not significantly reduce the utility of the data set. Overall, the SAR data set collected over the NCDPA was of extremely high quality. The average quality rating for the X-band data was 6.2, for the L-band data, 7.0, and for the C-band data, 7.0. No additional optical processing is required for this data set.

4
SUMMARY

Between 8 and 10 April, 1984, three SAR missions were flown over the North Carolina Digital Project Area (NCDPA) by the ERIM/CCRS CV-580 SAR System in order to collect multifrequency and multi-polarization SAR imagery over selected USGS test sites. A total of 22 SAR passes were collected over five different test sites. Approximately 790 line kilometers (7900 square kilometers) of high quality SAR data were collected.

These data were first optically processed into imagery. Copies were provided to USGS personnel, who then selected twelve areas to be digitized. A digitized SAR data set consisting of three frequencies (X-, C- and L-bands) and two polarizations for each frequency (VV and VH) was then produced on ERIM's Hybrid Image Processing Facility. First-order geometric and radiometric corrections were applied to the data. Thus, a data set has been generated to use in the evaluation of SAR imagery for detection of geologically-stressed vegetated areas.

In order to realize the full potential of the NCDPA SAR data set, users should realize that sophisticated analysis may need to be employed. First, to draw quantitative conclusions from the changes in radar backscatter from different passes, the SAR data must first be calibrated. Calibration of the SAR data requires reduction of the calibration array data and calibration signal data as well as following a careful set of procedures (see Appendix A or Larson, et al., 1985).

Second, higher-order geometric corrections (see Jackson, 1983) may be applied to the original SAR data in order to reduce radar lay-over and radar foreshortening. These higher-order geometric corrections would not only make the data easier to merge, but also could be used to account for scattering variations induced by changes in the local angle of incidence.

Finally, if analysis of the hybrid-digital data shows significant results, researchers should consider the use of digitally-processed SAR data. These data have a higher spatial resolution, lower noise levels, and higher dynamic range than the hybrid-digital data. In addition, image speckle can be reduced through multiple-look processing.

REFERENCES

- Ausherman, D.A., W.D. Hall, J.N. Latta, and J.S. Zelenka, Radar Data Processing and Exploitation Facility, Proc. IEEE International Radar Conference, pp. 493-498, 1975.
- Brunfeldt, D.R., and F.T. Ulaby, Active Reflector for Radar Calibration, IEEE Trans. Geosci. Remote Sens., GE-22, pp. 165-169, 1984.
- CCRS, CCRS CV-580, Ottawa, Ontario, in preparation, 1983.
- Jackson, P.L., Reflection and Identification Studies Applied to Terrain Imaging Radar, FTL-0331, University of Michigan, Ann Arbor, 78 pp., 1983.
- Kasischke, E.S., R.A. Shuchman, D.R. Lyzenga, R.W. Larson, and S.R. Stewart, SAR Data Collection and Processing Summary - 1983 Georgia Strait Experiment, ERIM Topic Report No. 168400-1-T, Ann Arbor, MI, 200 pp., 1983.
- Kasischke, E.S., R.A. Shuchman, R.W. Larson, D.R. Lyzenga, J.C. Clinthorne and P.L. Jackson, SAR Data Collection and Processing Summary - 1984 SARSEX Experiment, ERIM Topic Report No. 155900-21-T, 134 pp., 1985.
- Larson, R.W., D.T. Politis, and J.L. Walker, Calibration Procedures and Test Plan for Synthetic Aperture Radar, ERIM Final Report No. 157400-10-F, Ann Arbor, MI, 191 pp., 1982.
- Larson, R.W., P.L. Jackson, E.S. Kasischke and A.R. Dias, A Digital Calibration Procedure for Synthetic Aperture Radar Systems, IEEE Trans. Geosci. Remote Sens., (in press) 1985.
- Lyden, J.D., Altitude Inaccuracies During the 1978 Vancouver Island Experiment, ERIM Internal Memorandum RR-83-102, 1983.
- Rawson, R.F., F. Smith and R. Larson, The ERIM Simultaneous X- and L-Band Dual Polarized Radar, IEEE 1975 Radar Conference, pp. 505, 1975.
- Shuchman, R.A., P.L. Jackson, and G.B. Feldkamp, Problems of Imaging Ocean Waves with Synthetic Aperture Radar, ERIM Interim Technical Report No. 124300-1-T, Ann Arbor, MI, 111 pp., 1977.
- Shuchman, R.S., E.S. Kasischke, A.D. Nichols, and R.F. Rawson, Multi-frequency and Multipolarization P-3 SAR Facility, ERIM Topic Report No. 176900-1-T, Ann Arbor, MI (in press), 1984.
- Walker, J.L. and R.W. Larson, SAR Calibration Technology Review, ERIM Final Report No. 150400-7-F, 151 pp., 1981.

APPENDIX A
 CALIBRATION OF SAR DATA

Calibration of SAR data is a relatively straight-forward concept to understand in a theoretical sense, although the implementation of a total calibration algorithm requires a careful, routinized procedure in order to keep track of all the factors which can affect each step in the algorithm. In this Appendix, we will discuss the fundamentals of SAR image calibration. For a more in-depth discussion of calibration, the reader is referred to Walker and Larson (1981), Larson, et al. (1982, 1985) and Larson and Maffett (1985). In our discussion, we will use data collected during a SAR/ocean imaging experiment conducted for the Office of Naval Research (see Kasischke, et al., 1985) to illustrate the basic concepts behind SAR image calibration. Figure A-1 presents X- and L-band SAR data of internal wave surface patterns.

The goal of the calibration algorithm is to relate the measured intensity, P_I , from a processed SAR image to radar cross-section (σ). Assuming the SAR is operating within its linear region, this relationship can be expressed as

$$P_I = \frac{P_T G^2(\theta) \lambda^2 H_S \sigma}{(4\pi)^3 R^4} + P_n \quad (A-1)$$

where P_T is the transmitted power,

$G(\theta)$ is the antenna gain as a function of the incidence angle, θ ,

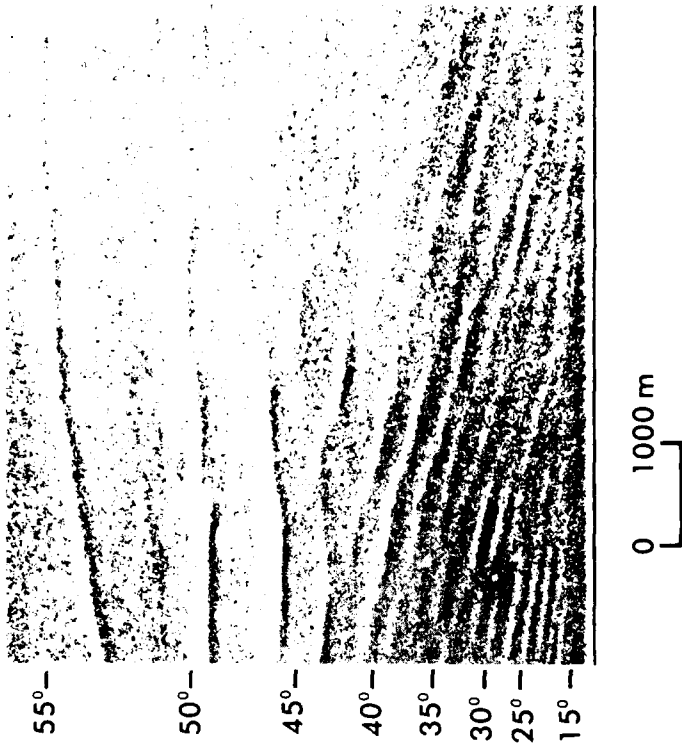
λ is the radar wavelength

H_S is the radar system transfer function or radar system gain

R is the slant-range distance to the target, and

P_n is the system noise.

L-BAND



55°—
50°—
45°—
40°—
35°—
30°—
25°—
15°—

X-BAND

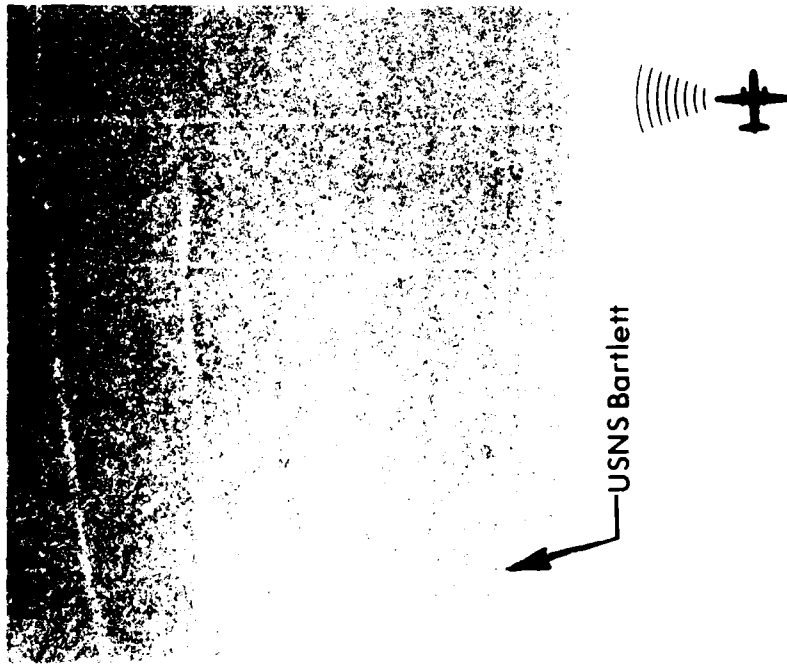


Figure A-1. Digitally-Processed X- and L-Band SAR Data Collected During SARSEX-4, Pass 5 (31 August 1984)

Using SAR imagery of calibrated reflectors of known radar cross-section (σ) and internal calibration signals, the basic calibration approach used at ERIM is as follows:

1. Inspect the candidate SAR imagery for artifacts and saturation to determine its potential for calibration,
2. Digitally process the SAR data set,
3. Calculate H_s and P_n for the scene to be calibrated using the calibration signals for that scene and the calibration reflector scene, and
4. Calculate σ for the image scene using P_I from that scene and the specific parameters for that scene (e.g., a new P_I and $G(\theta)$ and R).

Figure A-2 outlines the overall procedure used to calibrate SAR imagery. The first two steps (inspection and processing of the SAR data) appear to be straightforward, but in fact are crucial steps in the analysis and calibration process. The importance of this step cannot be overemphasized.

In selection of a SAR data set to address a specific analysis topic, it is necessary to determine if the SAR signatures are within the linear response region of the SAR system as well as determine whether or not the calibration signals are adequate for use in determining the SAR system gain. Once these two questions have been addressed, the SAR data can be processed into imagery and the calibration procedure begun.

Figure A-3 presents image intensity scans through the internal wave surface patterns present in Figure A-2. The scan was made in the range direction, with the ship present in the image being the center of the scan. The scan was generated by averaging 100 lines in azimuth and 20 elements in range. It is these intensity values which will be used to illustrate the calibration process.

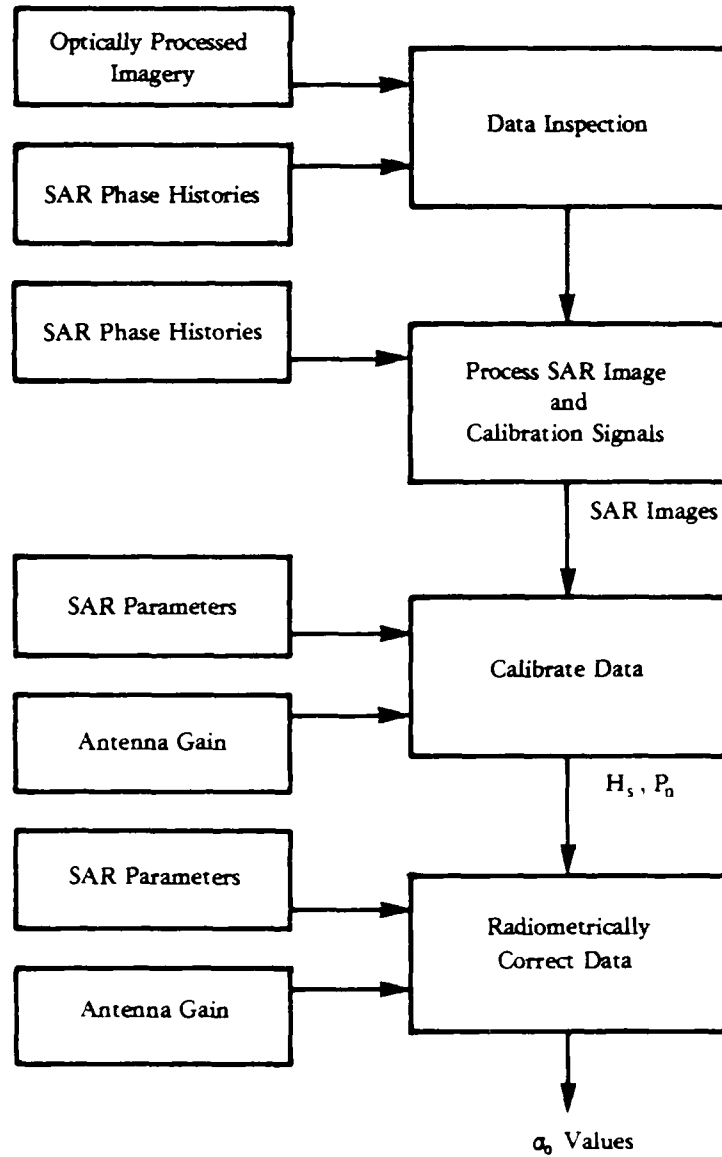


Figure A-2. Outline of Major Steps in SAR Image Calibration Procedure

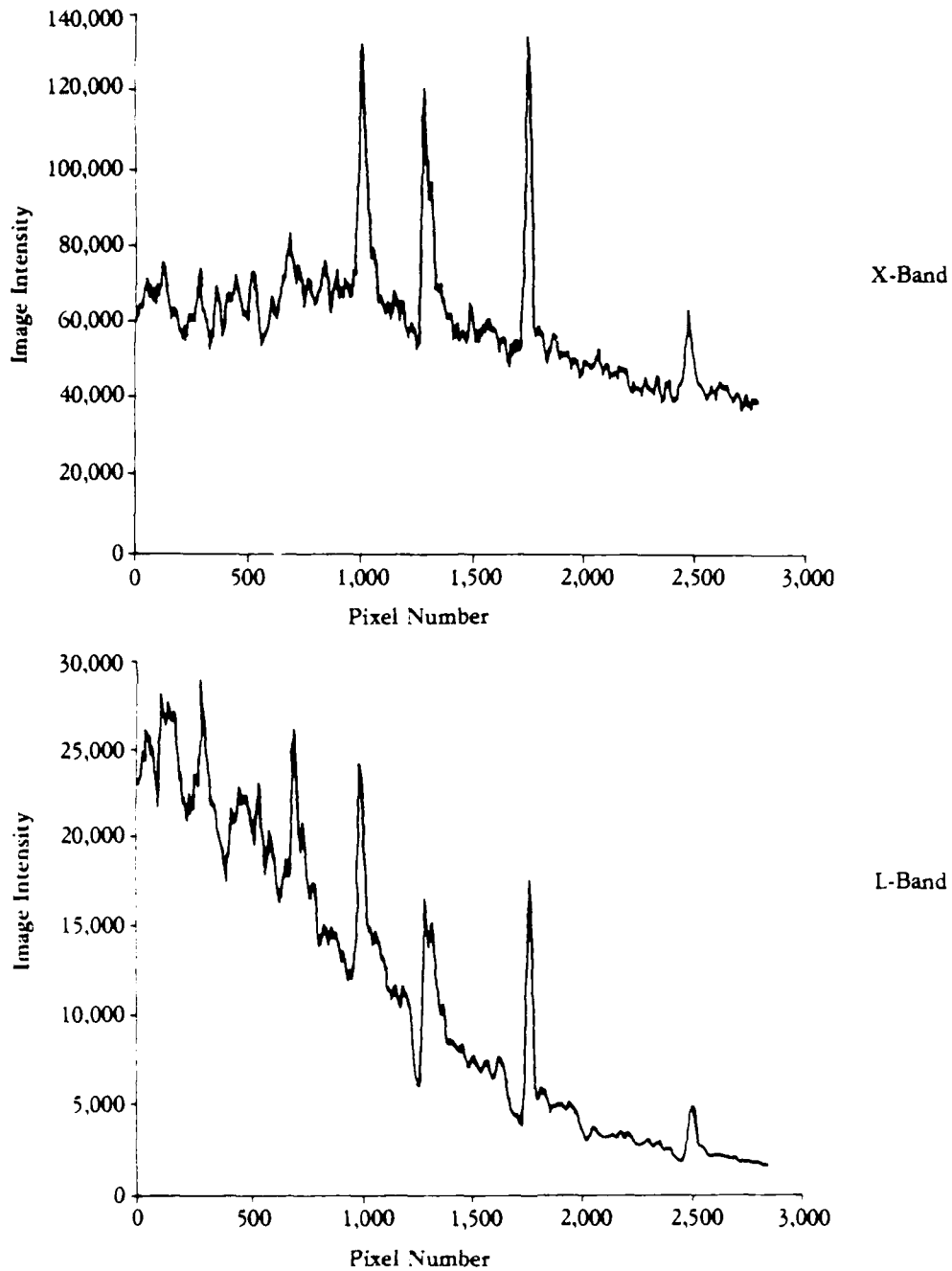


Figure A-3. Uncalibrated SAR Image Intensity Scans Through Surface Internal Wave Patterns From SARSEX-4, Pass 5

An examination of the intensities of the SAR signal histories will indicate whether the SAR system is operating in the linear region in the area of interest, i.e., whether the signals are saturated or not. To do so requires comparing the signals from an area of interest to a curve of the intensities from the calibration signals, some of which are saturated. The intensities of the SAR signal histories are illustrated in Figure A-4, which presents a curve generated from the internal calibration signals along with the location of the intensities of the ship, background level and brightest internal wave value.

The second step in the calibration procedure is to calculate each of the factors in Eq. (A-1). This includes using the SAR imagery of the set of calibrated reflectors. Once the SAR images of the reflectors are processed, an intensity, P , is extracted for each corner reflector in the scene. This intensity is calculated as

$$P = \sum_{i=1}^n \sum_{j=1}^m x_{ij}^2 \quad (A-2)$$

where x_{ij} is the power of a pixel,
 i is the line number, and
 j is the element number.

It is then necessary to calculate the background clutter for the area where the reflectors have been deployed. Once this clutter value (C) has been calculated and normalized to the same area as the area used for the reflector, then P_I is calculated

$$P_I = P - C \quad (A-3)$$

It should be noted that the same number of elements (i) and lines (j) should be used to calculate P_I for each reflector. Figure A-5 presents the P_I vs. σ curves generated for the calibration array imaged during the ONR experiment.

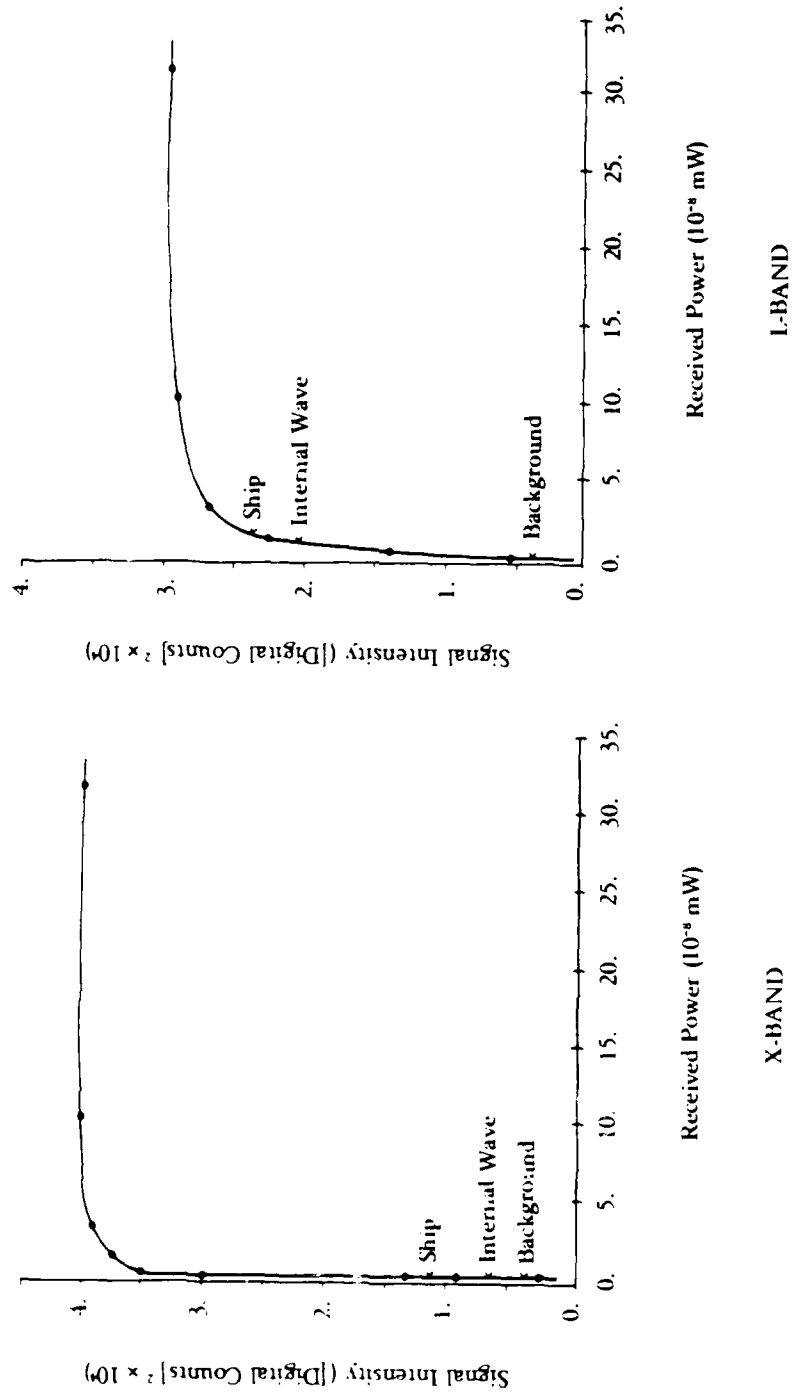


Figure A-4. X- and L-Band System Response Curves

AD-A160 173

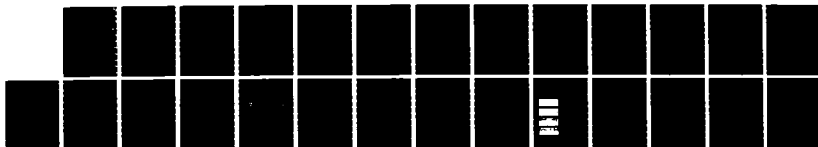
THE USGS (US GEOLOGICAL SURVEY) X- C- AND L-BAND SAR
DATA COLLECTION PROG. (U) ENVIRONMENTAL RESEARCH INST
OF MICHIGAN ANN ARBOR RADAR DIV E S KASISCHKE AUG 85
ERIM-173000-4-T

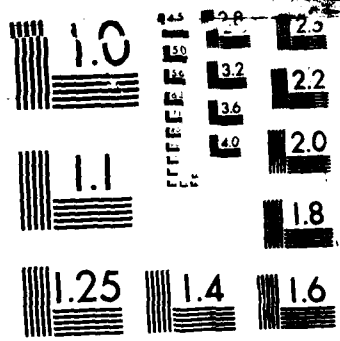
2/2

UNCLASSIFIED

F/G 17/9

NL





MICROCOPY RESOLUTION TEST CHART
1010A

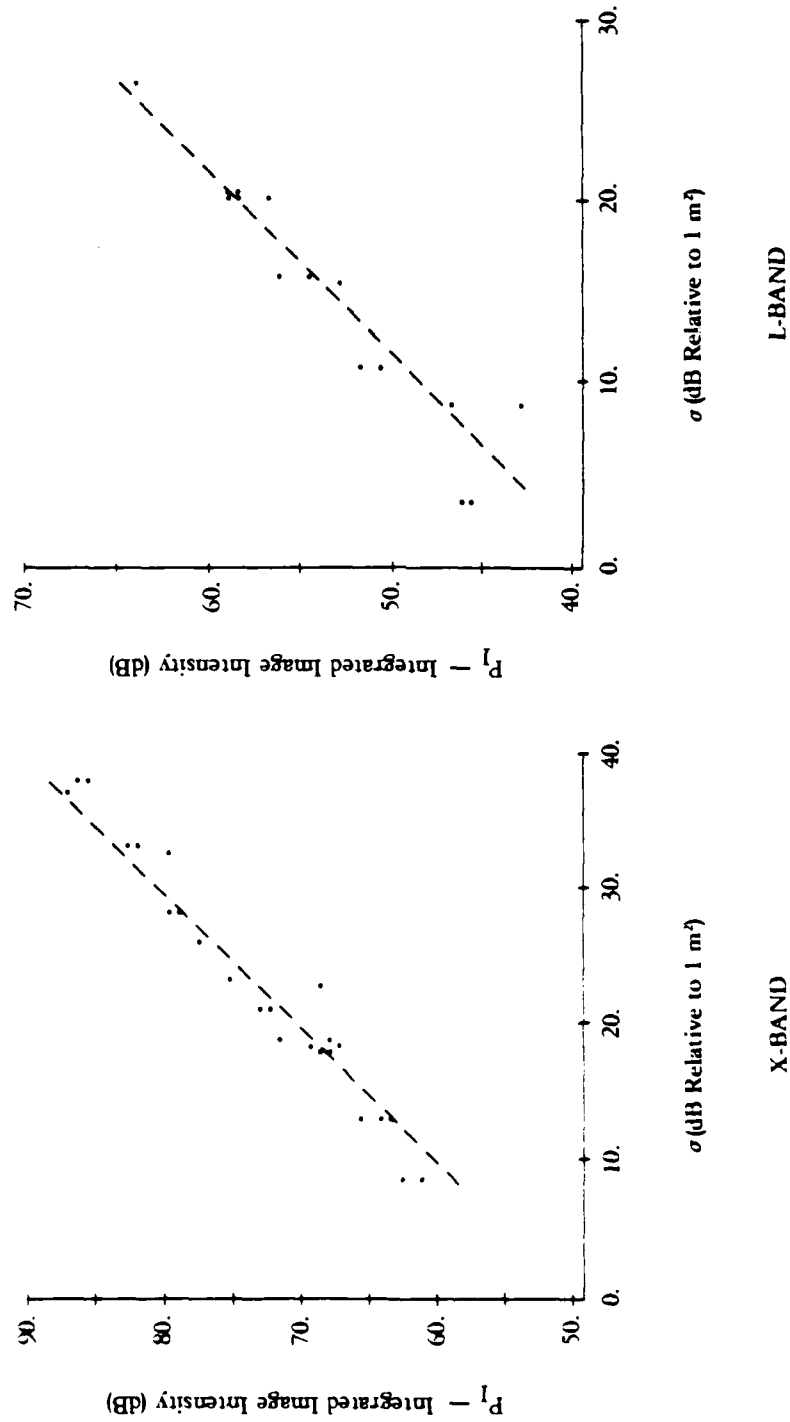


Figure A-5. Image Intensity Versus Radar Cross Section of Calibrated Reflectors From SARSEX-4, Pass 12 Data

Through the establishment of a linear relationship between σ and P_I , we can now arrange Eq. (A-1) to calculate H_S for the calibrated reflector array. Specifically

$$H_S = \frac{P_I (4\pi)^3 R^4}{P_T G^2(\theta) \lambda^2 \sigma} \quad (A-4)$$

Table A-1 lists the various factors to calculate H_S for the calibration array.

The next step in the calibration algorithm is to calculate the system gain, H_S , for the imaged scene. This is accomplished through measurement of the calibration signals generated before or after each pass of SAR imagery. These signals are measured in much the same manner as the reflector images using Eq. (A-3). However, instead of measuring a clutter factor, a system noise factor is calculated and subtracted from the power value (see Lyzenga and Shuchman, 1984). These power values are then plotted against the input power used to generate the signal. A curve is generated using both sets of calibration signals (for the calibration array and the SAR image to be calibrated). The difference between the linear portions of these curves (k) is the system gain difference between the two passes. The calibration signal curve at X-band for the two ONR data sets are presented in Figure A-6. The system gain for the image scene, H_S calculated from Eq. (A-4), is thus calculated by adding or subtracting k from H_S . For our example, k equals 18.0 dB at L-band and 18.5 dB at X-band.

Finally, a radar cross section for any pixel in the image scene can be calculated

$$\sigma = \frac{(P_I - P_n)(4\pi)^3 R^4}{P_T G^2(\theta) \lambda^2 H_S} \quad (A-5)$$

TABLE A-1
SAR SYSTEM PARAMETERS USED TO CALIBRATE
SAR IMAGERY

a.) Parameters for Calculation of H_S for Calibration Reflectors from SARSEX 4, Pass 12

<u>Parameter</u>	<u>X-Band</u>	<u>L-Band</u>
$\frac{P_I - P_n}{\sigma}$	76,504	5,248
λ	0.032 m	0.24 m
R	9,666 m	9,516 m
$G^2(\theta)$ for $\theta =$	48.6 dB	28.2 dB
P_T	1,741 W	5,650 W
H_S	$1.0301 \times 10^{19} \text{ W}^{-1}$	$3.9974 \times 10^{17} \text{ W}^{-1}$

b.) Parameters for calculation of σ values for SARSEX-4, Pass 5

P_n	11,442	204
λ	0.032 m	0.24 m
R	7,675 to 11,785 m	7,675 to 11,785 m
θ_I	29° to 55°	29° to 55°
$\theta_I(\text{Peak})$	62°	62°
$G^2(\theta)$	Variable Dependent on θ_I and $\theta_I(\text{Peak})$	
P_T	1,700 W	5,452 W
H_S	$7.2923 \times 10^{20} \text{ W}^{-1}$	$2.5222 \times 10^{19} \text{ W}^{-1}$
h	6696	6696

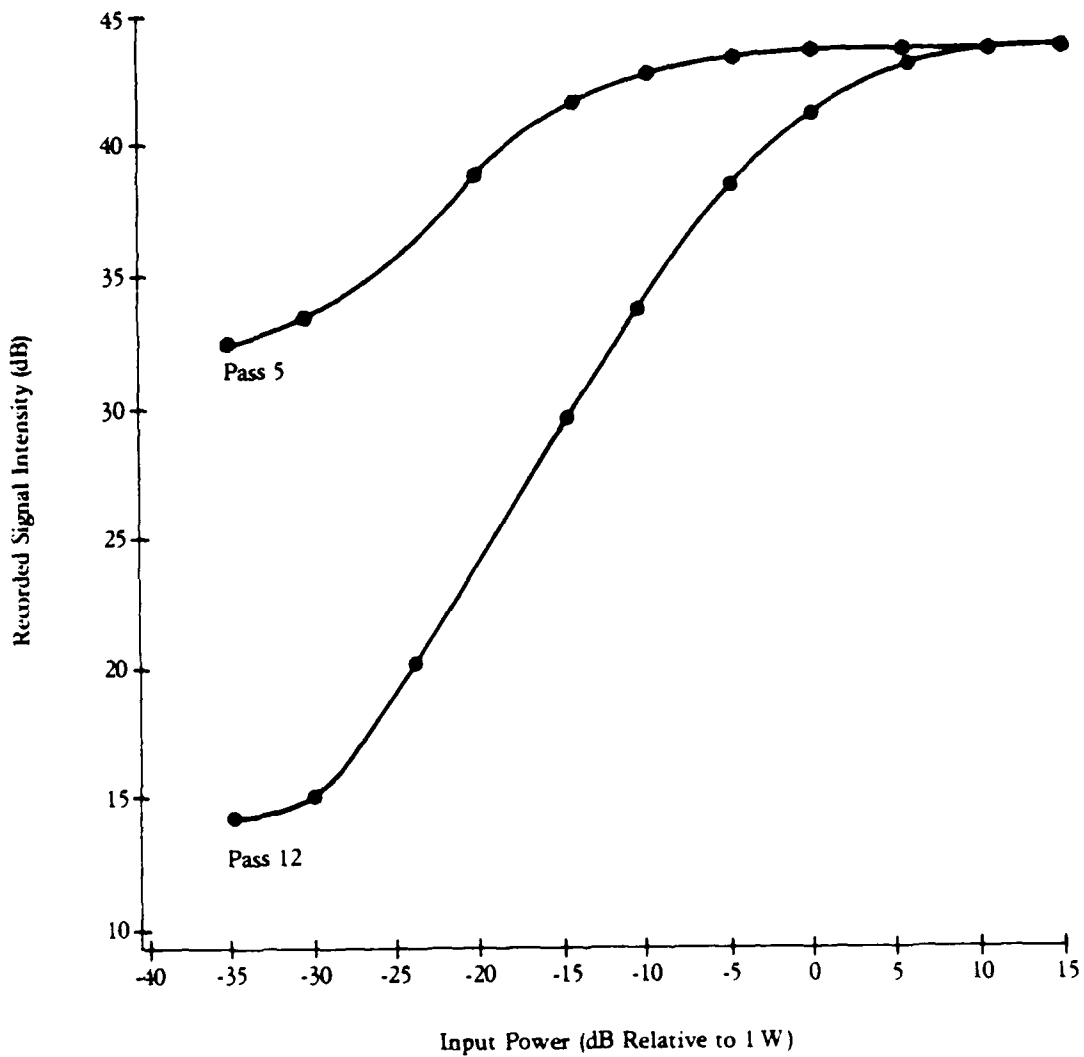
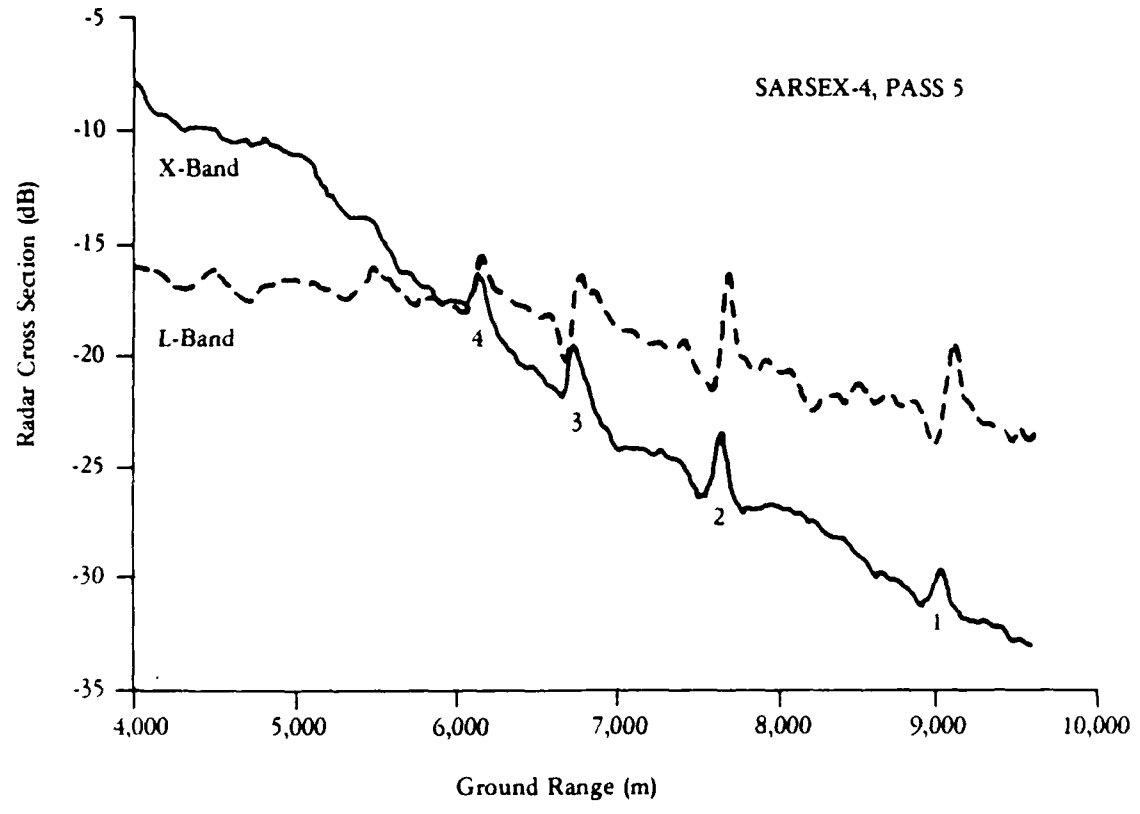


Figure A-6. X-Band System Response Curves Generated From Calibration Signals for SARSEX-4, Passes 5 and 12

where P_T is the transmitted power and P_n is the system noise for that scene, and R and $G(\theta)$ are calculated specifically for that pixel.

Using Eq. (A-5), a radar cross-section can be calculated for any pixel or area of the imaged scene. Figure A-7 presents the calibrated radar cross-section curves for the ONR SAR imagery.



Peak-to-Trough Signal Intensity

Wave	X-Band	L-Band
1	1.6 dB	4.5 dB
2	2.9 dB	5.3 dB
3	2.6 dB	4.0 dB
4	1.6 dB	2.9 dB

Figure A-7. Calibrated X- and L-Band Radar Cross Sections Obtained From SARSEX-4, Pass 5 Data

APPENDIX B

Dihedral Reflectors For Cross-Polarized Radar Imagery

by

P.L. Jackson
R.W. Larson
E.S. Kasischke

Submitted To

IEEE Journal of Geoscience And Remote Sensing

DIHEDRAL REFLECTORS FOR CROSS-POLARIZED RADAR IMAGERY

P.L. Jackson
R.W. Larson
E.S. Kasischke

Radar Division
Environmental Research Institute of Michigan (ERIM)
P.O. Box 8618
Ann Arbor, MI 48107

Abstract - Dihedral reflectors can be used for both cross- and like-polarized radar backscatter to calibrate intensity and provide locational accuracy for image registration. They can be economically constructed so that a large number can be used for calibration purposes across an imaging radar swath. Both rotating platform and SAR data demonstrated the dihedral's partitioning of reflected energy between cross- and like-polarization.

1. INTRODUCTION

Research in the uses of synthetic aperture radar (SAR) data is focusing more and more on measuring absolute and relative radar backscatter as well as merging multi-frequency and multi-polarization SAR data collected during different SAR overflights. Calibration of SAR data requires the use of calibrated reference reflectors and internal calibration signals [1]. Merging of multiple SAR data sets is aided by using reference reflectors whose positions are known.

Most SAR calibration experiments to date have used precision trihedral (corner) reflectors whose cross-section has either been calculated or measured. Recently, Brunfeldt and Ulaby have developed an active radar calibrator (ARC) which is essentially a transponder [2]. The ARC can be made to generate either like- or cross-polarized returns or both simultaneously.

An increasing amount of research is now being conducted on the analysis of cross-polarized SAR imagery. Trihedral reflectors do not return cross-polarized waves and thus cannot be used as a calibration source. ARCs can be used, but since it is necessary to have a large number of different sized calibration reflectors to generate a proper calibration curve, it would be quite costly to deploy a sufficient number for calibration purposes.

We wish to describe a dihedral reflector which returns both like- and cross-polarized EM waves. The dihedral reflector is relatively easy to construct and deploy, and cost-effective for a large number of emplacements. This type of reflector can be used to calibrate both like- and cross-polarized SAR imagery as well as to serve as a position reference to merge multiple-date SAR data sets.

II. DESIGN AND EMPLACEMENT

A polarized wave striking a conducting surface at a given angle ϕ will, upon reflection, be rotated in polarity by this angle. Two successive reflections, such as occur from a dihedral reflector, will cause the polarity to rotate by 2ϕ . If the dihedral is oriented so that the intersection of the plates is $\phi = 22\ 1/2^\circ$ with respect to the direction of the polarity and is perpendicular to the propagation direction of an incident radar beam, the polarity of the reflected beam will be rotated by 45° . Since a 45° rotation has equal components of like- and cross-polarizations, both polarizations can be sensed in the radar return.

Figure 1 schematically illustrates a dihedral reflector, which consists of two joined, perpendicular sheets of reflecting material with dimensions a and b. The proper orientation of the dihedral with respect to the polarity of the radar wave can be maintained by adjusting the heights of its front and back corners above a flat surface. These heights (see Figure 1) are adjusted as follows:

Let

$$A = (a/\sqrt{2}) \sin \theta ,$$

and

$$B = (a/\sqrt{2}) \cos \theta \sin \phi ,$$

where a is the dimension of the dihedral plate as shown in Figure 1, θ is the radar depression angle, and ϕ is half the angle of the desired polarity rotation upon reflection.

Then, for $\theta \geq \phi$

$$h_1 = A + B ,$$

$$h_2 = A - B ,$$

$$h_b = 0 ,$$

and for $\theta < \phi$

$$h_1 = 2A ,$$

$$h_2 = 0 ,$$

$$h_b = A - B ,$$

where the heights h_1 , h_2 , and h_b are shown in Figure 1. The dimensions h_1 and h_2 can be interchanged with the amount of rotation remaining constant but the direction being reversed. The backscatter cross-section of such a dihedral [3] is

$$\sigma_{\max} = \frac{8\pi a^2 b^2}{\lambda^2} ,$$

where σ_{\max} is the maximum cross-section, and λ is the radar wavelength.

The dihedrals can be constructed of sheet aluminum attached to a wooden frame, as shown in Figure 2. This dihedral (3 ft (0.9 m) x 4 ft (1.2 m)) has a σ_{\max} of 566 m² for L-band and 34,700 m² for X-band. It is readily emplaced with proper orientation in the field by tying the corners to construction stakes. To aid in field emplacement the proper heights of the dihedral corners can be listed in a table of SAR depression angles.

Prior to deployment of the dihedral reflector shown in Figure 2, laboratory measurements were obtained. A rotating platform in the field of a fixed antenna was used for this test [4]. Figure 3 illustrates polarity-partitioned radar returns from a dihedral reflector oriented at 22.5° with respect to the incident polarity when the dihedral faces the transmitter. The dihedral was rotated in the field of a transmit-receive antenna, and like- and cross-polarized radar returns plotted. The angle-dependent returns from both polarizations are equal or very similar in value within a rotating platform angle of 7° on either side of the maximum return.

III. FIELD TEST

A set of dihedral reflectors was deployed during a SAR data collection program conducted for the U.S. Geological survey in north-central North Carolina in April 1984. The ERIM-CCRS X-C-L SAR [5] was used for this purpose. X-band (3.2 cm) and L-band (23.5 cm) data collected over the Duke University Forest near Durham, North Carolina, demonstrated the effectiveness of these dihedrals for sensing both like- and cross-polarized radar backscatter. Figure 4 shows a portion of this imagery in both like- and cross-polarized SAR images. The dihedral reflector shown in Figure 2 was located near the center of each image, and is evident in both like- and cross-polarized images at both wavelengths.

Note that the image of the dihedral is stronger on the cross-polarized than on the like-polarized image, indicating that

the dihedral reflector was deployed at an angle greater than 22.5° with respect to the incident polarity direction at the actual SAR depression angle. Note also that the large (8300 m^2) trihedral reflectors, which return only like-polarized waves, are just visible on the X-band cross-polarized image. These reflectors produced such large like-polarized returns that they were detected across the -23 dB isolation between the like- and cross-polarized channels.

ACKNOWLEDGEMENT

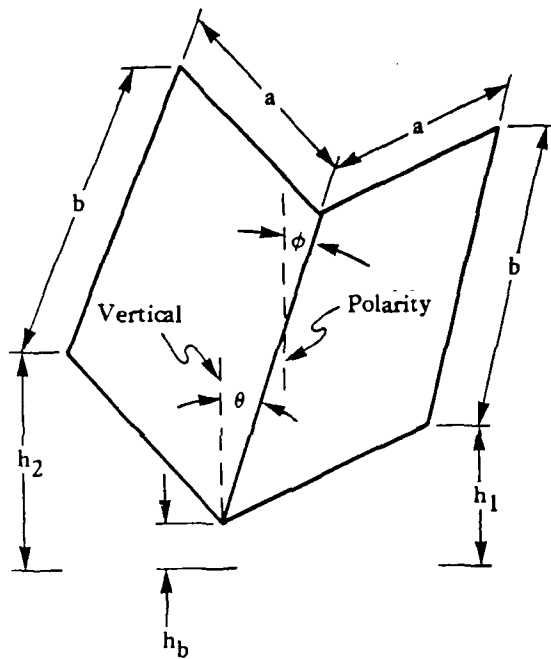
The research discussed in this paper was supported through funding provided by the U.S. Geological Survey (U.S.G.S) under Contract No. 14-08-0001-21748 and by the National Aeronautics and Space Administration (Johnson Space Center) under Contract No. NAS 9-16407. The authors would like to thank C. Ager and M. Powers of the U.S.G.S. for their assistance in deploying the dihedral reflectors, and Albert Fromm of ERIM for radar cross-section measurements.

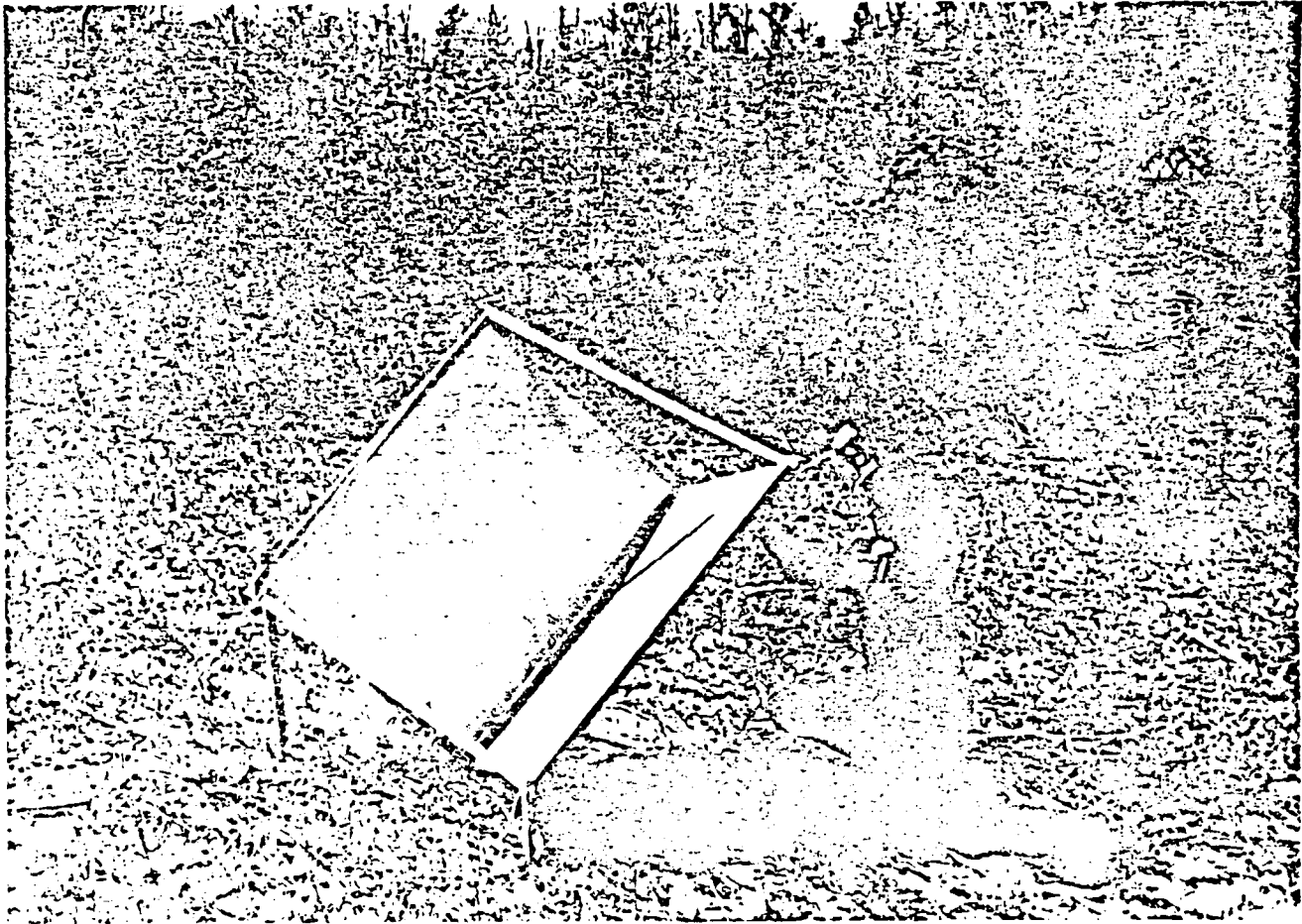
REFERENCES

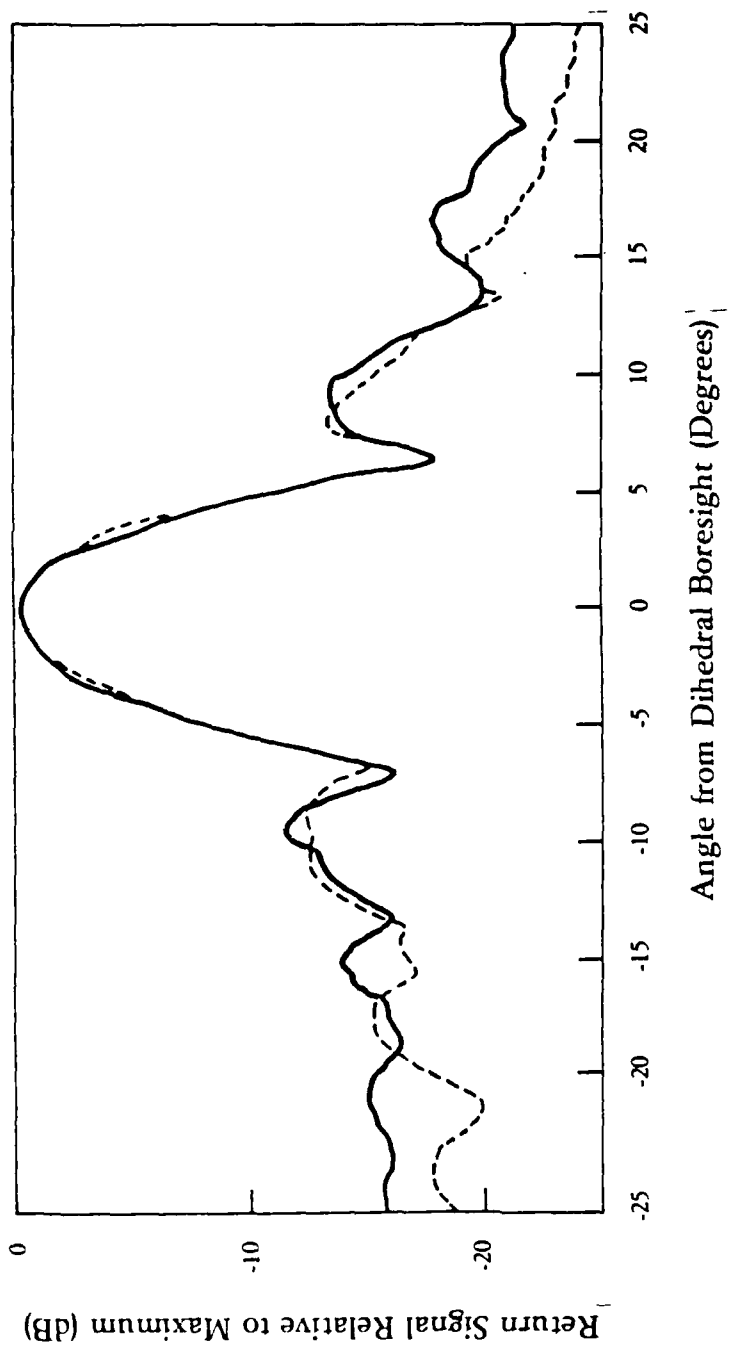
1. Larson, R.W., A. Dias, and R. Majewski, "Digital calibration method for synthetic aperture radar systems, IEEE Trans. on Geoscience and Remote Sensing (to be published 1985).
2. Brunfeldt, D.R., and F.T. Ulaby, Active reflector for radar calibration, IEEE Trans. on Geoscience and Remote Sensing, vol. GE22, pp. 165-169, 1984.
3. Ruck, G.T., D.E. Barrick, W.D. Stuart, and C.K. Krichbaum, Radar Cross Section Handbook, Plenum Press, N.Y., 1970.
4. Ausherman, D.A., A. Kozma, J.L. Walker, H.M. Jones, and E.C. Poggio, "Developments in radar imaging," IEEE Trans. on Aerospace and Electronic Systems, vol. AES-20, no. 4, pp. 363-400, 1984.
5. Rawson, R., F. Smith, and R. Larson, "The ERIM simultaneous X- and L-Band Dual Polarization Radar," Proc. of the IEEE International Radar Conference, Washington D.C., 1975

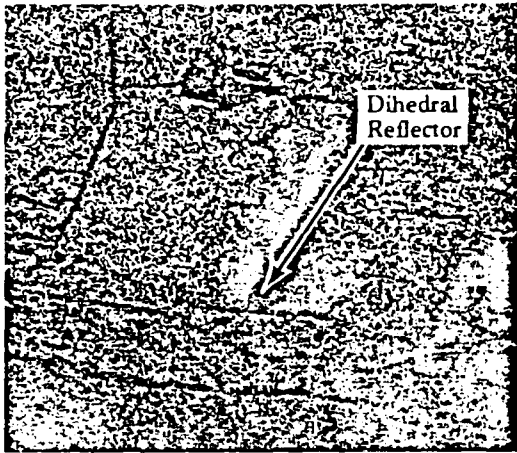
FIGURES

1. Schematic illustration of a dihedral reflector.
2. Field emplacement of dihedral reflector.
3. Like-Polarized (Solid Line) and cross-polarized (Dashed Line) backscatter vs angle of incidence. Rotating platform in field of fixed X-band antenna. Aluminum dihedral ($a = 6$ in, $b = 12$ in) positioned for 22.5° angle between incident angle and line of dihedral plate intersection.
4. L-Band and X-Band SAR data collected over Duke University Forest in April, 1984. Dihedral reflector is evident on all four like- and cross-polarized images. Small corner reflectors, located above and below the dihedral reflectors are evident on the like-polarized X-band image.



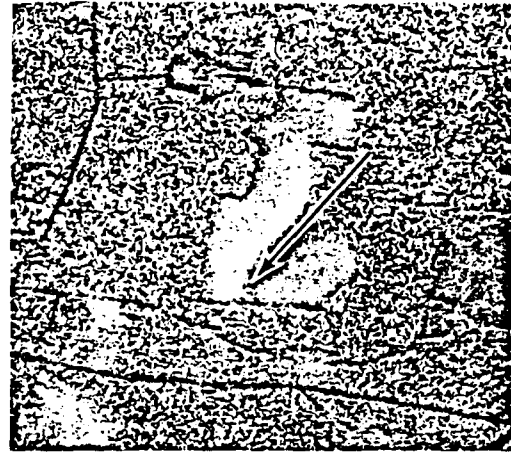




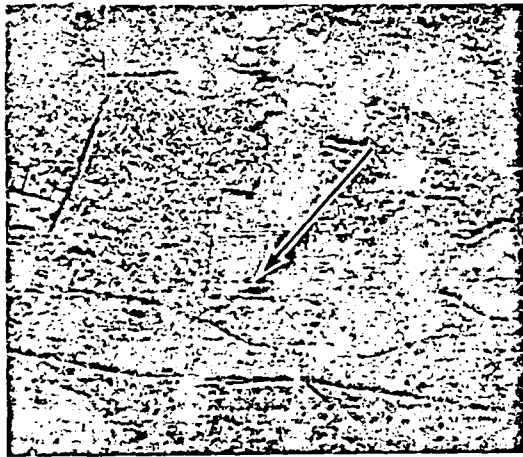


Like-Polarized

L-Band

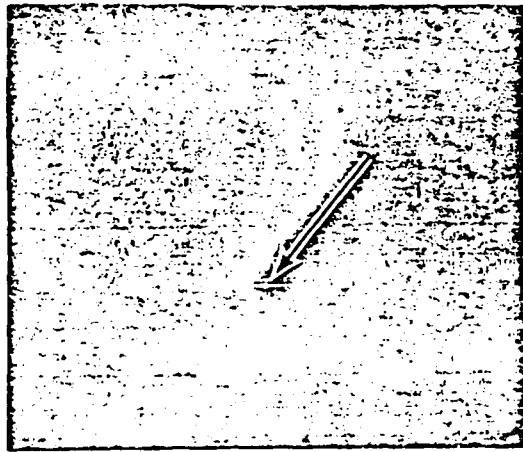


Cross-Polarized



Like-Polarized

X-Band



Cross-Polarized

APPENDIX C

Radar Data Processing and Exploitation Facility

by

D.A. Aushman

W.D. Hall

J.N. Latta

J.S. Zelenka

Reprinted From

Proceedings Of The 1975 IEEE Radar Conference

RADAR DATA PROCESSING AND EXPLOITATION FACILITY

D.A. Ausherman
W.D. Hall
J. N. Latta
J. S. Zelenka

Radar and Optics Division
Environmental Research Institute of Michigan
P.O. Box 618, Ann Arbor, Michigan 48107

ABSTRACT

A system is described which is dedicated to the signal processing and image exploitation aspects of synthetic aperture radar (SAR). The system utilizes coherent optical, hybrid optical-digital, and wholly digital approaches to SAR data processing. The subsystems using each one of these processing media are briefly reported. Examples of processed imagery are included and an application to radar remote sensing of the earth's surface is given as an example of one use of the facility.

INTRODUCTION

A system has been developed which is dedicated to the signal processing and image exploitation aspects of synthetic aperture radar (SAR). The overall system is capable of utilizing coherent optical, hybrid optical-digital, and wholly digital processing technologies in the generation, enhancement, and subsequent display of radar imagery. The ERIM Radar Data Processing and Exploitation Facility has proven applicability in many imaging radar applications, including the remote sensing of earth's resources.

The concept of Synthetic Aperture Radar is well documented [1-3]. The most common SAR utilizes the sidelooking radar configuration shown in Figure 1. The objective of such a system is to generate a two-dimensional continuous image of the terrain strip illuminated by a microwave beam as the radar vehicle moves in the azimuth (along-track) direction at a constant velocity. Range (cross-track) resolution is obtained by transmitting dispersed pulses and applying pulse compression techniques to the returned signals. Azimuth resolution is obtained by recording the Doppler frequency shifts associated with the returns from point scatterers as they migrate through the antenna beam. Knowledge of the Doppler frequency vs. time relationship for a point scatterer at a given range allows one to precisely locate the scatterer in azimuth in a manner analogous to the pulse compression applied in the range direction. The uncompressed radar echoes are usually recorded and subsequent two-dimensional signal processing is applied to form an image. The signal storage medium is usually optical analog (on film) or digital, depending on the processing medium to be used for signal compression. The system described herein also allows

optical recording and subsequent digital processing of the signal histories.

For coherent optical signal compression, film is the usual storage medium. The radar returns are coherently mixed to video frequencies and used to modulate the intensity of a CRT spot as its image is swept across a photographic film at a constant velocity. The video signal maintains a small carrier frequency to avoid any spectral folding, and it is recorded about a D.C. bias level to enable the proper recording of bipolar signals. The resultant film recording is a linear correspondence between slant-range (time-delay) and the spatial dimension across the film. Subsequent pulses are recorded side-by-side along the film as the film is moved past the CRT at a rate proportional to the radar vehicle velocity. The spatial dimension along the signal film is therefore linearly related to the azimuth dimension of the terrain. The developed film forms the input to the optical processor.

OPTICAL RADAR SIGNAL PROCESSING

The optical processor acts as a two-dimensional filter matched to the signal generated by a point

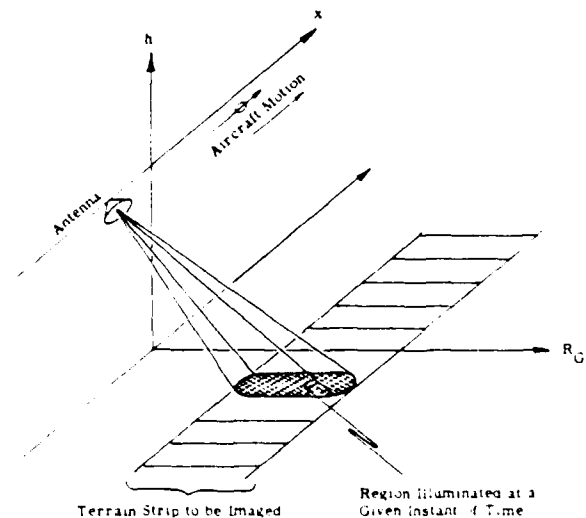


FIGURE 1. Schematic Representation of Strip-Map Mode Imaging Radar.

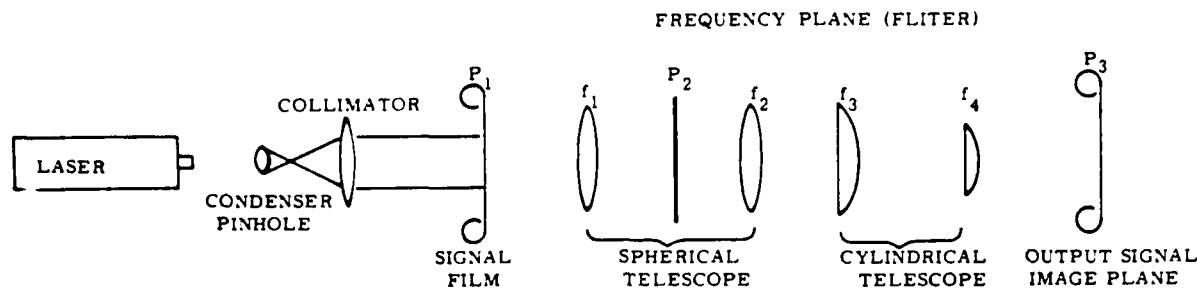


FIGURE 2. Tilted Plane Optical Processor

scatterer. Thus, the required two-dimensional pulse compression can be viewed as the convolution of an appropriate reference function with the recorded radar signal. In the optical processor this convolution is performed by configuring the lenses such that the impulse response of the processor is identical to the desired reference function. The primary advantage of the optical approach is the nearly instantaneous processing capability for two-dimensional signals with very high information content.

The optical processing facility usually utilizes a configuration known as the tilted plane optical processor. This optical system has been previously reported [4] and will not be described in detail herein. For a brief description consider the schematic diagram of the processor shown in Figure 2. A spherical telescope, usually of unity magnification, is comprised of spherical lenses L_1 and L_2 . A cylindrical telescope of variable magnification, consisting of lenses L_3 and L_4 is in tandem. The signal-film transparency S is illuminated with collimated, monochromatic (laser) light by utilization of a point source P and collimator L_0 . The desired image forms at the output plane I , where it can be viewed directly or recorded on photographic film. Frequency plane filtering can easily be accomplished by placing the appropriate slits and weighting masks in plane F , which is the spatial two-dimensional Fourier transform of the input data. Such filtering is used primarily to limit the passband of the processor. For certain forms of coded radar pulses the desired matched filtering occurs as a consequence of the lens action and free space transformations associated with the optical configuration.

If the ranging signal transmitted by the radar is a linear frequency modulated (chirp) pulse, the slant-range image is formed near the signal film due to the propagation effects between the film and the image. This is analogous to the formation of a holographic image. This image is then re-imaged via the spherical telescope to the output plane I . The azimuth signal history is a true microwave hologram [3] which forms an image, usually in a different plane and of different magnification than the range image. By adjusting the magnification and the position of the cylindrical telescope (with no effect on the range image), the range and azimuth image planes can be brought into coincidence with unity aspect at plane I . For processing of long image strips both input and output films must be

translated through the processor in synchronism, forming a continuous convolution in the azimuth direction.

The above processing method is complicated in that the azimuth image plane is tilted with respect to the signal film while the range image is parallel to the signal film*. The solution is to tilt the input and output planes the proper amount to bring the planes to a common focus [4]. When the input plane is rotated about the azimuth coordinate, the slant range image formed by the unity telescope rotates the same amount. The azimuth image, however, is demagnified by the cylindrical telescope and therefore rotates a proportionally lesser amount. A tilt angle usually exists which brings the two image planes into focus.

Frequency plane filtering is required in the processor to remove the conjugate (the negative frequency band) and undiffracted (D.C.) wavefronts which result from the holographic signal recording. A frequency plane slit is used to insure that these signal components do not corrupt the final image. In addition, aperture weighting masks can be inserted in the frequency plane to provide the desired processor impulse response.

The use of film as the hardcopy image storage medium limits the output dynamic range of the system to approximately 25 dB. The next section will describe a hybrid optical-digital system capable of providing direct digitization of the output image with increased dynamic range.

HYBRID OPTICAL-DIGITAL RADAR SIGNAL PROCESSING

The image dissector and digitization (IDD) facility consists of a coherent optical processor interfaced to a computer system which provides digitization, recording, and display of processor outputs. The hybrid concept effectively combines the power and speed of coherent optical data processing with the flexibility and precision of digital processing methods. The system can be used for digitization

*The azimuth image plane is tilted due to the fact that the Doppler frequency vs. azimuth position relationship is a function of the range of the scatterer. This in turn implies that the azimuth holographic signals have focal lengths which vary linearly with range.

of film-recorded SAR signal histories or of optically processed imagery having a dynamic range of up to 40 dB. If the digital phase histories are digitally processed into imagery, it can result in a very large dynamic range (50 to 60 dB) previously only available as a light distribution in the output plane of an optical processor. Such imagery is ideal for subsequent exploitation processing. The unique design parameters for this system were dynamic range response, resolution, linearity, and total system stability.

A block diagram of the hybrid facility is shown in Figure 3. The key to the optical-digital interface is the image dissector camera manufactured by ITT Aerospace/Optical Division. The image dissector has been described as a photomultiplier with a small electronically movable photocathode area, thus acting as an all-electronic, low-inertia microphotometer. The dissector camera is positioned such that the output image of the optical processor is focused upon the photocathode. Electrons are emitted from the back of the photocathode, forming an electronic image with current density modulated according to the image input. The electron image, focused by magnetic deflection, falls upon an aperture plane at the other end of the drift tube. The aperture samples the image by allowing only a small, well defined area of the electron image to pass through to the electron multiplier, which then multiplies the sampled photoelectrons by a factor of approximately 5×10^3 . The entire electron image is deflected, allowing the aperture to sample different points in the input image.

In the IDD system the aperture is "scanned" only in the range direction. The aperture is effectively displaced in the azimuth direction as the input film is translated between successive range scans. The dissector aperture used is rectangular, measuring 0.01 mm in the range direction and 0.5 mm in the azimuth direction. The effective width of the azimuth aperture can be reduced by placing a slit of the desired width in the output plane of the optical processor and then re-imaging the output on the dissector photocathode surface. The spatial frequency response of the dissector exhibits approximately 40% modulation at 30 line pairs per millimeter.

As shown in Figure 3 the dissector system with its associated control electronics is interfaced to the PDP-8/E minicomputer. This computer buffers a scan line of data from the dissector interface and

writes the data on a 9-track, computer compatible tape system, one line at a time. The PDP-8/E also has the ability to perform a real-time photonormalization on each scan line of data for removal of the nonuniform response characteristic of the photocathode (typically $\pm 11\%$ variation). The correction to be applied is automatically determined from data collected in a special calibration mode of operation.

The images are digitized to 8 bits, giving 256 image intensity levels. An alternate circuit is selectable which square roots the video prior to digitization. In this manner 256 levels of image amplitude information is obtainable. The dynamic range achievable with the IDD is approximately 40 dB, compared with a 20 dB dynamic range typically achievable if the image were recorded directly on film.

The control electronics enable the user to select the number of picture elements (pixels) digitized per scan line up to a maximum of 3000 per 30 mm scan length. In addition, the scan length can be selected by setting thumb switches to the desired scan start and scan stop address or by adjusting the dissector deflection voltages. The integration time per pixel is selectable in increments of 10 usecs from 10 usecs to 990 usecs. (Integration is required to filter out electron shot noise introduced in the multiplier stages.) Finally, a point-skip control allows the user to vary the scan line resolution by skipping up to ten pixels between digitizations. Azimuth sample spacing is determined by the speed of the precision film drive used to translate the input film. The film drive unit has a long-term stability of 5×10^{-3} per cent and a short-term jitter of less than one micron.

The IDD system is capable of both hardcopy and softcopy display of the digitized data. Hardcopy is provided with a 70 mm CRT film recorder while softcopy is accomplished with a PEP-400 analog scan converter image display interfaced to a PDP-11/40 control computer.

The hardcopy CRT film recorder is interfaced to the PDP-8/E and used for displaying digitized data stored on the magnetic tape unit. The CRT is a fiber optics direct coupled line scan recorder capable of recording images up to 3000 elements in range and virtually any length in azimuth (limited by film length). The recording spot size is approximately 20 microns in diameter and recording linearity is ± 0.1 per cent in range and ± 1 per cent in azimuth. Although not as accurate as the digitization process, this display technique is useful for hardcopy visual presentation of digitized imagery.

The softcopy display consists of a PEP-400 Conrac display interfaced to a PDP-11/40 minicomputer which receives scan data via the PDP-8/E control computer. The PEP-400 is an analog scan converter which utilizes a silicon dioxide image storage tube. The storage tube is capable of holding a 1024×1024 image matrix for 15 minutes before it fades and has available 32 shades of grey for display. The Conrac TV monitor is a 1229 line display synchronized to the PDP-400 controller. In addition to the conventional contrast and brightness control, the PEP-400 controller has a zoom control and selective X-Y image position control which provides more detailed image examination.

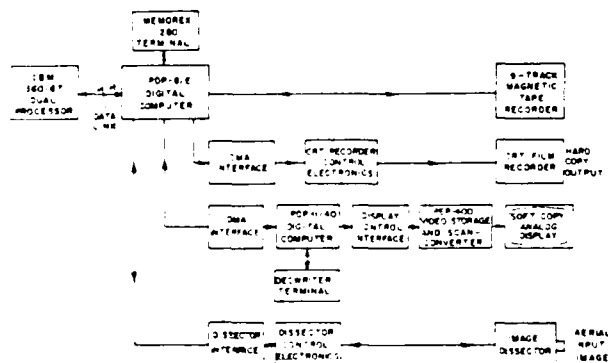
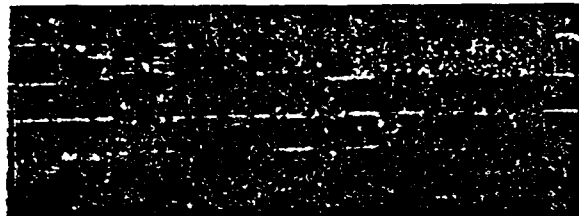


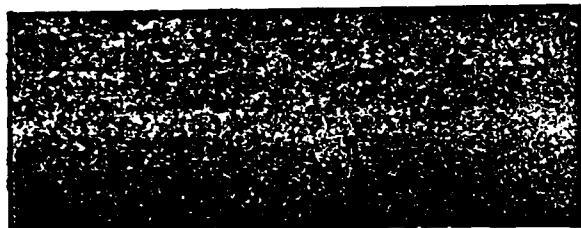
FIGURE 3. Image Dissector and Digitization (IDD) Facility

The softcopy display provides a capability for real-time operator interactive processing. Special interactive processing techniques such as coherent optical spatial filtering are possible on a real-time basis. The principle modes of operation are: (1) Direct display of data during digitization; (2) direct display of Fourier transformed data during digitization; (3) data plots of FFTs of image data for initial set up and system performance evaluation; and (4) data tape verification after digitization.

Examples of SAR imagery processed and digitized on the hybrid IDD facility are shown in Figure 4. The images were produced with the ERIM four channel multiplexed radar system [5,6] which on a single pass produces phase histories at two wavelengths (3.2 and 23 cm) with two polarization configurations for each wavelength (horizontal transmit, horizontal receive and horizontal transmit, vertical receive). The phase histories were processed



a) 3.2 cm Horizontal-Horizontal Polarization



b) 3.2 cm Horizontal-Vertical Polarization



c) 23 cm Horizontal-Horizontal Polarization



d) 23 cm Horizontal-Vertical Polarization

FIGURE 4. Sar Imagery Optically Processed, Digitized and Displayed using the Hybrid IDD Facility.

to 30 ft resolution in both range and azimuth and were digitized with 6.67 ft sample spacing in both coordinates. The images were then reconstructed on the CRT hardcopy film recorder. The area imaged was a portion of the NASA soil moisture test site near Phoenix, Arizona.

DIGITAL SAR SIGNAL PROCESSING AND IMAGE EXPLOITATION

Digitized phase histories and images, including those generated on the hybrid IDD system serve as inputs to the digital radar data processing and exploitation facility. The goal of this facility is twofold: (1) the development of two-dimensional digital signal processing techniques applied to SAR image formation; and (2) the development of manual and automatic exploitation techniques, which will improve the practicability of imaging radars in various applications. The facility comprises a minicomputer based system of specialized hardware in a multi-user operating environment. The system has been specifically tailored for efficient SAR processing and image exploitation.

A block diagram of the digital facility appears in Figure 5. The basic component of the system is a Digital Equipment Corporation PDP-11/45 central processing unit which utilizes 262,144 bytes of on-line memory through the use of memory management hardware. An advanced operating system (RSX-11D) allows multiple real-time tasks to run concurrently on the machine, with a single task addressing up to 65,536 bytes of memory. Intertask communication is permitted, which implies that several tasks could potentially be working on a single processing problem. Several computer terminals are provided so that several users can be utilizing the facility simultaneously.

Special provisions have been made for offline storage. Due to the vast amounts of data associated with SAR phase histories or images, a 116 million byte random access disk unit has been included in addition to a DEC RK05 disk unit (2.4 million bytes) used for operating system and user program storage. The magnetic tape system consists of two 9-track and one 7-track dual density type drives, allowing tape-to-tape processing in formats compatible with virtually all industry standards, except the newer 6250 bpi format.

To aid in implementing SAR digital processing algorithms a hardwired FFT processor has been included in the system. The FFT processor (Time Data, Inc. FPE4) can perform a 1024 point complex FFT in 200 msec. The data frame size for the FFT is controllable from 4 complex points up to 4096 complex points in powers of 2. In addition to real and complex, direct and inverse transforms, the processor can perform frequency domain Hanning filtering as well as auto and cross spectrum averaging. Software has been generated which uses the FFT processor to perform a large array two-dimensional FFT (up to 1024 x 1024 complex points).

An interactive digital image display is currently being integrated into the digital facility. The RAMTEK display, which has a solid-state shift register refresh memory, is capable of displaying digital imagery in two modes (1) 512 x 512 x 6 bits on a black and white TV monitor; and (2) 256 x 256 on a color TV monitor with 6 bits each controlling

the red, green and blue intensities for each picture element. Overlay channels are provided so that graphical information such as object outlines or annotation data can be superimposed on the displayed images without destroying the contents of the display memory. In addition, a trackball controlled cursor allows the user to extract positional information from the displayed images. A diagram of the interactive display system is shown in Figure 6.

An additional feature of the display are the programmable table-lookup memories installed between the display memory and D/A converters which provide the video intensities. Under program control these memories can be loaded with intensity transfer functions which are then applied to the images on a point-by-point basis in real time as they are displayed. The transfer function can be constructed to provide contrast enhancement, thresholding, image intensity inversion, pseudo-color encoding or any of a number of single point image manipulations, the results of which are nearly instantaneously visible to the operator. The display will be used to view digitally processed SAR imagery and to examine image exploitation techniques.

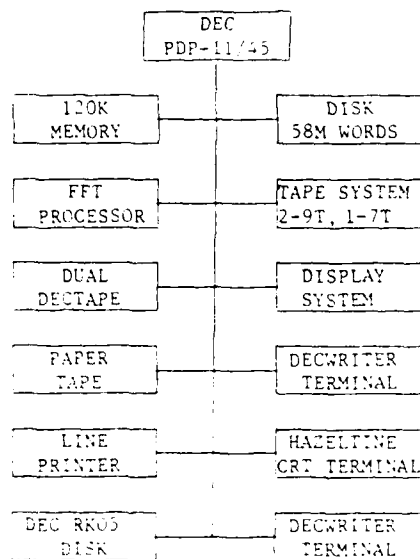


FIGURE 5. Digital Radar Data Processing and Exploitation Facility

SAR digital processing consists primarily of two-dimensional pulse compression techniques applied to digital signal histories. The digital facility serves as a general purpose tool for examining such techniques. The 2-D pulse compression is generally implemented as two one-dimensional digital matched filtering operations in conjunction with range and azimuth prefiltering operations analogous to the frequency plane filtering used in the optical processing technique previously described. The FFT hardware is useful for performing the various types of digital filtering operations. The digital facility has been structured for highly controlled experimental processing rather than emphasizing real-time applications.

Once digital SAR imagery is available, exploitation processing can be applied. Such techniques are directed towards either improving manual interpretation or implementing machine automated interpretation of the imagery. The digital facility is applicable to both types of analysis.

The goal of processing for manual interpretation is to increase the flow of information from display to observer. Most conventional image processing techniques are applicable here, ranging from interactive extraction of mensuration data using the cursor, to spatial frequency filtering for image enhancement. Emphasis is being placed on single point operations to take full advantage of the real-time, programmable enhancement capability of the image display.

Automated interpretation involves the use of pattern recognition algorithms on features extracted from the radar imagery. Applications include automatic target identification and classification of land use or conditions on the basis of multi-channel radar returns. For example, the four images shown in Figure 4 are being analyzed in an effort to determine soil moisture content, surface roughness characteristics, and vegetation type associated with the field patterns in the image. The four channels have been digitally registered and multivariate discriminate analysis is being applied to derive decision rules based on the four radar returns for each picture element [7]. In addition, texture analysis [8] is being applied to individual images in an effort to determine the relationship between each surface condition and the spatial characteristics of the radar returns.

SUMMARY

A system has been described which is designed specifically for signal processing and image exploitation of SAR data. The total facility utilizes coherent optical, hybrid optical-digital, and wholly digital processing technologies to generate and effectively display SAR imagery. The optical system uses a state-of-the-art tilted plane processor to process optically recorded SAR signal histories into imagery. The hybrid facility makes use of an image dissector device as a bridge between the optical-analog and digital realms to effectively combine the speed and power of coherent optical processing with the flexibility and precision of digital techniques. A unique digital system which includes a hardwired FFT processor and an interactive digital image display can then be used to investigate digital SAR processing and both manual and automated interpretation techniques.

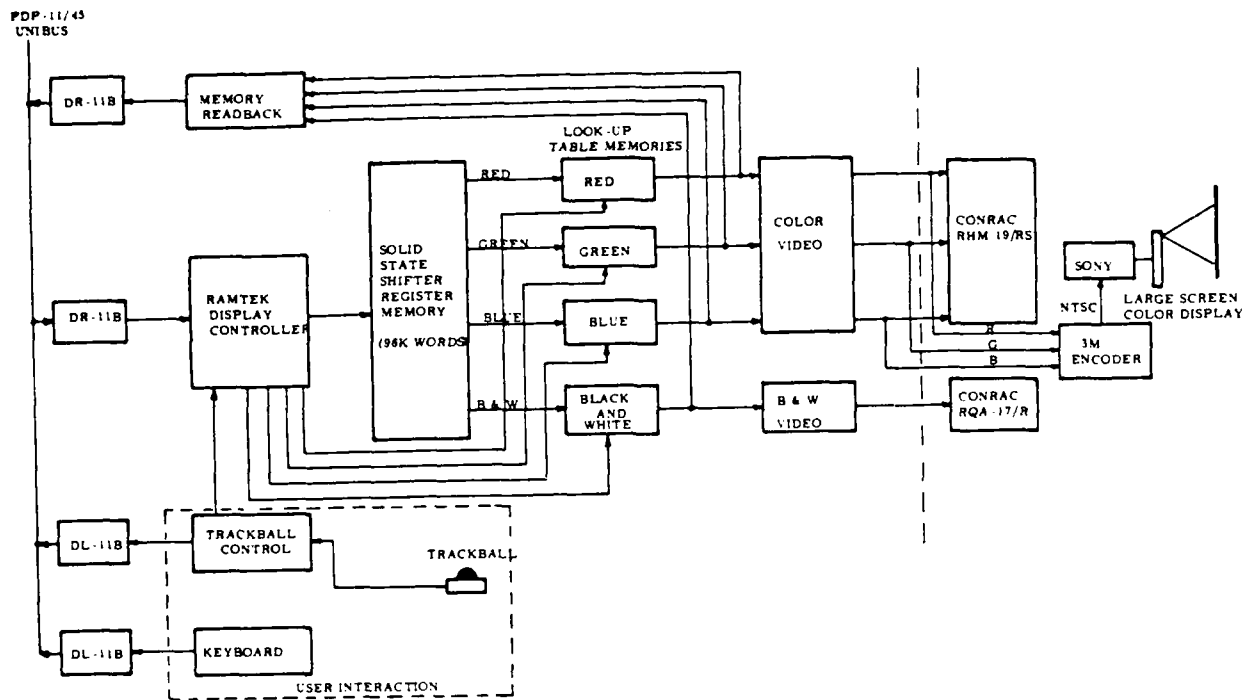


FIGURE 6. RAMTEK Digital Image Display Block Diagram

REFERENCES

1. W. M. Brown, "Synthetic Aperture Radar," IEEE Trans. on Aerospace and Electronic Systems, AP-13, March 1977, pp. 217-229.
2. W. M. Brown and L. J. Perrella, "An Introduction to Synthetic Aperture Radar," IEEE Spectrum, Vol. 1, September 1964, pp. 51-61.
3. W. M. Brown, "Synthetic Aperture Radar Techniques in the Microwave Region," Proceedings of the IEEE, AP-19, No. 4, September 1971, pp. 1305-1318.
4. R. F. Rawson, N. G. Leith, and N. G. Massey, "Tilt-Insensitive, 2-D Processor," Appl. Opt., Vol. 10, No. 7, August 1971, pp. 1766-1771.
5. R. Rawson and F. Smith, "Four Channel Simultaneous X-L Band Imaging SAR Radar," 9th Int. Symp. of Remote Sensing of Environment, Ann Arbor, Michigan, April 1974, pp. 251-270.
6. R. F. Rawson, F. Smith, R. Larson, "The ERIM Simultaneous X- & L-Band Dual Polarization Radar," IEEE International Radar Conference, Washington, D.C. April 21, 22, 23, 1975.
7. R. B. Crane, et al., A Study of Techniques for Processing Multispectral Scanner Data, ERIM Technical Report No. 11650-155-T, Sept. 1973.
8. D. A. Ausherman, Texture Discrimination Within Digital Imagery, Ph.D. Dissertation, University of Missouri-Columbia, December 1972. Available from University Microfilms, Inc., Ann Arbor, MI.

APPENDIX D
DATA TAPE FORMAT

The following is a description of ERIM digital data tape format (SAR IPL data):

1. Each CCT (Computer Compatible Tape) has been recorded on 9 track tape at a density of 6250 BPI.
2. There are 8 files on each tape, with 2 end of volume marks immediately following the last file.
3. The first record of each file contains a header record from the original data. The first 96 bytes of this record are used to store the following information:
 - A. Data type number
 - B. File number
 - C. Flight date
 - D. Band
 - E. Polarization
 - F. Bite
 - G. File size (prior to geometric correction)
 - H. Resolution in meters (range)
 - I. Data Compression method (square root)
 - J. Processing date

All header data is in an ASCII Convention.

4. Processed SAR data (beginning with record 2 of each file) consist of fixed length unformatted records. The SAR data is in a byte convention (quantized to 8 bits, one byte per image element). Information on the number of records and record length in bytes of each file has been included, as well as an example of header information.

ENTR
DITIC

7-86